Energy and Electron Transfer in Porphyrin-Phthalocyanin-Porphyrin Heterotrimers.

A study by Transient Absorption Spectroscopy, Fluorescence Upconversion, and Time Correlated Single Photon Counting.

DISSERTATION

zur Erlangung des akademischen Grades
doctor rerum naturalium
(Dr. rer. nat.)
im Fach Physik

eingereicht an der
Mathematisch-Naturwissenschaftlichen Fakultät I
Humboldt-Universität zu Berlin

von
Diplom-Physiker Sebastian Tannert

Präsident der Humboldt-Universität zu Berlin:
Prof. Dr. Jan-Hendrik Olbertz

Dekan der Mathematisch-Naturwissenschaftlichen Fakultät I:
Prof. Dr. Stefan Hecht

Gutachter:

1. Frau Prof. Dr. Beate Röder
2. Herr Prof. Dr. Jörg Enderlein
3. Herr Prof. Dr. Karsten Heyne

eingereicht am: 15. Oktober 2012
Tag der mündlichen Prüfung: 8. August 2013

Abstract

This thesis contributes to the comprehension of energy and electron transfer within novel supra-molecular structures, denominated triads, consisting of a central phthalocyanine axially-coupled to two porphyrins. In the course of this thesis, two of the trimers, were quantitatively characterized regarding their intramolecular transfer processes. Both feature a dative bond between the porphyrins and the phthalocyanine via the central silicium atom of the latter. These investigations aimed at answering whether this class of compounds allows the desired combination of light harvesting and charge separation. To perform the required analysis, the setups of the Röders group had to be upgraded to enable the measurement of fluorescence and absorption kinetics at a sub-picosecond timescale. As a result, two new setups are now available; one facilitating fluorescence upconversion via sum frequency generation, while the other one enables recordings of transient absorption. Both setups utilize a short laser pulse to optically generate a time gate in the range of 100 fs, enabling the time-resolved detection of the measurement signal by an integrating detector. In addition, data analysis of time-correlated single photon counting was extended by the method of global analysis, allowing the reconstruction of decay-associated spectra.

The rate constants of both investigated trimers in two solvents with different polarity were determined by the combination of data from a variety of measurement methods. An efficient charge transfer from the porphyrins to the phthalocyanine and a hole transfer from the phthalocyanine to one of the porphyrins occurs in all investigated cases. This result confirms the prospect that light harvesting and charge separation can occur combined in one molecule. Depending on solvent polarity and the structure of the porphyrines, electron transfer parallel to the energy transfer and a charge back transfer takes place in addition to both above-mentioned processes. However, the charge-separated state of the investigated substances decays to fast, still preventing a practical utilization of these compounds in solar cells and necessitating further developments.

Keywords:
artificial photosynthesis, organic solar cell, energy transfer, electron transfer

Zusammenfassung

Diese Dissertation leistet einen Beitrag zum Verständnis des Energie- und Elektronentransfers innerhalb von neuartigen supramolekularen Strukturen, die aus einem zentralen Phthalocyanin und zwei axial angekoppelten Porphyrinen bestehen. Zwei solcher Trimere, welche die koordinative Ankopplung von Porphyrinen über ein Silizium-Zentralatom des Phthalocyanins nutzen, wurden im Rahmen der Arbeit zum ersten Mal quantitativ bezüglich auftretender innermolekularer Transferprozesse charakterisiert. Ziel war die Beantwortung der Frage, ob diese Substanzklasse die wunschgemässe Vereinigung von Lichtsammlung und Ladungstrennung ermöglicht. Hierfür war es erforderlich, die in der Arbeitsgruppe Röder zur Verfügung stehenden Messaufbauten so zu ergänzen, dass Fluoreszenz- und Absorptionskinetiken auch im sub-Pikosekundenbereich messbar wurden. Als Ergebnis stehen zwei neue Messplätze zur Verfügung. Der eine ermöglicht die Fluoreszenz-Aufwärts-Wandlung der Probenfluoreszenz über Summenfrequenzgeneration, der andere die Messung der transienten Absorption der Probe. Beide Aufbauten nutzen einen kurzen Puls zur optischen Erzeugung eines Messfensters im Bereich von 100 fs, um die Kinetik des Messsignals mittels eines integrierenden Detektors zeitaufgelöst detektieren zu können. Weiterhin wurde die Datenauswertung der Appartur zur zeitkorrelierten Einzelphotonenzählung um die Methode der globalen Datenanpassung ergänzt, um Zerfallszeit-assozierte Spektren messen zu können.

Aus der Kombination der Messdaten, aufgenommen mit einer Vielzahl von Messverfahren, konnten für die beiden untersuchten Trimere in zwei unterschiedlich polaren Lösungsmitteln die Ratenkonstanten der Energie- und Ladungstransferkanäle ermittelt werden. In allen Fällen findet ein effizienter Ladungstransfer von den Porphyrinen zum Phthalocyanin und ein Lochtransfer vom Phthalocyanin zu einem der beiden Porphyrine statt. Dieses Ergebnis bestätigt die Erwartung, dass Lichtsammlung und Ladungstrennung in diesem Molekül vereint auftreten. Zusätzlich zu den beiden oben erwähnten Prozessen findet je nach Lösungmittelpolarität und Struktur der Porphyrine ein dem Energietransfer paralleler Elektronentransfer und ein Ladungsrücktransfer statt. Allerdings zerfällt der ladungsseparierte Zustand zu schnell, was eine praktische Nutzung der untersuchten Verbindungen in Solarzellen noch verhindert und ihre Weiterentwicklung erfordert.

Schlagwörter:
Artifizielle Photosynthese, organische Solarzelle, Energietransfer, Ladungstransfer

Contents

1 Introduction

One of the most visible colors on Earth is green, a color quite pleasant to our eyes. It originates from the chlorophylls, which nature evolved to capture sunlight — being the fundamental energy source for life on earth. The utilization of the energy of light starts with absorption of light quanta in the light harvesting complexes (LHCs) of plants, not considering its effect by trivial heating of any absorbing matter. Absorption is followed by directed energy transfer of the excitation to reaction centers (RCs), where multiple electron transfers separate charges for their further utilization in driving chemical reactions. The subsequent biochemical processes result in growth of biomass, which partly became fossil fuels in the past. Since production of fossil fuels is a very slow process and mankind is consuming more and more energy, the resources of fossil fuels are running out.

Many concepts are used and discussed nowadays to substitute fossil fuels as the main source of energy for mankind. The two main alternatives are nuclear power technologies and regenerative energy technologies. The latter subdivide into numerous different approaches. One approach is solar energy conversion by mimicking the primary steps of photosynthesis. Since an important amount of consumed energy is required as electricity, artificial photosynthesis aims at direct usage of the separated charges. For achieving this, different tasks have to be addressed. See figure 1.1 for a schematic drawing of an artificial light conversion system. *Firstly*, the incoming photons need to be absorbed by a light harvesting network and to be funneled into the *second* stage, the charge separation unit (CSU). In a *third* step, the charges need to be transferred into electrodes, from where they can start flowing as an electrical current. Finally, all parts have to be held together at the right distances by some material. This thesis will deal with the first two steps only, light harvesting and charge separation (CS). Difficulties that so far arose for the optimal realization of both tasks originate from unwanted dissipation of energy into heat, fluorescence, and population of long living

triplet states not being involved in energy or charge transfer. Furthermore, the charge transfer efficiency is often decreased by charge back transfer. To put artificial organic light converters into practical application, the main goal is to fine-tune electrochemical, photophysical and geometrical properties of the used compounds.

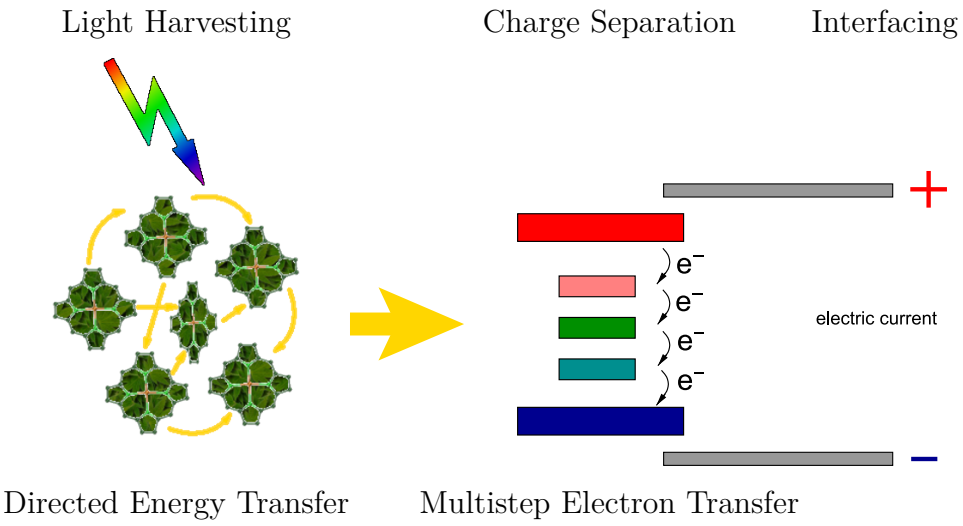

Figure 1.1: Scheme of an artificial organic light converter mimicking the initial steps of photosynthesis. Light gets absorbed by the chromophores of the LHC. Directed energy transfer delivers the excitation between several chromophores and funnels it finally into the charge separation unit. Here, a multistep electron transfer cascade producing separated charges is shown. The generated charges have to be drained by an interface.

It is the aim of this thesis to contribute to the understanding of artificial systems designed to model the primary steps of photosynthesis. A new concept of creating porphyrin-phthalocyanine-porphyrin (P-Pc-P) heteromers was realized by Ng et al. (Li and Ng, 2000). The synthesized compounds were designed to exhibit energy and charge transfer within the same molecule. It was the goal of this work to characterize the interactions of the chromophores, and to proof if the new simplified synthesis strategy is a promising route to create materials combining light harvesting and charge separation properties, as expected. To be able to observe the expected ultrafast decay of fluorescence emission and changes of absorption, techniques of ultrafast spectroscopy had to be established, therefore. Furthermore, it turned out

that the obtained data could analyzed in a meaningful manner only by applying global data fitting. As part of this work the necessary software was developed.

The thesis is organized as follows: Chapter 1 introduces the concept of artificial organic light converters and summarizes the tools to investigate the properties of such compounds. Chapter 2 leads to an understanding of methods of ultrafast optical spectroscopy, which were used in this study. During this PhD work two setups were built to establish ultrafast spectroscopy in the photobiophysics workgroup of Prof. Röder. The setup for fluorescence up-conversion in the femtosecond time domain was built during a diploma work (Werncke, 2005) under supervision of the author, and the setup for the measurement of transient absorption spectra in the femtosecond time domain by the author himself, supported by a diploma student (Völker, 2003). Chapter 3 describes the transient absorption setup in detail.

To gather and extract information from a combination of methods used to investigate complex molecular systems, global data analysis is a necessary tool. Its basics and implementation are subject of chapter 4. Used materials and methods are described in chapter 5. The novel class of P-Pc-heteromers is introduced in chapter 6. The obtained results are presented and discussed here as well. Chapter 7 is summarizing the whole work, discusses the relation to other scientific work, and formulates tasks for future work.

1.1 Artificial Organic Light Converters

Based on the more and more accepted fact that mankind needs a sustainable source of energy, which is not polluting the environment, the use of organic, bio-compatible and easy-to-produce materials seems favorable. The idea of just copying the charge separation unit from plants sounds promising and has been a research objective for many decades. Indeed, it is believed and expected that devices, based on nature's realization of energy conversion will have higher efficiencies than inorganic solar cells and will require less energy during production. (Barbour et al., 2007)

Reviewing the development of organic photovoltaics one can not ignore the roots of photovoltaics in general, which were of inorganic origin. It was E. Becquerel discovering the photoelectric effect for the first time in 1839 (Becquerel, 1839). Later, in 1876 W. Adams and R. Day recognized that selenium, being illuminated, produces an electrical current (Adams and Day, 1876). Using thin layers of selenium and gold, in 1883 Fritts developed the ancestor of todays inorganic solar cells (Fritts, 1883). Shortly after the photoelectric effect was discovered an enhancement of that process by organic dyes was observed by Moser, which he designated as "optical sensibilization" (Moser, 1887). However, all these devices were too inefficient to produce power in an usable amount and the selenium cell was used as a light sensor only. In 1911 W. Ostwald was writing about a hypothetical "photo-electrical element constructed suitably to convert the radiation of sun directly into electrical energy." He states, "Having this machine built, industry and transportation could do everything with this electricity what currently is based on hard coal." These ideas were presented in the framework of explaining the carbon cycle between plants and animals and the role of sunlight to drive the "Mill of Live" (Ostwald, 1911). However, the development of inorganic solar cells was so far of greater success than mimicking photosynthesis for electrical power production until now. Already in 1954 an inorganic solar cell with a conversion efficiency of about 6 % was presented (Chapin et al., 1954). In 1958 the photoelectric effect could also be shown by using organic substances as tetramethyl p-phenylenediamine and magnesium phthalocyanine (Kearns

and Calvin, 1958). At this time the details of photosynthesis were still unknown and under investigation (Bradley and Calvin, 1955). Nevertheless, people were inspired by the natural way of converting sunlight into chemical energy and tried to mimic photosynthesis for electrical power generation by artificial organic molecules. Porter (1978) stated in his Bakerian lecture in 1977 that "It is not impossible that, by putting together these separate parts, a much simplified *in vitro* system may be synthesized which is nevertheless capable of carrying out the essential parts of the photosynthetic process and perhaps one which is more suited to some of Man's needs."

Thus, at least three different branches of solar light to charge separation techniques have been developed over time. Two of them are very closely related to the photoelectric effect, namely the inorganic and the organic solar cells. The third branch, artificial photosynthesis, had its starting point in understanding the primary processes of photosynthesis. Soon after knowing the ingredients of the photosynthetic light harvesting complexes and the reaction center, researches tried to mimic it by synthesizing similar organic compounds. Also, the supra-molecular systems investigated in this thesis were synthesized in the realm of this branch. Therefore, this overview will start about "mimicking the early steps of natural photosynthesis". However, to use artificial photosynthetic model systems for the generation of electricity, they have to be embedded in structures which are in common with organic photovoltaic (OPV) cells, here two of the branches join again. Furthermore, there was also a tremendous development in the field of dye sensitized organic solar cells (DSSCs). DSSCs are in-between organic and inorganic solar cells. Like in photosynthesis, electron transfer plays an important role for DSSCs and energy transfer may enhance their conversion efficiency. Therefore, they also need to be discussed in this context.

In 1818 Pelletier and Caventou (1818) isolated the compound giving leafs the green color and named it "Chlorophyle". Since about 1900 quantitative research was investigating the dependence of photosynthesis in leafs on incident light (Brown and Escombe, 1905; Emerson and Arnold, 1932b,a). The exploration of the molecular assembly involved in photosynthesis started with the studies of Willstätter and Fischer who discovered the chemical structure

of chlorophylls (Willstätter and Stoll, 1913; Fischer, 1920). Many years later, in 1984, Michel, Deisenhofer and Huber firstly resolved a detailed crystal structure of a reaction center complex (Deisenhofer et al., 1984). Nowadays, structures of different LHCs and RCs are available and allow a reasonable understanding of the photosynthesis in many of its steps (Hohmann-Marriott and Blankenship, 2011; Pan et al., 2011; Umena et al., 2011; Guskov et al., 2009; Deisenhofer et al., 1995). All results of these enormous efforts show that the natural paragons, the light harvesting complexes and reaction centers, are large proteins in which chlorophylls, quinones, caretenoids and metal centers are embedded.

In addition to the elucidation of nature's structural realization of energy conversion, many theories had to be developed to understand the occurring physico-chemical processes. In particular, the theory of radiation-less energy transfer and the theory of electron transfer were milestones permitting a deeper understanding of the processes underlying photosynthesis. Förster started the development of the theoretical framework of energy transfer (Förster, 1948, 1949b). His successful theory was later extended by Dexter (Dexter, 1953) and many others. Recent publications summarize the history, expand the theory, and give perspectives for the future (Olaya-Castro and Scholes, 2011; Megow et al., 2011). Marcus, Hush and Jortner were the founders of the electron transfer theory (Marcus, 1956, 1965; Marcus and Sutin, 1985; Marcus, 1993; Hush, 1961; Jortner, 1976). This theory elucidates the kinetics of electron transfer and the principles of having a much lower electron transfer probability for backward than for forward transfer. The energetics of electron transfer is described by a theoretical approach named "Rehm-Weller equation" (Rehm and Weller, 1969).

One may trace back the genealogy of artificial photosynthesis to the time of 1944 when O. Warburg discovered the change of quinone's redox state under illumination when mixed with suspensions of green algae (Warburg, 1946). Interestingly, it was not known at this time that also quinones play a role as electron acceptors intrinsically in photosynthesis. Later Tollin et al. (Harbour and Tollin, 1972) demonstrated that charge transfer occurs in chlorophyll-quinone solutions. In a next step, Kong and Loach (Kong and

Loach, 1978) bound a quinone covalently to a porphyrin (P) for the first time, see figure 1.2. The distance of electron donor and acceptor was now constrained by a so called "linker". This was a crucial step to investigate the charge transfer undisturbed by diffusion of the two moieties.

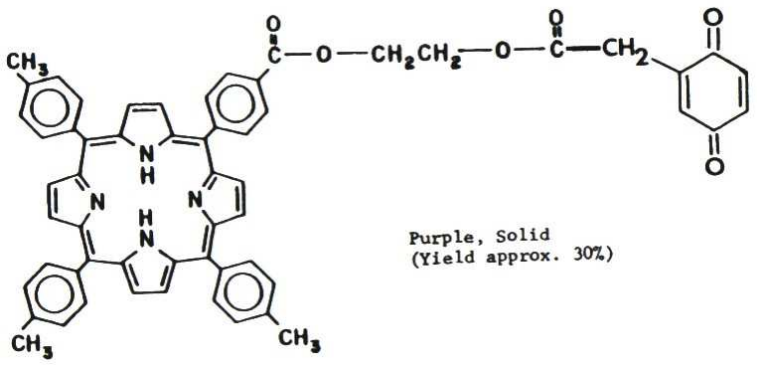

Figure 1.2: Chemical structure of the first synthetic compound modeling photosynthesis, the P-quinone-dyade by Loach and coworkers (Kong and Loach, 1978).

Others followed this approach establishing similar syntheses (Dalton and Milgrom, 1979; Tabushi et al., 1979). In 1982, Lindsey and Mauzerall (1982) and later Staab et al. (Weiser and Staab, 1984) followed the insight that only predictable distances between electron donor and acceptor allow a distance-dependent quantification of charge transfer kinetics. Having systems with rigid geometry, the electron transfer theory was investigated and in 1984 the group of Closs et al. (Miller et al., 1984) verified the prediction of the inverted region of the Marcus theory.

In the early times of mimicking photosynthesis, the major approach of design was covalent coupling of compounds that had been identified to be part of the natural systems. A number of systems, called dyads, consisting of an electron donor and one acceptor, were synthesized. With better understanding of electron and energy transfer and getting more insight into the native structure, it became clear that simple dyads will not be able to realize the dream of artificial photosynthetic reaction centers. Ionic and hydrophobic interaction sites were introduced to imitate the situation within

the natural occurring RC, and more and more complex systems (Wasielewski, 1992) were developed. The dyads were followed by triads (Johnson et al., 1993), tetrads (Wiehe et al., 2001a) and even pentads (Gust et al., 1993). By replacing chlorophylls and quinones with Ps, phthalocyanines (Pcs) and fullerenes[1] the systems became chemically more stable and the synthesis easier. As a consequence, a large number of derivatives could be synthesized to study the effects of orientation, distance (Harriman et al., 2009), solvents (Heitele et al., 1989), and ligands (Imahori et al., 2002) on electron transfer.

Two main strategies were followed for designing and studying artificial photosynthetic systems, in the early seventies of the 20th century. Both were devoted to light harvesting followed by electron transfer, they only differed slightly in their molecular engineering. (Tran-Thi, 1997) Whereas the first route uses linearly arranged electron donors (i.e. Ps), the second approach rather exploits the properties of the special pair, by co-facial arranging of the Ps or similar extended π-systems. Both routes used quinone or methylviologen as an electron acceptor in the beginning. While searching for more optimal systems, both, electron donors and electron acceptors, were later replaced by molecules exhibiting similar redox- and photo-physical properties. Since a tremendous number of different systems and arrangements was synthesized, only some examples will be mentioned. These include P-quinone (Wasielewski, 1992), P-fullerene (Guldi, 2002; Kim et al., 2004), Pc-quinone (Gouloumis et al., 2006), Pc-fullerene (El-Khouly et al., 2004, 2007; Martin-Gomis et al., 2007), subPc[2]-fullerene (El-Khouly et al., 2008, 2010), subPc-P (Xu et al., 2010), and boron bipyrromethene-P-fullerene (Liu et al., 2011) systems. Also chlorophylls, carotenes, perylens, viologens and ferrocene were used as electron donors or acceptors.

Over the time it became apparent that the most promising substances for artificial systems are fullerenes, Ps, and Pcs. Therefore, newly synthesized model systems are mainly build of these compounds. In this thesis two supra-molecules from the class of P-Pc systems were investigated. This class is introduced in chapter 6 in detail.

[1]Fullerenes are introduced in Kroto et al. (1985) and Taylor and Walton (1993).
[2]SubPcs are introduced in Claessens et al. (2002).

Today, artificial systems with long-living charge-separated states exist (Harriman, 2004; Ohkubo et al., 2004; El-Khouly et al., 2010; Liu et al., 2011), but other challenges became evident. It is not only a long-living charge separated state which makes a molecul an useful source of electrical energy. In order to use the material under real-life conditions, many more issues need to be solved. This includes an efficient channeling of the charges away from the organic material. Furthermore, the organic compounds must be long-time-stable, or alternatively, there has to be an affordable mechanism to refresh them. In addition, the production of the organic material and the whole conversion system must be compatible with mass production. Given the huge efforts needed to synthesize only a few milligrams of promising molecules acting as artificial photosynthetic reaction centers up to now, many chemists are working on simpler synthesis protocols.

Closely related to the strategy of mimicking the light harvesting and charge separation of photosynthesis are organic solar cells[3]. There are two main streams of solar cells utilizing organic compounds: OPV cells and DSSCs (Bauer et al., 2011). The OPV cells are organic counterparts of conventional inorganic solar cells, whereas, strictly speaking, DSSCs are systems using charge transfer from an organic dye to the inorganic semiconductor titanium dioxide (TiO_2).

OPV cells consist of a conductive and light transparent cathode, typically indium-doped tin oxide (ITO), a layer of two blended organic compounds acting as electron donor and acceptor and an aluminum anode. This structure is deposited on glass or on a polymer. The report of Tang in 1986 about a Cu-Pc and perylene derivative based cell is the starting point of the expanding investigation of OPV cells (Tang, 1986). Modern approaches to this concept include structuring the organic compounds (Hirade et al., 2011) and the use of very new materials such as graphene (Wan et al., 2011). A recent overview about OPV cells can be found in in the review of Brabec et al. (2010) and in Lin et al. (2011a).

Although OPV cells reached a higher conversion efficiency in the beginning, their development stagnated in terms of conversion efficiency for a long

[3]The boundaries even become blurred more and more as concepts are mixed.

time. Already in 1991, which is seen as the birth year of usable DSSCs, the first efficient DSSC had a conversion efficiency comparable to the best OPV cell currently available (O'Regan and Grätzel, 1991; Lin et al., 2011a). The DSSC is also known as "Grätzel cell", named after Michael Grätzel, who was awarded with "The 2010 Millennium Technology Grand Prize" for his invention (Meyer, 2010).

Just like OPV cells, DSSCs are made from a conductive and transparent electrode deposited on glass or polymer, typically ITO. The next layer are TiO_2-semiconductor-nanoparticles doped with a dye sintered onto the transparent electrode. The circuit is closed by a redox electrolyte (mostly I_3^-/I^-) used to deliver the electrons from the platinum counter-electrode to the dye. Up to now the most successful sensitization is achieved by dyes, based on ruthenium complexes which were used from the early times on (Grätzel, 2009; Kalyanasundaram et al., 2011).

However, there is ongoing research to substitute the ingredients of the DSSCs by compounds which are cheaper, easier to handle, long-term-stable, and not as rare as ruthenium. Of course promising candidates for sensitizing dyes are seen in those compounds which were already identified as good candidates for artificial photosynthetic models. Therefore, DSSCs, sensitized with different Ps, were characterized (Lee et al., 2010; Brumbach et al., 2009; Bessho et al., 2010; Chang et al., 2011; Imahori et al., 2009; Wang et al., 2005). Furthermore, covalently coupled pairs of Ps were tested (Mai et al., 2010). Also, theoretical approaches were used to screen for the best sensitizer (Ma et al., 2010). Naturally occurring large π-systems like chlorophyll *a* and pheophorbide *a* (Pheo) were checked for their ability to serve as sensitizer as well (Koyama et al., 2009). Surely, various Pcs were investigated as sensitizing dye (Zanotti et al., 2011, 2010; An et al., 2010; Rawling et al., 2009; Cid et al., 2009; Eu et al., 2008). A recent review (Martinez-Diaz et al., 2011) summarizes the efforts made with Pcs. Due to their high extinction coefficients and good tuneability quantum dots were also tested as sensitizer (Rühle et al., 2010).

Despite optimizing the DSSCs by exchanging materials by new ones, there are also approaches to modify the design of the cell in general. One of

these approaches is co-sensitization. Inspired by the LHCs, chlorophyll *a* was chosen as co-sensitizer by Wang et al. (2009, 2010b,c). Another kind of light harvesting is presented by Marek et al. (2011): zinc-P aggregates mimicking chlorosomes are proposed to extend the overall absorption band of OPV cells or DSSCs. Zeolite L nanorods filled with organic dyes acting as light harvesters share the same approach of making more energy of the incident light available for conversion (Ince et al., 2011; Calzaferri, 2010; Calzaferri et al., 2002).

Inspired by nature as well is the approach of Takechi et al. (2010) to introduce another sensitizer at the cathode, realizing a kind of Z-scheme of energy levels. In addition, surface plasmon resonance of silver nanoparticles could improve the conversion efficiency by about 25 % by enhancing the absorption (Jeong et al., 2011).

The work of Chang et al. (2011) raises the hope that already established model systems can be used as sensitizers for DSSCs. His group successfully used a covalently linked supra-molecule with carbazole as an electron donor and a cyanoacrylic acid as acceptor.

Not only the sensitizing dye is a topic of research, also the electrodes and the redox electrolyte are on focus for improvement to reach the goal of an all solid state DSSC with a high performance. Efforts to increase the electron mobility and the light scattering of the anode by 3D structuring could increase the open circuit voltage by 110 mV (Tetreault et al., 2011). Using mesoporous TiO_2 beads instead of standard TiO_2 for photocatalysis pushed the conversion efficiency above 10 % (Sauvage et al., 2010). The expensive platinum counter electrode could already be substituted by cobalt sulfide (CoS). The conversion efficiency of DSSCs with CoS has still a reasonable value of 6.5 % (Lin et al., 2011b; Wang et al., 2010a). Two new redox electrolytes were investigated recently, butyronitrile (Sauvage et al., 2011) and 5-mercapto-1-methyltetrazole (Wang et al., 2010a). Both showed acceptable conversion efficiencies of more than 6 %, and exhibited a couple of advantages, like less absorption and less corrosive effect to the electrodes compared to the common iodide electrolyte.

Reviews about all aspects of DSSCs are available in Hagfeldt et al. (2010);

Kalyanasundaram and Grätzel (2010); Grätzel (2007, 2003). The review of Clarke and Durrant (2010) is an excellent introduction and summary about the charge generation and transport in organic solar cells. The topic of electron transfer in DSSCs is addressed by the recent publication of Bauer et al. (2011). A recent review about "Energy Conversion in Natural and Artificial Photosynthesis" summarizes many aspects of the current state of the art (McConnell et al., 2010). This paper contains also a nice comparison of energy level diagrams for natural photosynthetic systems, artificial models, and the standard DSSC. The overall big goal is to come close to the proposed Shockley and Queisser conversion efficiency limit of 30 % (Shockley and Queisser, 1961; Snaith, 2010).

1.2 Requirements and Modern Strategies for the Design of Artificial Photosynthetic Units

Based on current understanding of the principles appearing in natural photosystem (PS) and the lessons learned from model systems, some general demands to artificial systems can be formulated.

a) Broadband absorption in the UV/VIS

Natural LHS contain a variety of pigments with different absorption spectra. The absorbing chromophores should cover the spectrum of sunlight as good as possible.

b) Efficient excitation transfer

In natural PS most of the absorbed photons lead to a charge separation. To realize high quantum yields in this sense, the excitation transfer rates need to be much higher than the sum of the dissipation rates.

c) Optimized number of antenna chromophores per CSU

Being idle, an efficient RC combined with efficient excitation transfer is wasteful. Therefore, the number of absorbing chromophores surrounding the CSU must be chosen in such a way that the charge separation chain is permanently active.

d) Stable and long-living CS state

Natural RCs separate charges within nanoseconds, while the separation lasts for some hundred microseconds. To achieve a high electron transfer quantum yield and allow the created charges to result in useful electrical work, the CS state lifetime should be as long as possible. A more than ten times slower back electron transfer rate compared to the CS rate is equally important.

e) Robustness against degradation

Degraded absorbing chromophores should change the efficiency not more than accounting for the missing absorption. Either an easy route to refresh degraded components should exist or the lifetime of the active material must ensure for a profitable runtime of the device.

f) Robustness against changing environmental conditions

External perturbations, such as changing temperature, should have only little effect on the overall efficiency and should furthermore not induce irreversible alterations.

To fulfill the requirements formulated above, a number of design principles and strategies were developed. Nowadays, the idea of a one-to-one copy of the elementary pieces of natural PS has nearly vanished. Instead of chlorophylls and quinones, more stable compounds are used. However, general observations like "Interestingly, it was found that antenna complexes display an amazing diversity in contrast to the reaction centers." (Blankenship, 2002) are still valid hints on how a successful artificial system could be created. The exploited natural systems also allow for defining ranges of suitable arrangements. Reviewing the available data, Noy et al. (2006) states that: "We find that the basic physics of the transfer processes, namely, the time constraints imposed by the rates of incoming photon flux and the various decay processes allow for a large degree of tolerance in the engineering parameters. Moreover, we find that the requirements to guarantee energy and electron transfer rates that yield high efficiency in natural photosystem are largely met by control of distance between chromophores and redox cofactors." These findings encourage and give hope that there are working configurations besides the ones

realized by evolution. Many chemists synthesized many compounds in the hope to find structures with such suitable properties. Over time, Ps, Pcs, and fullerens were established as very promising and stable building blocks for photoinduced CS systems.

In a couple of cases the linking was achieved by metal coordination, since "A simple but elegant way to obtain linked donor-acceptor entities involving metallomacrocycle complexes with fixed distance and orientation is the use of coordination of axial ligands to metallomacrocycle complexes." (Fukuzumi et al., 2009) Frequently silicon phthalocyanine (SiPc) was used a a coordination center owing to its useful qualities. "Among the reported phthalocyanines, the axially substituted silicon phthalocyanines have gained attention recently, because they are not able to aggregate in solution due to their special structural features; in addition they have longer fluorescence lifetimes than the more common zinc phthalocyanines." (El-Khouly et al., 2009)

To join the necessary educts, self assembly (Ermilov et al., 2011; Haycock et al., 2000), metal coordination (Harriman and Sauvage, 1996; Choi et al., 2004), and click chemistry (Kolb et al., 2001) are favored methods in order to keep reactions simple and cheap.

2 Fast and Ultrafast Optical Spectroscopy

Optical spectroscopy is the first choice if one wants to study inter- and intramolecular transfer processes like electron and energy transfer. Numerous spectroscopic methods have been developed up to now. A subgroup of them measures optical properties time-dependently. Initially based on human vision and sense, time-resolved techniques were slow in the beginning [Gen 1, 3–5]. Over the years, detectors with faster response times, and sources being able to emit short pulses of light were developed. Both tools, detectors and excitation sources need to be improved if one wants to examine faster and faster variations of optical properties. To follow the kinetics, the initial perturbation (excitation) needs to be much shorter than the transition itself[1].

Whereas in the beginning of photosynthesis research (Brown and Escombe, 1905), mechanical shutters, driven by a water turbine, flashed sunlight, already in 1932 the light pulses were produced by electric discharging flash lamps (Emerson and Arnold, 1932a). The induced processes were not yet monitored spectroscopically, but chemically, in these experiments, however. Nevertheless, an important consideration used in ultrafast spectroscopy was already utilized: even very slow but integrating detectors may be used in conjunction with time gating to gain a higher time resolution than the detector allows for. If the monitored process can be initiated periodically, this increases the sensitivity manyfold, furthermore.

Shortly later, time-resolved recordings of photoinduced reaction kinetics were performed by means of measuring changes in optical absorption of the reaction partners. This technique was developed further by Norrish and Porter (1949) (Thrush, 2003) and was termed “flash photolysis”. Their apparatus, which used flash lamps, was the ancestor of modern transient absorption spectrometers using sophisticated femtosecond laser systems. That time, it allowed to explore faster reactions in more detail, than before. The

[1]There may be cases were the system can be investigated succesfully at different stationary points.

development of short and ultrashort pulsed lasers pushed the resolution limit to faster and faster kinetics. These efforts led to the nobel price to A. Zewail fifty years after Norrish's and Porter's paper. He received the nobel prize "for his studies of the transition states of chemical reactions using femtosecond spectroscopy" (Nobel Prize).

Time resolved spectroscopy can be performed in the frequency or in the time domain. There is a long and ongoing struggle of which is the superior method. The most positive result of this competition is the continuous development of both strategies. In this study, only methods following the time domain approach are used and described below.

A common (but physically unprecise) classification divides time-resolved spectroscopic methods in fast and ultrafast ones. The "fast" methods often utilize detectors with a fast time response (raftly $<$500 ps), whereas the "ultrafast" methods are solely based on time gating of the measured signal and slow integrating detectors. From a technical point of view, the limit is set by the time response of the fastest detectors available, which is in the range of some tens of picoseconds. One could argue that being able to perform experiments with "ultrafast" time resolution, the "fast" methods become obsolete. However, technical reasons grant the old "fast" methods their rights if one has to measure slower processes.

The time resolution of "ultrafast" methods is no longer determined by the response of the detector, but by the gate in front of it. Ultrafast spectroscopy uses femtosecond pulses to perturb and probe samples in the time domain. If absorption is measured, the limited duration of the probe pulse acts as a gate itself. In case of probing emission, ultrafast gating is achived by processes like sum frequency generation (SFG) or the optical Kerr effect (OKE).

2.1 Fundamentals

Optical Spectroscopy

Electromagnetic waves do not only transport energy, but also carry detailed information about their origin and previous interaction with matter. The recognition of this fact led to the development of modern spectroscopy (Kirch-

hoff and Bunsen, 1860). Later, the development of the quantum theory of light by Einstein (1905) and that of the quantitative photochemistry by Warburg (1924) were some of the milestones on the way to ultrafast optical spectroscopy which is nowadays available to investigate physico-chemical processes of different nature.

The main actors involved in energy and electron transfer within photosynthesis are chromophores absorbing and possibly fluorescing in the ultraviolet to near infrared wavelength range. Commonly, the essential states and transitions of a chromophore are depicted in a simplified Jabłonski diagram as shown in figure 2.1.

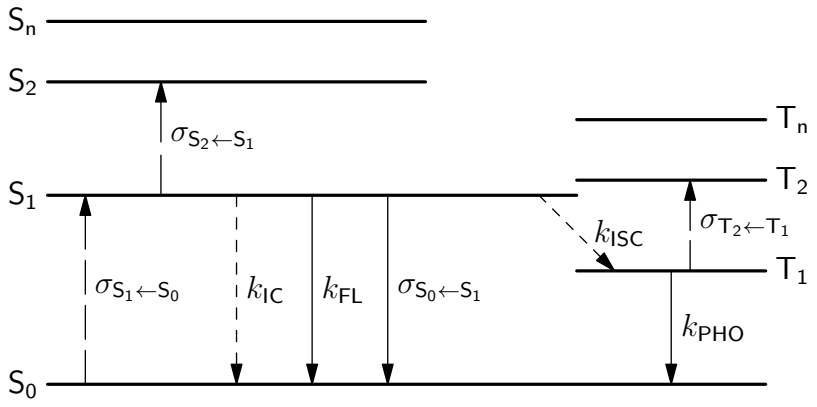

Figure 2.1: Jabłonski diagram depicting the electronic energy states (S_0, S_1, S_2, S_n, T_1, T_2, T_n) of a molecule and the transitions between them. $\sigma_{S_1 \leftarrow S_0}$: absorption cross section, k_{FL}: fluorescence rate constant, k_{IC}: internal conversion rate constant, k_{ISC}: intersystem crossing rate constant, k_{PHO}: phosphorescence rate constant, $\sigma_{S_2 \leftarrow S_1}$: induced absorption cross section, $\sigma_{S_0 \leftarrow S_1}$: stimulated emission cross section, $\sigma_{T_2 \leftarrow T_1}$: induced triplet absorption cross section. See text for further details.

The electronic ground state of most molecules is the singlet state S_0. By absorbing a photon, they can be excited into the first excited singlet state S_1. Once being in this state, a molecule can follow two pathways by further stimulation of a second photon, and three spontaneous pathways, leading to the depopulation of the first excited singlet state. Residing in the first excited singlet state, the molecule may absorb a second photon of proper energy and reach the second excited singlet state S_2 or a singlet state of even

higher energy denoted by S_n. Another fundamental transition starting from the S_1 state is stimulated emission, whereby an incoming photon stimulates the emission of another one exhibiting the same energy, phase and direction (Einstein, 1916; Dirac, 1926, 1927), see figure 2.2.

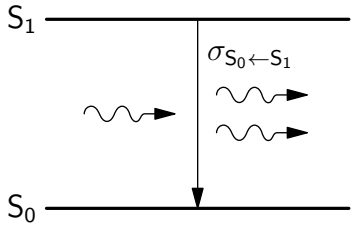

Figure 2.2: Jabłonski diagram showing the process of stimulated emission. The interaction of a photon with an excited molecule stimulates the emission of a second photon, thereafter two photons with identical phase, direction and energy exist.

The best observable spontaneous depopulation process of the S_1 state is fluorescence, whereby one photon is emitted while passing back to the S_0 state. Furthermore, a molecule can dissipate excited state energy radiationless into the surrounding environment, for instance, into a liquid solvent by internal conversion (IC). A third possible transit is intersystem crossing (ISC) which brings the molecule into the first excited triplet state T_1. For this, the spin configuration must change. ISC is a strongly forbidden process, unless a considerable amount of spin-orbit or spin-spin coupling exists (Turro et al., 2009; Marian, 2012). The transition from the T_1 state to the singlet ground state involves spin flipping again, therefore the triplet state is a long-living state and its lifetime is typically on the order of microseconds or longer. In case of being radiative, this process is called phosphorescence. Due to the long lifetime of the T_1 state, a molecule may absorb a second photon while being in this state and reach the second excited triplet state T_2 or a triplet state of higher energy denoted by T_n.

In addition to these elementary transitions, energy and electron transfer processes play an important role in photosynthesis. In terms of optical spectroscopy, they show up with specific patterns. Both processes occur between at least two interacting molecules, commonly known as donor and acceptor.

In the case of "energy transfer" the energy stored in the excited state of the donor molecule is transferred to the acceptor, whereas a transfer of a net charge (i.e. an electron) takes places in case of "electron transfer".

2.2 Tracing the Excited States

By tracing the population of the first excited singlet states of a photosynthetic model system, one can measure transfer rates of energy and electron transfer. Two elementary processes allow to determine the population density of the excited state, fluorescence and excited state absorption.

The majority of chromophores related to artificial photosynthesis research exhibit fluorescence from the first excited singlet state with a reasonable large rate constant. Detecting this emission is the method of choice due to its sensitivity compared with measuring the induced absorption.

Typical life times of the first excited state of Ps and Pcs range from one to ten nanoseconds. If additional energy or electron transfer processes depopulate the excited state, its life time can become even shorter than ten picoseconds. Applicable methods to measure the fluorescence in a time-resolved manner, and in the appropriate time ranges, are time-correlated single photon counting (TCSPC) and fluorescence up-conversion with femtosecond time resolution (fsUPC).

The number of emitted photons γ per time interval $\mathrm{d}t$ is directly proportional to the rate constant of fluorescence k_{fl} and to the excited state concentration $c^*(t)$, as expressed by the rate equation:

$$\frac{\mathrm{d}}{\mathrm{d}t}\, c^*(t) = -\underbrace{k_{\mathrm{fl}} \cdot c^*(t)}_{=\gamma} - (k_{\mathrm{IC}} + k_{\mathrm{ISC}}) \cdot c^*(t)$$

The largest signal measured by TCSPC and fsUPC is proportional to $k_{\mathrm{fl}} \cdot c_0^*(t)$, with c_0^* being the concentration of excited states directly after excitation, favouring the detection of photons in case of strong depopulation channels. This is in contrast to steady state detection where only the total number of emitted photons is recorded. This number is getting very small when strong depopulation channels exits, even if the product $k_{\mathrm{fl}} \cdot c_0^*(t)$ stays the same.

Fluorescence Up-Conversion

If the emitted fluorescence of a sample vanishes faster than within ten picoseconds then the method of TCSPC is not suitable anymore to record the decay, since the resolution limits of detectors and electronics are reached. The idea of fluorescence up-conversion is to use the nonlinear effect of sum frequency generation (SFG) as an ultrafast gate in front of the detector. This gating, as fast as the laser pulses are short, makes this method even faster than TCSPC.

The operation scheme is as follows: the sample is excited by an ultrashort pulse. A well defined time later the gate pulse enables SFG of the samples fluorescence with the gate pulse. SFG takes place for the short duration of the gate pulse only. By varying the delay between excitation and the gate pulse and recording the sum frequency signal, the decay of the fluorescence is sampled.

Light-matter interaction induces a polarization of the material, being a source of new radiation. The electric polarization P of a material induced by an electrical field E can be described by the Taylor series:

$$P = \varepsilon_0 \sum_n \chi^{(n)} E^n.$$

In nonlinear optical materials the optical susceptibility $\chi^{(n)}$ has non-zero higher orders. These may lead to measurable new generated frequencies if the photon flux density and the materials coupling coefficients (like $\chi^{(2)}$ for SFG) are large enough. The sum of the nonlinear terms, i.e. having an order higher than one, is called P^{NL}. Using it, the wave equation for nonlinear optical materials can be written as:

$$\nabla^2 E - \frac{n^2}{c_0^2}\frac{\partial^2}{\partial t^2} E = \frac{1}{\epsilon_0\, c_0^2}\frac{\partial^2}{\partial t^2} P^{\mathrm{NL}}$$

Thus the nonlinear polarization can be understood as a driving force of the electrical field. The electrical field of two collinear light beams of fre-

quency ω_1 and ω_2, with the corresponding wave vectors $\vec{k}_1$ and $\vec{k}_2$, reads:

$$E(\vec{x},t) = E_1\,\mathrm{e}^{i(\omega_1\,t-\vec{k}_1\cdot\vec{x})} + E_2\,\mathrm{e}^{i(\omega_2\,t-\vec{k}_2\cdot\vec{x})} + \text{c.c.}$$

In a nonlinear material these two beams induce a polarization[2] which is proportional to $E_1\,E_2\,\mathrm{e}^{i(\omega_3\,t-\vec{k}_3\cdot\vec{x})}$. This term is describing the SFG. The emitted intensity of the sum frequency field is directly proportional to the product of the incident beam intensities, $I_3 \propto I_1 \cdot I_2$, which is one requirement to use this effect as an ultrafast linear gate. The rays interfere constructively only if the phases of the waves fulfill a condition, known as the phase matching condition $\vec{k}_3 = \vec{k}_1 + \vec{k}_2$ or rewritten using the refractive index of the material $\omega_3\,n(\omega_3) = \omega_1\,n(\omega_1) + \omega_2\,n(\omega_2)$. To fulfill the phase matching condition one needs to use birefringent materials, where the refractive index can be tuned by crystal orientation according to the polarization of the beams.

2.3 Detecting the Dark States

Charge separated states and triplet states exhibit only very weak or no emission at all in most cases. For that reason they are called "dark states". To monitor their population density, one can measure the time dependent absorption by means of Transient Absorption Spectroscopy (TAS).

The major interest of detecting "dark states" in case of investigating the energy and charge transfer of P-Pc-triads lies in the detection of the charge separated state and in measuring the refilling of the singlet ground state. Triplet state population is not of interest, since energy and electron transfer mostly depopulate the singlet states very fast, so that the triplet states are populated only in a negligible manner.

Transient Absorption Spectroscopy

Transient absorption spectroscopy measures the absorptive properties of a sample in a time-resolved manner. The method follows a classical pump-probe scheme. Initially ($t = t_0$), the sample is brought into a non-equilibrium

[2]Note, there are other terms as well.

state, often by means of a short and strong optical pulse (pump pulse). Hereby the population density of the energy levels is altered. Typically, the ground state is depopulated and higher excited states get populated. Shortly after ($t = t_0 + \Delta t_n$), the absorption of the sample is recorded during a short period for many delay times Δt_n. The measurement at one delay time may be repeated to improve the signal to noise ratio. The series of measurements for all delay times reveals then the kinetics of relaxation processes like internal conversion, fluorescence, energy and electron transfer, charge recombination and others. Depending on the duration of the light pulses used for measuring the absorption (probe pulses), different time domains of the kinetics can be accessed.

Under certain assumptions, light attenuation by matter follows the Beer-Lambert-Bouguer law (McNaught et al., 1997). The light intensity I behind the sample depends on the incident light intensity I_0. The alteration of I_0 by absorption depends on the wavelength dependent optical density $OD(\lambda)$.

$$I(\lambda) = I_0 \cdot 10^{-OD(\lambda)}$$

The optical density is directly proportional to the product of the molar extinction coefficient (ε) (an intrinsic property of the sample), the concentration (c) of the sample, and the optical pathway l through the sample.

$$OD(\lambda) = \varepsilon(\lambda) \cdot c \cdot l$$

Dealing with different contributions[3] to the optical density, the formula is usually rewritten to a form containing the molecular cross section σ, and the molecule density n.

$$OD(\lambda) = \sigma(\lambda) \cdot n \cdot l \cdot \ln 10$$

In contrast to steady state absorption spectroscopy, the first excited singlet state gets substantially populated during application of the pump pulse. Therefore, the probe pulse may lead to transitions from the first ex-

[3]Notably, there is no established terminology about a stimulated emission counterpart of the molecular absorption coefficient. Therefore, the terms of stimulated emission are usually introduced late into the formulas.

cited singlet state into higher excited states or may cause stimulated emission, as well.

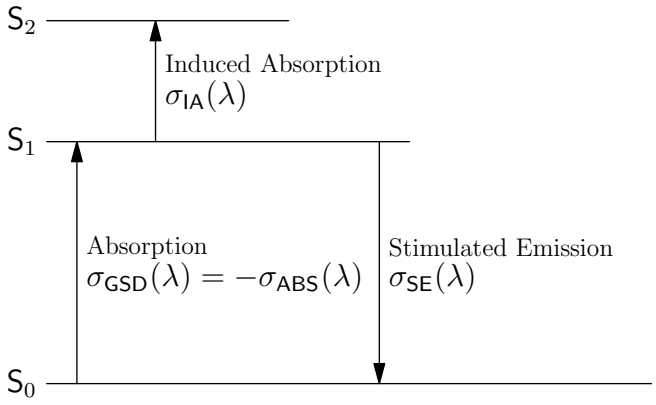

Figure 2.3: Energy level system of three singlet states, S_0 the ground state, S_1 the first and S_2 the second excited state. The three most prominent contributions to the transient absorption signal are shown, namely ground state depletion caused by absorption, induced absorption, and stimulated emission.

Hence, the wavelength-dependent optical cross section σ has at least three components, depicted in figure 2.3, absorption from the ground state, absorption from the first excited state, and stimulated emission from the first excited state. For various reasons it is helpful to relate the optical density after excitation to the optical density of the unexcited sample. By subtracting the equilibrium ground state absorption $OD^o(\lambda) = OD(\lambda, t < t_0)$ one gets

$$\Delta OD(\lambda, \Delta t_n) = OD(\lambda, t_0 + \Delta t_n) - OD^o(\lambda).$$

This so called "delta OD"-signal $\Delta OD(\lambda, \Delta t_n)$ is a superposition of three time- and wavelength-dependent fractions generated by the pump and the test pulse: ground state depletion (GSD), induced absorption (IA) and stimulated emission (SE)

$$\Delta OD(\lambda, \Delta t_n) = l \cdot \ln 10 \cdot \Big(\begin{array}{lll} n_{\mathrm{GSD}}(\Delta t_n) & \sigma_{\mathrm{GSD}}(\lambda) & + \\ n_{\mathrm{IA}}(\Delta t_n) & \sigma_{\mathrm{IA}}(\lambda) & + \\ n_{\mathrm{SE}}(\Delta t_n) & \sigma_{\mathrm{SE}}(\lambda) & \end{array} \Big).$$

Each of these components features a time-dependent molecule density $n(\Delta t_n)$ and a static wavelength-dependent pattern or spectrum[4] $\sigma(\lambda)$. It is the scope of data analysis to unravel this linear combination into separated traces. One can use the following a priori information and properties of the three contributions to aid the complex mathematical problem:

Ground State Depletion: Its spectral pattern $\sigma_{\mathrm{GSD}}(\lambda)$ is identical to the steady state absorption spectrum $\sigma_{\mathrm{ABS}}(\lambda)$, since the signal originates from all molecules not being in the ground state and, therefore, being unable to absorb like unexcited molecules. It follows from the definition of ΔOD that n_{GSD} becomes negative (expressing molecules missing from the pool of those being in the unperturbated ground state) and decays to zero at infinite long times, if the sample is not transformed or destructed by photochemical reactions.

Stimulated Emission: Its pattern $\sigma_{\mathrm{SE}}(\lambda)$ can be calculated from the spontaneous steady state fluorescence spectrum $\sigma_{\mathrm{FLU}}(\lambda)$ with the relation describing the coupling of the Einstein coefficients

$$B_{21} = \frac{\lambda^3}{8\pi\, h} A_{21}.$$

Stimulated emission generates photons, expressed by a negative value of $n_{\mathrm{SE}}(\Delta t_n)$, which follows the kinetics of the excited states. In most cases the prominent source of stimulated emission is the first excited singlet state.

Induced Absorption: It originates from transitions between transiently populated levels (like the first excited singlet state) and higher levels. Therefore, the spectrum of this fraction is unknown a priori and accessible only by TAS. It may be a complex superposition of more than one possible transition. Each of these transitions may exibit different kinetics, resulting in an individual term $n^i_{\mathrm{IA}}(\Delta t_n)\,\sigma^i_{\mathrm{IA}}(\lambda)$. Also transiently occuring ionic forms of the sample can lead to new absorption bands which can be categorized as an induced absorption.

[4]Cross sections are usually defined as non negative numbers.

Despite the theoretical feasibilty to calculate absorption spectra from the molecular structure, accurate and reliable values are not available from all theortical methods known, yet. Therefore, the cross sections and the relative distances of the energy levels are solely based on experimential results. Nevertheless, as a rule of thumb, induced absorption spectra are quite unstructured and have a wide bandwidth compared to the ground state spectra.

Experimentially, the optical density of the sample is calculated from the light intensities of the probe beam measured before (I_0) and after (I) passing the sample.

$$OD(\lambda) = \log\left(\frac{I_0(\lambda)}{I(\lambda)}\right)$$

To aquire the ΔOD-signal, the optical density has to be recorded after the delay Δt_n following perturbation by the pump pulse, too. This obtained data is indicated by *.

$$OD^*(\lambda, t_0 + \Delta t_n) = \log\left(\frac{I_0^*(\lambda, t_0 + \Delta t_n)}{I^*(\lambda, t_0 + \Delta t_n)}\right) \quad \text{sample excited at } t = t_0$$

In the time range of pico- and femtoseconds, the delay is introduced by varying the length of the light pathway of one of the beams (pump or probe beam). For adequate statistics of the recorded signals, measurements are repeated for each delay time. In addition, the optical density OD^o of the unexcited sample has to be measured, too. This can be done in two ways: one can measure the optical density in parallel by passing the beam through regions of the sample that were protected from excitation light, or it may be measured in an independent measurement when the pump beam is blocked. Here, the latter approach was realized.

$$OD^o(\lambda) = \log\left(\frac{I_0^o(\lambda)}{I^o(\lambda)}\right) \quad \text{sample not excited}$$

Overall, ΔOD is derived from four intensity measurements:

$$\Delta OD(\lambda, \Delta t_n) = OD^*(\lambda, t_0 + \Delta t_n) - OD^o(\lambda) = \log\left(\frac{I_0^*(\lambda, t_0 + \Delta t_n) \cdot I^o(\lambda)}{I^*(\lambda, t_0 + \Delta t_n) \cdot I_0^o(\lambda)}\right)$$

By using polychromatic test light, one obtains a set of spectra $\Delta OD(\lambda, \Delta t_n)$ representing the energy level population of the sample over time. The span of the test light spectrum defines which transitions can be detected, whereas the duration of the test pulse sets a limit to the fastest kinetics that can be resolved. A model has to be fitted against the set of spectra to deduce the pathways and the couplings between the energy levels within the sample, finally.

3 Design and Assembly of a fsTAS-Setup

Being a classical pump-probe technique, TAS in the time domain of femtoseconds to picoseconds (fsTAS) requires the following building blocks:

- Laser system generating ultrashort light pulses
- White light generation
- Delay stage
- Flow cell for liquid samples
- Spectrally resolving detectors
- Optical setup
- Computer-operated data acquisition system and control electronics.

Laser system, detectors and data acquisition system are synchronized by the control electronics. The opto-mechanical components (delay stage, polarizers, shutters) and the data acquisition system are operated by means of a computer. The optical setup delivers the light from the laser to the white light generation and further on through the sample, encased in the flow cell, onto the detectors and the energy meter. In the following sections these blocks are described in more detail.

3.1 Requirements

A necessary basis for investigating molecular structures, in which ultrafast processes lead to a redistribution of charges and energy, is the ability to monitor the absorption of the system with high temporal and spectral resolution and sufficient sensitivity. The objective was to build a setup fulfilling the following requirements. With the setup it should be possible to:

- Characterize non coherent transfer processes in the order of femto- to picoseconds.
- Excite samples in the spectral range of 400 nm to 700 nm.
- Detect transient absorption spectra with a spectral resolution of about 2 nm in the range of 450 nm to 720 nm simultaneously at each delay time.

In the design of a transient absorption spectrometer, general aspects need to be considered. They are discussed next, before the selected components are described in detail.

3.2 Realization

The temporal resolution of a pump-probe experiment is determined primarily by the width of the available light pulses. Furthermore, the interval between light pulses exciting the sample and probing the absorption of the sample needs to be variable, yet well defined. Working in the femtosecond time scale, the only way to achieve a stable and well defined delay between the pump and probe pulses, is to generate them by the same initial source. Simultaneous broadband detection of the absorption requires a light source exhibiting a wide spectrum with short pulse duration. Only nonlinear effects in condensed matter or fluids facilitate the generation of the required super-continuum with durations of about 100 fs. Once generated, the test light has to be transmitted by optics and through air. Also a reference beam needs to be split off and has to pass the sample as well. Since all transmittive optics disperses the multicolored beam, reflective optics was chosen, as far as possible, in the beam path before the light interacts with the sample.

Finally, the probe beams need to be analyzed by its wavelength. The detection is accomplished by a light sensitive multi-channel sensor. Its readout time scales linearly with the number of channels, unless massive parallel processing is utilized. The data are also less distorted by read noise if reading is done slower. Thus, an overall compromise has to be found between spectral resolution, i.e. the number of channels, and an acceptable readout

time. Definitely, no light must fall onto the detector during readout. For this reason the laser control electronics must ensure blanking of the pulses during readout. A mechanical shutting of the light would be to slow.

In the following section the realized setup is introduced and the interaction of its components is illustrated.

The Laser System

Well established state of the art lasers, generating femtosecond light pulses, use sapphire crystals doped with titanium ions (Ti:Sa) as the active medium. The advantages of this material are the large spectral bandwidth, a high saturation threshold, and the nonlinear properties which enable the use of the the laser medium as a passive mode locker itself. ("Kerr-lens-modelocking") However, the spectral range of a Ti:Sa-laser is limited to wavelengths ranging from 690 nm to 1100 nm. This limitation is circumvented by utilizing nonlinear processes in anisotropic crystals to generate and amplify new frequencies. A multi-stage laser system is necessary to provide the required energy as the overall efficiency of the wavelength conversion processes is about 10 %. Nowadays, the chirped pulse amplification (CPA) technique (Strickland and Mourou, 1985) is preferred to generate short pulses of high power. CPA ensures that the energy density in the gain medium is below saturation. The seed pulses are temporally stretched in a defined manner using a grating, followed by amplification and re-compression by another grating. Therefore, a CPA-system consists of a seed oscillator, a pulse stretcher, a pump-laser, the amplification stage, and a pulse compressor. The seed oscillator produces low energy pulses of the desired pulse duration, which are chirped by the pulse stretcher in a defined way. These pulses, having henceforth a much longer pulse width, are amplified in the active medium. Its population inversion is achieved by the pump-laser. The amplified pulse is then re-compressed back to its original duration in the pulse compressor. Using these intermediate long pulses, physical limitations in the active medium and of the optics which would cause damage of components or limit stability and maximum power are not reached.

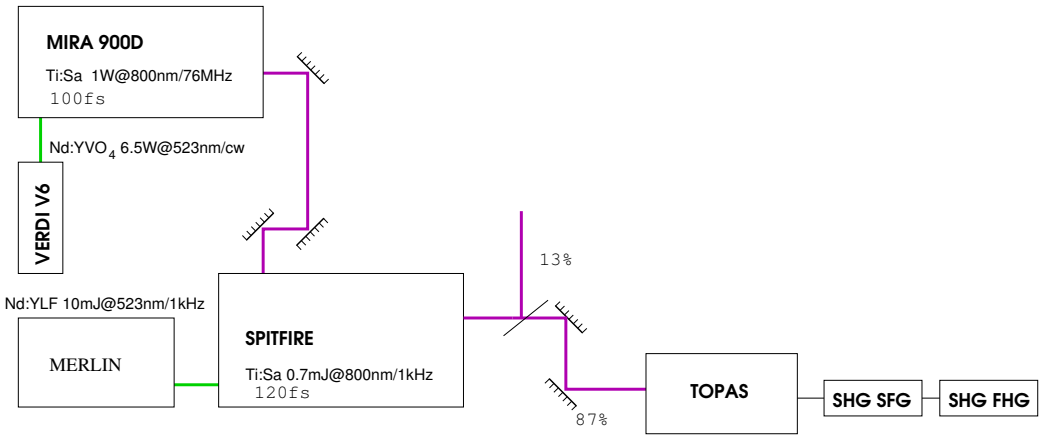

Figure 3.1: Laser system for the generation of ultrashort pulses. See text for a detailed description of the components.

The ultrashort pulses for the experiment where generated by a CPA-system (Spitfire, Spectra Physics). To seed this amplifier a femtosecond laser (Mira 900D, Coherent) was used. The seed-oscillator was pumped by a continuous wave, frequency doubled Nd:VO_4-laser (Verdi V6, Coherent) with 6.5 W output power and an emission wavelength of 532 nm. The Mira was configured to generate pulses of about 100 fs pulse duration with a frequency of 76 MHz at a wavelength of 800 nm. Its energy per pulse was about 660 nJ. The pump-laser of the amplifier was a frequency doubled, Q-switched, arc-lamp pumped Nd:YLF-laser (Merlin, Spectra Physics) with a repetition frequency of 1 kHz, a pulse width of 200 ns, a pulse energy of 10 mJ, and a radiation a wavelength of 532 nm.

The beam exiting the amplifier, with a pulse energy of about 700 µJ, was splitted into two parts, one part with a portion of about 13 % was used to generate probe pulses, while the remaining part was transformed by an optical parametrical amplifier (TOPAS, Light Conversion Ltd) into pulses with selectable wavelength. The further use of second harmonic generation (SHG)-, and SFG-modules gave a final tuning range of of 230–1200 nm. The output pulse width was about 70 fs.

Optical Setup

The pump-probe experiment operates as a polarization-sensitive two-ray absorption photometer in principle. Unlike its steady-state counterpart the probe beams are ultra-short and spectrally broad-band pulses. In addition to the specifications required due to the short pulse duration and the high spectral width, the necessity to detect weak changes in absorption of the sample requires a careful selection and arrangement of optical components.

The setup consists of several parts: generation and delay of the polarized test beam, splitting and projection of the test beam onto the detectors, and dispersion and detection of signal and reference light.

For generation and delay of the polarized test beam about 13 % of the 800 nm beam is split off. Using a sufficient number of mirrors which are placed in a suitable distance of each other, the light split off by the beam-splitter passes somewhat less than exactly the same pathlength as the pump beam to the sample. The distances are chosen so that the test beam reaches the sample about 10–20 ps before the pump beam. The delay path consisting of a motorized linear stage and two mirrors allow to increase the pathlength additionally by a propagation delay of about 1 ns. To ensure an unchanged

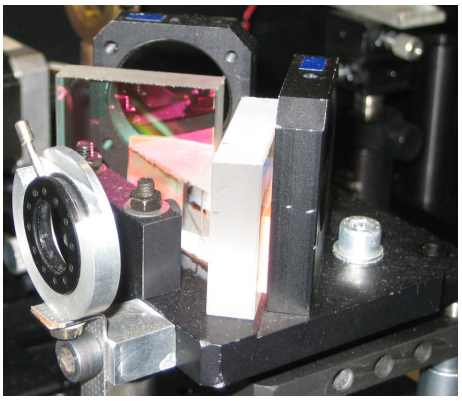

Figure 3.2: Delay line retro-reflector, built from two mirrors, and a glass prism.

position of the test beam, relative to the pump beam within the sample, the mirrors have to be adjusted very precisely, i. e. the angle between them

has to be exactly 90° and their surfaces have to move exactly perpendicular to the beam in vertical as well as horizontal direction when the mirrors are displaced. To guarantee the exact relative orientation of both mirrors to each other, they were pressed onto the edges of a commercially available glass prism (see figure 3.2). The second requirement was met by mounting the pair of mirrors onto a prism holder which allows rotation in addition to its tilting ability. Using this construction, the mirrors can be adjusted perpendicular to the incident beam in vertical as well as in horizontal direction independently of the moving direction of the linear stage, which might not be exactly parallel to the direction of the incident beam. To minimize the influence of a remaining tilt of the beam, the delay path is positioned at the shortest possible distance to the sample.

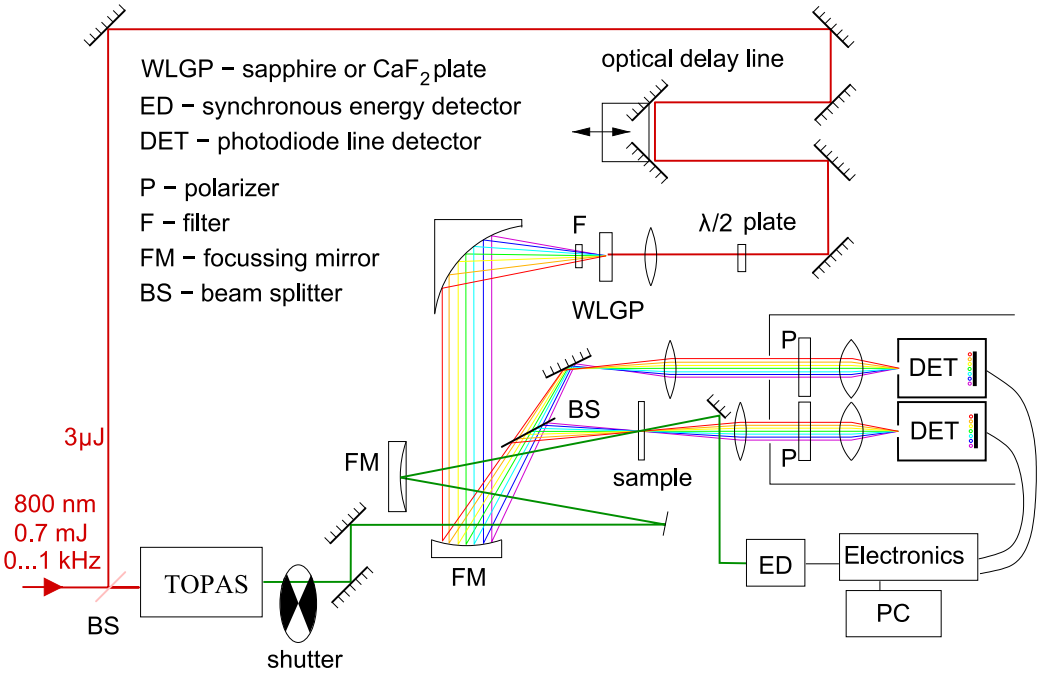

Figure 3.3: Scheme of the optical path of the transient absorption setup.

After passing the delay line, the intensity of the beam is decreased by a variable beam attenuator (iris and variable neutral density wheel) to generate a stable spectral continuum. It passes then an appropriately aligned $\lambda/2$ plate which determines the polarization of the test beam. Having a diameter

of 7 mm, the beam is focused onto a sapphire plate using a lens to produce the photon flux density required to generate a broad band continuum and to obtain a sufficiently small point source of this continuum.

The frequencies generated within the sapphire plate are emitted with a somewhat higher divergence than that of the entering beam. For projection of the white light, the divergent beam is first parallelized by an off-axis parabolic mirror and then directed towards a focusing mirror with a focal length of 500 mm. A part of the light has to be split off in order to generate a reference signal for the optical density measurement of the sample. As dispersion has to be at minimum for the signal path, the reflected light of the beam splitter is used for passage through the sample while the transmitted beam serves as reference. The flow cell containing the sample is placed at the focal plane of the reflected beam. Behind the flow cell the beam was collimated by an achromatic lens to pass a polarizer. An analog pathway was established for the reference beam. Finally, two achromatic lenses imaged the collimated signal and reference beam onto the entrance slit of two identical polychromators (MS125, Lot-Oriel GmbH, Germany), see figure 3.4.

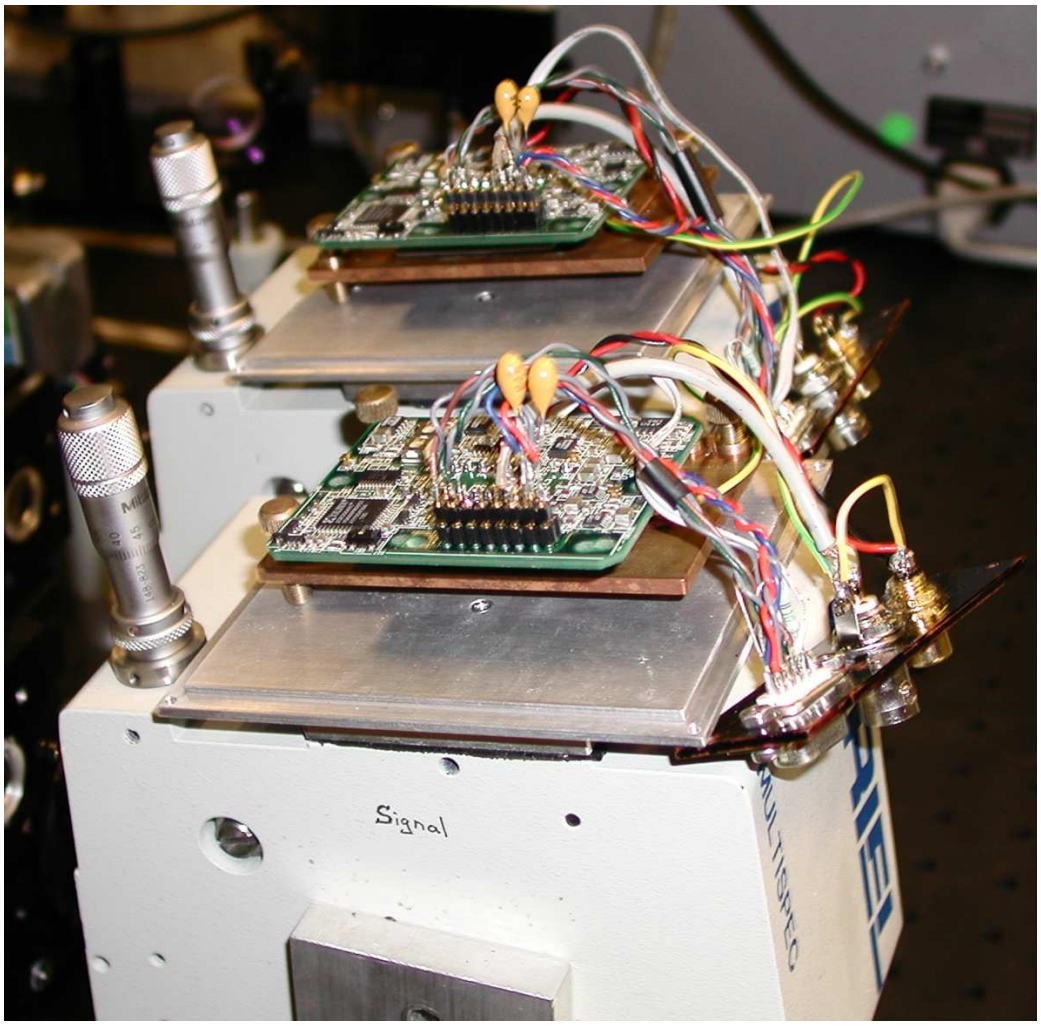

Figure 3.4: Photodiode lines (not visible) and readout electronics attached to the Polychromators, housing detached.

Flow cell

Samples within this study were molecules dissolved in liquid solvents. Since thermal lensing and photo-bleaching play an important role and must be avoided, simple non-flow cuvettes cannot be employed. Liquids can be brought into the beam path enclosed by a cuvette or as a free running stream. Since potentially harmful solvents such as toluene and dimethylformamide were used, a flow cell was utilized. A dedicated flow cell was designed to withstand organic solvents (see figure 3.5). All tubings and connectors (Bohlen-

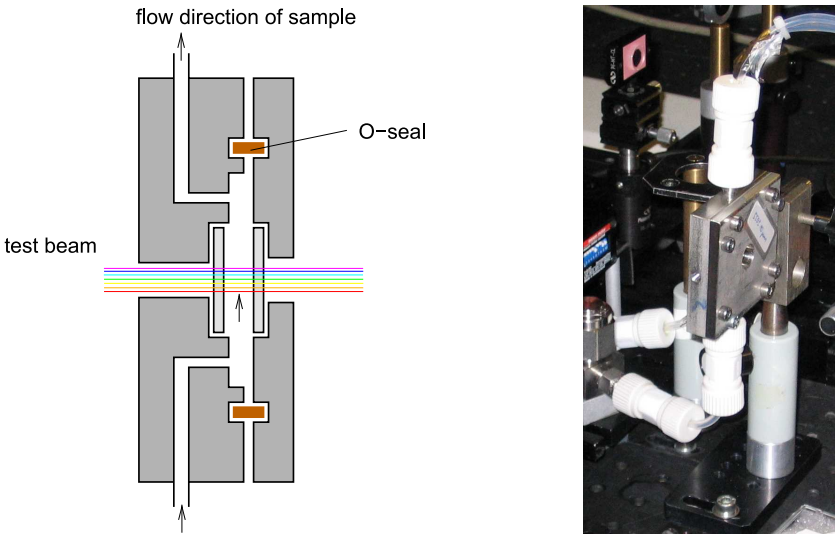

Figure 3.5: A) Schematic drawing of the flow cell. B) Image of the flow cell installed in the setup.

der, Germany) are made from poly(tetrafluoroethylene) also known by its brand name Teflon. Fused silica windows of 0.17 mm thickness were glued into the steel housing to build a transparent cell. Quartz glass was chosen because of its lower dispersion compared to standard glass types. The flow circuit is assembled by the cell, and a pear shaped flask as sample reservoir. The sample flow is driven by an annular gear pump (mzr-7223, HNP Mikrosysteme, Germany).

Detector and Control Electronics

The role of the detectors is to convert the wavelength-dependent intensity distribution of the two test beams (signal- and reference-beam) into computer processable data. This task requires the dispersion of the light into its different wavelengths at first and the detection of the respective intensities afterwards. The dispersion is achieved by grating-based polychromators in Czerny-Turner configuration (MS125, Lot-Oriel GmbH, Germany).

Two main strategies can be followed to record the different wavelengths. If one uses a single detector, sequential scanning of the wavelengths has to be performed by moving the dispersing element. The drawback of this method is the inability to get a full spectrum for specific sample conditions. Parallel recording by multiple detection elements, (i.e. with charge coupled device (CCD) sensors or photo-diode line sensors), is an alternative without this limitation and was used in this work.

The available light intensities and requirements for the signal to noise ratio (SNR) decide what kind of detector type should be used. The main influencing factor is the overall SNR. Mainly three types of noise sum up vectorially, the shot noise of the light itself, dark noise, and readout noise of the detector and the readout electronics.

$$\sigma = \sqrt{\sigma_{\text{shot}}^2 + \sigma_{\text{dark}}^2 + \sigma_{\text{read}}^2}$$

Shot noise σ_{shot} is the noise associated with the random arrival of photons at any detector. Shot noise exists because of the discrete nature of light and electrical charge. The number of counted photons is governed by Poisson statistics. For a CCD or photodiode-line detector,

$$\sigma_{\text{shot}} = \sqrt{N_{\text{e}}}$$

where N_{e} is the signal expressed in generated electrons by the inner photo-electrical effect. Shot noise is also sometimes called “Poisson noise”. This type of noise depends on the signal strength and becomes relatively smaller as the signal increases.

Dark noise σ_{dark} is the noise created by thermal effects. Even in the absence of light, electron-hole pairs are generated inside the sensor. The rate of generation depends exponentially on the temperature and typically doubles every 7 K. The thermally generated electrons N_{dark} cannot be separated from photo-generated electrons, and obey the same Poisson statistic, so

$$\sigma_{\text{dark}} = \sqrt{N_{\text{dark}}}$$

One can subtract the average dark signal, but the shot noise associated with it remains. The accumulated number of the dark counts depend on temperature and integration time. Dark noise is minimized by cooling of the detector and plays a significant role only for long acquisition times, typically in very low light conditions as for instance in astronomy.

Readout noise σ_{read} occurs during the process of converting the detectors electrical signal to digital counts. Readout noise is determined by the quality of the detector's electronics. This constant source of noise is independent of signal strength, temperature and integration time.

The signal to noise ratio is defined as:

$$\text{SNR} = \frac{S}{\sigma}$$

where σ is the overall noise of the signal S. In the case of the above mentioned detectors the SNR for a specific temperature and integration time is given by:

$$\text{SNR} = \frac{S}{\sqrt{\sigma^2_{\text{shot}}(S) + \sigma^2_{\text{dark}} + \sigma^2_{\text{read}}}}$$

In TAS, very small changes of a large signal have to be detected, as the changes of transmitted light intensity (change of absorption) are very small compared to the transmitted intensity itself. However, the number of available photons is not strongly limited. These conditions call for a high SNR when the signal S is large.

Comparing CCD- and photo-diode line detectors, reveals that read and dark noise is smaller for the CCD type detectors, but the maximum de-

tectable signal is much higher for photo-diode line detectors. This difference originates from the technological design and the physics of the detectors themselves. A capacitor of one photo-diode line element can store more charges than one element of a CCD. Evaluation of the SNR shows that dark and read noise is small compared to shot noise in the case of TAS, where integration times are very small and the signal S is large. Therefore, one can estimate the SNR by:

$$\mathrm{SNR} = \frac{S}{\sigma_{\mathrm{shot}}(S)} = \frac{S}{\sqrt{S}} = \sqrt{S}$$

Clearly, the higher well capacity (number of maximum stored charges) of a photo-diode line improves the SNR. For that reason photo-diode line detectors were chosen. To have stable and low dark noise, thermo-electrically cooled detectors were used.

The temperature was stabilized by a proportional controller circuit depicted in figure 8.1. A temperature-dependent resistor serves as sensor. Its value is compared with the nominal one by a differential amplifier. The deviation is transformed into a current which drives a Peltier element. Incorporating both, the photo-diode line and the Peltier element, inside the evacuated housing of the integrated circuit, condensation of water on the detector is prevented. The photo-diode line is directly mounted onto the cold side of the Peltier element whereas the hot side is connected to the metal housing. This design leads to a heating of the front window as well and avoids condensation at that place, too. The photo-diode line housing is mounted onto a copper block which is cooled by an air stream of a fan to remove the heat.

The chosen photo-diode lines (see figure 3.6) consist of 512 light sensitive elements. Each is made up of a photo-diode, a capacitor and a driving transistor. Light falling onto the photo-diode generates a current by the inner photoelectric effect. That current discharges the capacitor. To read out all elements individually, a clock and driving circuit turns on the driving transistors sequentially, one after the other. That way, each capacitor is connected once a readout cycle with the read line. During readout of each

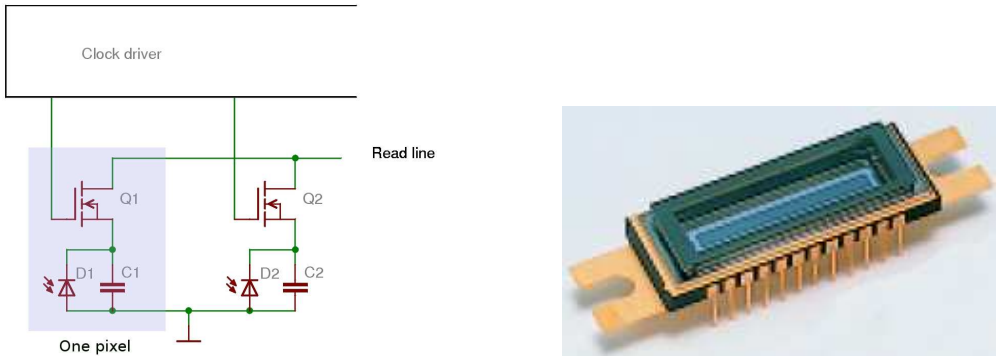

Figure 3.6: A) Schematic representation of a photo-diode line sensor. Each picture element (pixel) consists of a light sensitive sensor area (photo-diode D), an integrating capacitor C and a driving transistor Q. For an explanation of operation see text. B) Picture of the S3902/512 photo-diode line sensor device.

element, the capacitor is recharged until a preset voltage is reached. A charge integration circuit transforms the amount of the charge necessary to recharge the capacitor into voltage. This voltage is proportional to the light fallen onto the cell during the period between recharging. Readout electronic requires a low noise circuit design, which is well adapted to the photo-diode lines. It was, therefore, purchased from the manufacturer of the photo-diode lines.

To integrate the detectors into the whole system one main clock circuit is used to derive all signals to drive the detectors and the laser (see Appendix). The base clock is generated by a crystal-stabilized oscillator. Its 2 MHz clock is divided by a factor of 4 to achieve a clean duty cycle of 50 %. This 500 kHz clock drives the pixel clock of the photo-diode line driver. To generate laser driving and read start pulses, this 500 kHz clock is divided by a factor of 500 further on. With the resulting frequency of 1 kHz the laser is triggered to generate pulses at this frequency. In order to be able to accumulate the light of several laser pulses in the photo-diode lines the laser trigger pulses are fed through a divider being part of the A/D interface card. Thus, after every n-th laser pulse (n controllable by software), a readout of the photo-diode line is initiated. Since the read start pulses have to be coincident to

the pixel clock, a dedicated circuit built from D-flip-flops synchronizes the asynchronous read initiating pulse to the pixel clock, forming the read start pulse. Since readout lasts longer than a laser trigger period, the laser is blanked during readout. This blanking is achieved by masking the trigger pulses for the pockels cell driver.

Synchronous Energy Detector

Ideally, the pump pulses should exhibit a constant energy over the runtime of an experiment. In practice, the per shot energy of the used laser system varied up to 10 % and from time to time much bigger deviations occurred due to misalignment and temperature effects. To be able to detect improper operation of the laser and to correct for minor deviations the pump pulse energy was monitored by an energy detector. In order to sample exactly these pump pulses which excite the sample during the accumulation of the spectra it needs to be synchronized with the read cycles of the photo-diode lines. The design of the energy detector followed the principle of the photo-diode sensor lines (see Appendix for circuit schemes). At the begin of a new read cycle a capacitance is charged up to a precisely defined value. The photon-generated current of a photo-diode exposed to the pump pulse light discharges this capacitance. Since the photo-current is linearly dependent on the energy impinging on the diode and the voltage of the capacitance is linearly-dependent on the charge held by the capacitor, the voltage drop is linearly-dependent on the deposited energy. The voltage of the capacitor is sensed with the high impedance of an operational amplifier. A second operational amplifier converts the drop into a raise of the signal and shapes it into a proper voltage level for transmission to the analog to digital converter, coupled to a single chip microprocessor. The microprocessor controls the conversion of the voltage and stores the results into its external memory. Furthermore, it communicates to the PC to transfer the digital representation of the energy to the control program for further processing.

Control Programm

Data acquisition and operation of the optomechanical components is achieved by dedicated computer hardware. To realize the control of all components in the desired way, a computer program was written by the author in C using Minimalist GNU for Windows (mingw), an open source programming tool to write native Microsoft Windows applications. The graphical user interface (see figure 3.7) was designed and programmed using GIMP Toolkit (gtk+). It allows to set all necessary parameters for data acquisition and instrument

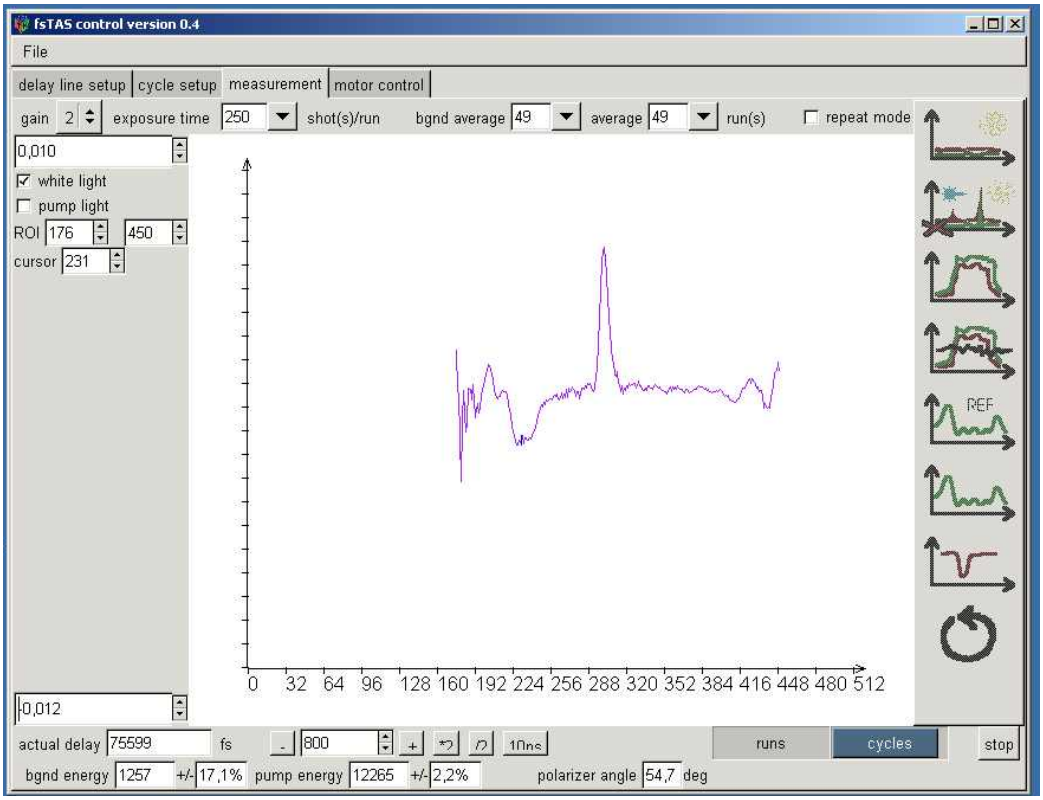

Figure 3.7: Screen-shot of the control program for fsTAS.

control like exposure time, preamplifier gain, shutter states, and current optical delay. Furthermore, it records and displays various data sets for adjustment of the setup and in preparation of a measurement. The most important tool is the on-line display of the spectra of both detectors and its ratio, to check and guide the alignment of the two optical pathways. Prior to any

signal measurement, the background with and without excitation light has to be recorded. This measurement can be triggered separately or is done within a complete measurement cycle. To align the excitation beam, a single or repeated measurement of the ΔOD signal can be initiated. For a complete measurement cycle one can generate a list of delay values at which the ΔOD signal will be measured. This list can be built up by linearly or logarithmically-spaced values. Once the list is complete and all recording parameters are set, the program conducts the whole experiment and stores the data.

Summary of technical parameters

excitation wavelength	tunable between 230 — 1300 nm
excitation pulse width	$\approx$ 70 fs
excitation pulse power	$\approx$ 10 µJ
detection wavelength range	500 — 720 nm
number of detection channels	512
detection wavelength resolution	2 nm
temporal scan range	-20 — 1000 ps
mechanical scan resolution	1 fs
necessary sample volume	$\approx$ 15 ml
optical path length through sample	1 mm
allowed solvents	organic solvents except methanol and acids

3.3 Measurements

Porphyrin-Quinone-Tetrad

This supra-molecule was designed to mimic the bacterial photosynthetic reaction center, and thus, to function in analogy of the primary steps of photosynthesis. Two porphyrins and two quinones were covalently coupled to form

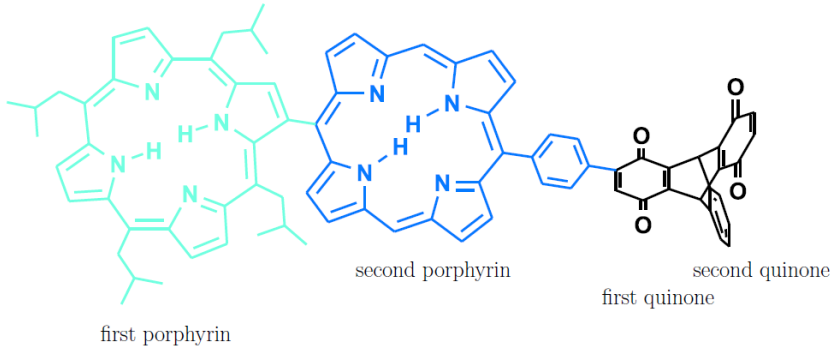

Figure 3.8: Chemical structure of the porphyrin-quinone-tetrad mimicking a bacterial reaction center.

an electron donating "special pair", and to model the electron accepting quinones (see figure 3.8). This specific assembly features a rigid spatial arrangement for the two quinones. Its chemical synthesis was described in Wiehe et al. (2001b). Tannert (1999) reported that both porphyrins can be described as not strong electronically coupled in the ground state (see figure 3.9 for the absorption spectrum). Deduced from the crystal structure, twisting of the porphyrin cores is supposed to induce bathochromic shifts of the energy levels of both porphyrins and changes of their oscillator strength compared to the unlinked precursors. Under these assumptions a selective excitation of the first porphyrin can be achieved at an excitation wavelength of 440 nm. By analyzing the fluorescence of the first porphyrin, its S_1 state decay time was estimated to 97 ± 20 ps (data not shown). The second porphyrin emitted no measurable fluorescence at all. In this former study the kinetics of the porphyrin ground states were not recordable fast enough to be resolved. The new transient absorption setup allowed to close this gap. Transient absorption spectra were recorded every 10 ps after excitation of

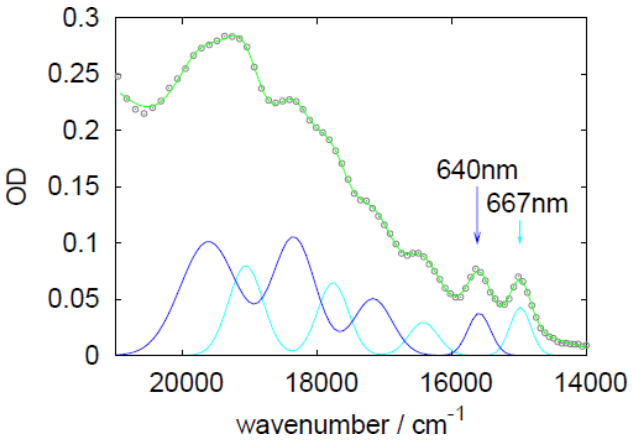

Figure 3.9: Absorption spectrum (gray circles) of the tetrad, Q bands only. The colored curves are the result of a band analysis. The cyan spectrum was assigned to the first porphyrin, the blue spectrum was assigned to the second porphyrin, the sum is shown in green. Taken from [Tannert (1999)].

the first porphyrin until the monitored ground state was refilled once again at about 300 ps (see figure 3.10 B). The average ground state recovery time of the first porphyrin was found to be 90 ± 20 ps. This value is remarkably small, assuming a charge separated state. The second porphyrin showed only a very weak transient at 640 nm which could not be analyzed due to noise. However, one can observe that there is no buildup of ground state depletion of the second porphyrin during the recovery of the ground state of the first porphyrin (see green and brown curve in figure 3.10 A and compare the peak at 670 nm versus the peak at 640 nm). Therefore, energy transfer from the first to the second porphyrin is unlikely. As the existence of electron transfer was clearly proven by oxidizing and reducing the quinones, the most likely hypothesis is the occurrence of a very fast back electron transfer from the quinones to the porphyrins explaining the short ground state recovery time of the first porphyrin.

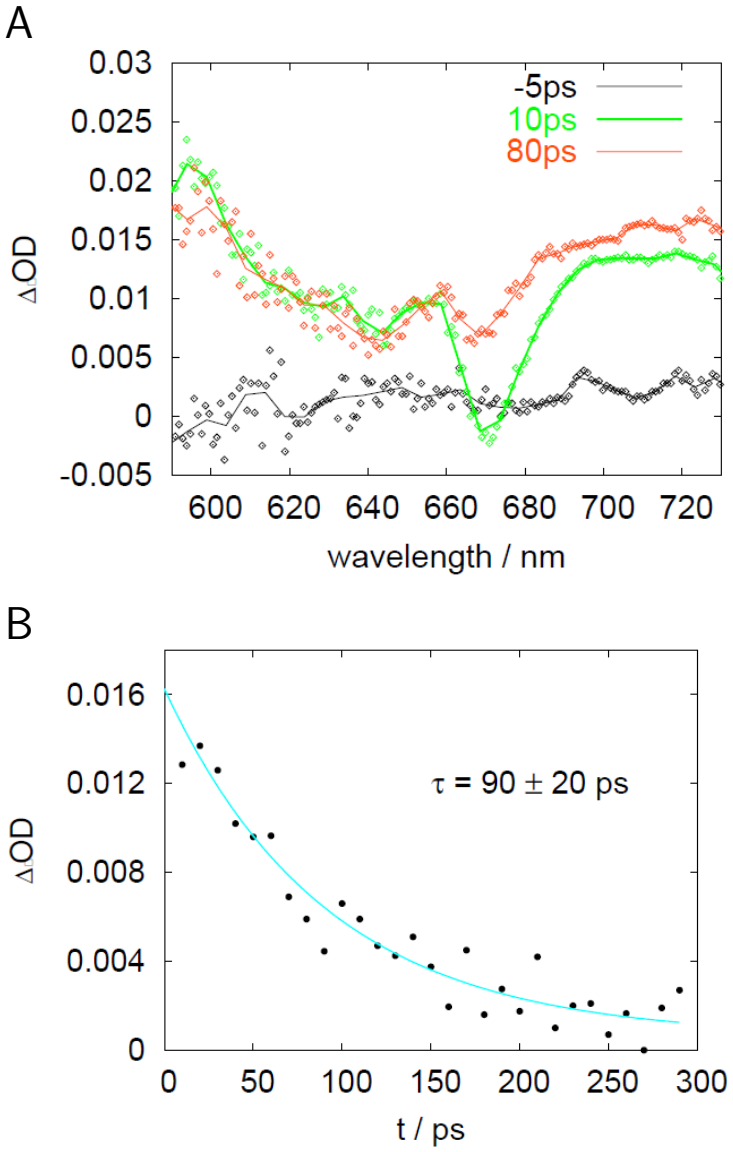

Figure 3.10: A) Transient absorption spectra of the tetrad at three different delay times after pulsed excitation at a wavelength of 440 nm. B) Ground state recovery of the first porphyrin after excitation, probed by the transient of the optical density at 667 nm relative to the optical density at 700 nm to account for baseline shifts. The magenta curve is the optimal fit of a mono exponential decay function.

Pheophorbide a-loaded diaminobutane dendrimers

Energy migration in pheophorbide *a* (Pheo)-loaded diaminobutane (DAB) dendrimers is a very fast process due to the high packaging density of the dyes. These dendritic structures are promising candidates as multipliers in

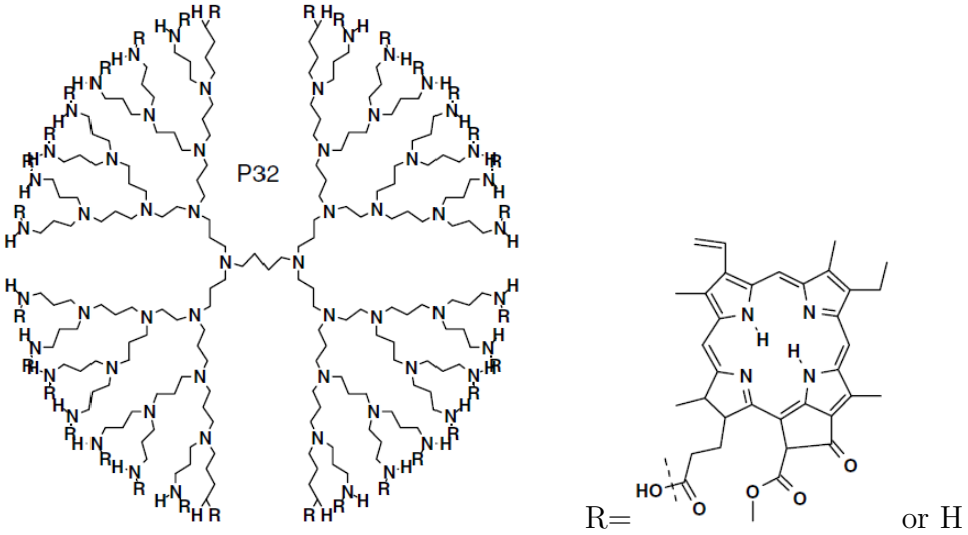

Figure 3.11: Chemical structure of P32, a DAB dendrimer of fourth generation being able to bind 32 pheophorbide *a* molecules. About 75 % of the residues (R) are dyes all others are single hydrogen atoms.

photodynamic therapy in order to increase the number of singlet oxygen producing photosensitizers per addressator (Hackbarth et al., 2005). In addition, they might be used as light harvesting complexes. A dendritic structure that can get loaded with thirty two Pheo molecules (P32) is depicted in figure 3.11. Finally, about 75 % of all binding sites could be filled with sensitizing dye molecules (Hackbarth et al., 2005). As a consequence of the restricted space, available for the dye molecules, the inter dye distances become small and, thus, allow efficient energy transfer between the dyes. Furthermore, a significant drop of singlet oxygen production was observed for P32 compared to monomeric Pheo molecules (Hackbarth et al., 2005, 2001), a fact which seems to strongly limit the usefulness of this multiplier approach. However, after cellular uptake the dyes become free and reestablish there ability to generate singlet oxygen (Paul et al., 2003). This way, the strongest initial quenching

of singlet oxygen generation is even favorable to avoid photo-toxicity before reaching the target structures. It is therefore important to understand the underlying mechanisms of energy transfer and energy quenching, to tune the quenching.

To get insight in the ongoing processes, absorption as well as fluorescence was investigated in a time-resolved manner for P32 dissolved in ethanol. Three different fluorescence decay times were obtained, 4.75 ns, 630 ps, and 40 ps. Transient absorption spectroscopy revealed two recovery times of the

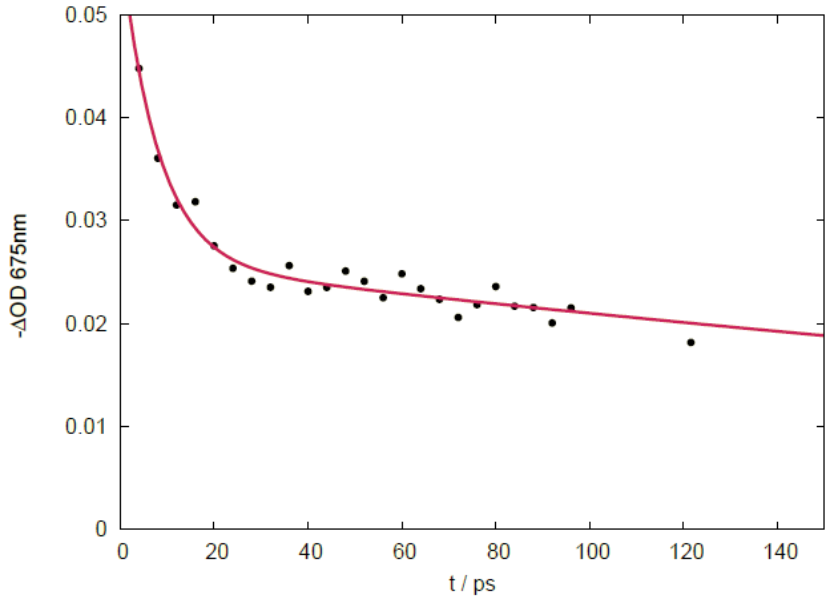

Figure 3.12: Recovery of the ground state depletion of P32 monitored at 675 nm (black dots). The red curve shows a bi-exponential fit with decay times of 8 ps, and 580 ps.

ground state population of the Pheo dyes in the sub nanosecond timescale (see figure 3.12, and 3.13). with recovery times having a value of 8 ± 1 ps and of 580 ± 180 ps. This finding confirms that at least two different distance distributions between the Pheo dyes exist. Homo-Förster energy transfer can not explain the dissipation of energy in such short time scales as observed by time-resolved fluorescence spectroscopy, quantitative detection of singlet oxygen production, and transient absorption spectroscopy (Tannert et al., 2004). Energy trapping by Pheo dimers is proposed as the quenching pro-

cess like in concentrated dye solutions (Lutz et al., 1981). Eichwurzel et al. (2000) investigated the properties of the Pheo dimer and estimated a maximum center-to-center distance of the two monomers of about 6 Å. According to their findings, the disc-shaped Pheo molecules are stacked planar to each other close to the van der Waals distance of 3 Å exhibiting a lateral displacement in the range of a few angstroms. Considering the planar size of Pheo of about 8 Å, this means a very close arrangement. So far, the ground state recovery time for the Pheo dimer is not known. Estimating it in a very crude way from the reduced fluorescence quantum yield of the dimer compared to the Pheo monomer by a factor of more than 10^4 (Eichwurzel et al., 2000), one yields a time in the range of 60 fs, shorter than the laser pulses used in this study, and therefore difficult to observe. Assuming a Förster radius R_0 of 62 Å for the energy transfer from a monomeric Pheo to the Pheo dimer trap, and a first excited state lifetime τ_{S_1} of 5.7 ns (Hackbarth et al., 2005), the ground state recovery times τ_{GSR} of 8 ps and 580 ps translate into a center-to-center distance R of the Pheo dye to the Pheo dimer trap of 21 Å and 43 Å (see formula 3.1).

$$R = R_0 \sqrt[6]{\frac{\tau_{GSR}}{\tau_{S_1} - \tau_{GSR}}} \tag{3.1}$$

Presuming the validity of the dimer trap hypothesis, the obtained ground state recovery times can be assigned to the (last) energy transfer from a monomeric Pheo molecule to a Pheo dimer trap. The energy transfer steps between monomeric Pheo molecules do not show up, since these events keep the number of occupied and unoccupied ground states constant. These values are in good agreement to molecular mechanics calculations predicting a dye-to-dye distance of less than 20 Å (Hackbarth et al., 2001). The ratio of two between the distances fits into the picture of a only 75 % dye loaded DAB dendrimer, where some of the binding sites are occupied by a hydrogen atom only and create a double sized gap.

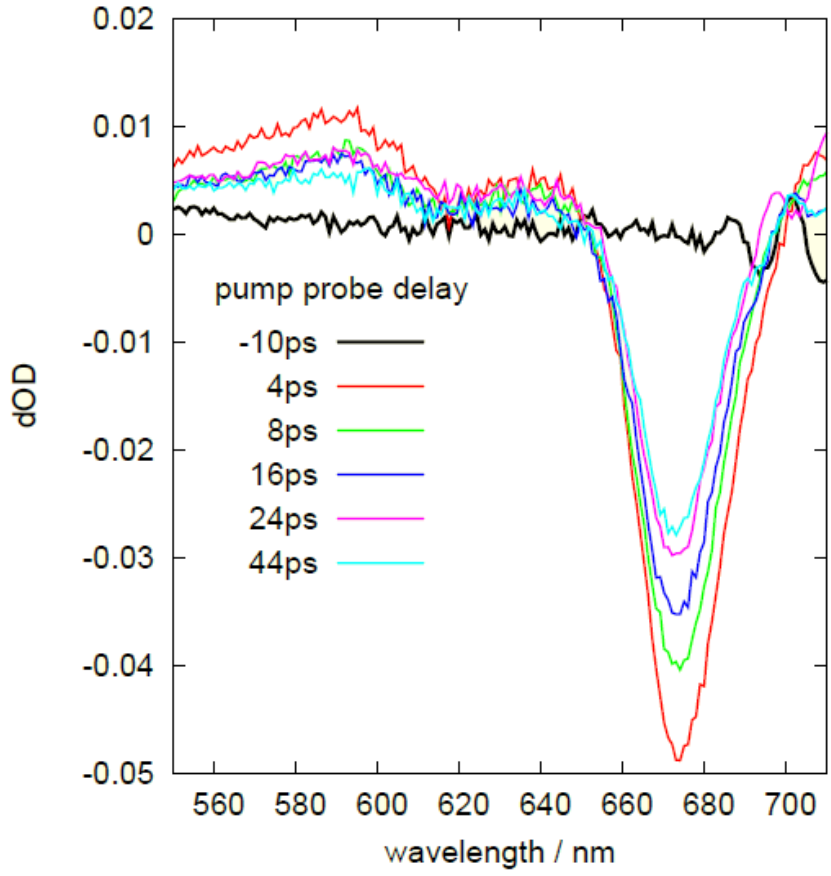

Figure 3.13: Transient absorption spectra of P32 at various delay times after excitation. The prominent peak at 675 nm is due to ground state depletion of Pheo.

4 Global Data Analysis

Spectroscopic measurements result in large amounts of numerical data. However, often the information one wants to collect is hidden in the data. It needs a mathematical procedure to extract the information out of the raw measured data. If one is investigating complex samples, often different experiments need to be performed to gather all the data, that allow the extraction of the wanted information. Even more knowledge is obtained by recording data under different conditions. See figure 4.1 for an overview of these two cases. If all the measured data are analyzed using one model to describe the whole set of aquired data, the procedure is called "Global Data Analysis".

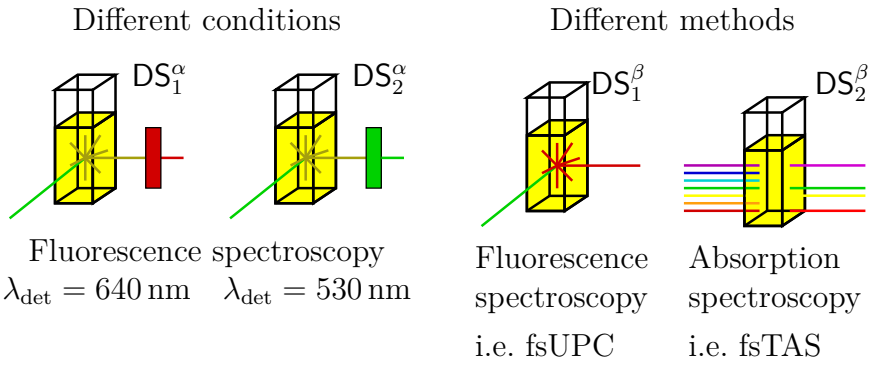

Figure 4.1: Investigating complex systems typically comprises the recording of data obtained under different conditions or from different methods. These sets of data (DS_1^α, DS_2^α, DS_1^β, DS_2^β) are the basis for global data analysis.

4.1 Motivation for Global Techniques

A multichromophoric system (i.e. the investigated triad), wherein energy and electron transfers occurs, is said to exist in different states. Each one is characterized by its specific energy and charge distribution. One state might be that where all moieties are in their ground states, another one is the charge separated state. To characterize the system fully, one wants to

know the transition rates between these states. Therefore, the dwell time of each state has to be measured. Since each state has its own properties, commonly, different measurement methods need to be applied under different conditions. All data together give a complete set of the systems kinetics.

The easiest approach for data analysis would be to analyze the data of each experiment independent of the other ones. Afterwards one would compare the information extracted from one experiment with all the others. Typically one has to check if all measurements gave consistent results. A major drawback of this approach is the fact, that interrelations of parameters are easily missed and it is hard to judge if results are consistent or not.

A more rigorous approach is "Global Data Analysis". It assumes a model describing the system under investigation for all used methods and for each measured condition. In the most suitable case the theoretical model is based on physically meaningful parameters. This case is called "Global Target Analysis". This global approach essentially has advantages only. No parameter is determined twice or more times and needs to be checked for consistency, all the knowledge about the system is tested in one place. Of course, a test of the validity of the model itself still has to be performed. Furthermore, having a model based on physical meaningful parameters, also the confidence intervals may be derived directly.

4.2 Parameter Estimation and Error Analysis

The determination of transition rates between molecular states involves mostly nonlinear curve fitting of the measured data $d(t_l)$, sampled at discrete time points t_l. Mathematically, the sought rates are parameters p of a model function $f(p, t_l)$, which are adjusted by an algorithm to minimize the deviation between the model and the measured data. One figure of merit to judge the deviation between model and data is χ^2:

$$\chi^2 = \sum_{l}^{N} \left(\frac{f(p, t_l) - d(t_l)}{\sigma(t_l)} \right)^2$$

This figure of merit can be derived from the general theory of maximum

likelihood under the assumption of Gaussian distributed errors σ (Hauschild and Jentschel, 2001). It holds even true for Poisson distributed noise in the large signal case, where the Poisson distribution is well approximated by a Gaussian shape. Numerical evaluation shows that in case of data acquired by TCSPC the approximation is valid if the total number of counts per decay histogram exceeds about 25,000 counts (Maus et al., 2001).

Being in the fortunate situation to know the individual errors for every measured discrete point $\sigma(t_l)$ one expects χ^2 to be equal to the number of discrete points N. Considering the correlation amongst the parameters p introduced by the model function, the so called reduced χ^2 is defined as:

$$\chi^2_{\mathrm{red}} = \frac{\chi^2}{N - N_p}$$

in which N_p is the number of parameters. Thus, a model with a well optimized set of parameters gives a χ^2_{red} of unity. However, one should be aware of the fact that the χ^2-test is a mathematical measure of deviation only, even a physically wrong model may describe the data mathematically well. Therefore the model functions need to be chosen by the experimenter by means of his a priori knowledge and careful evaluation of all possibilities.

As stated above, a well chosen model function depends directly on the physical parameters of interest. Therefore, methods for the determination of confidence intervals of the estimated parameters directly provide confidence intervals of the parameters of interest. Furthermore, interrelations of the parameters can be treated in a rigorous manner in that case easily.

Model functions $f(p, t)$ to analyze the data acquired in this work are sums of exponential functions, mostly convoluted ($\otimes$) with the response characteristic of the excitation source and the measurement system IRF(t):

$$f(p, t_l) = \left(\sum a_k \, \exp(-t/\tau_k)\right) \otimes \mathrm{IRF}(t)$$

Due to the complexity of the investigated samples, global analysis was a key technique for successful data elicitation in this work. It was used for two different applications. The first case was the separation of K different species

exhibiting overlapping fluorescence spectra, but different fluorescence lifetimes. In case of non-interacting species exhibiting ordinary photo-physics, one expects the fluorescence lifetime τ_k of species k to be independent of the wavelength λ. Whereas, at constant excitation intensity the measured amplitude $a_k(\lambda)$ is varying with wavelength and resembling the fluorescence spectra of species k. For a mixture of K species and sampling the intensity decay at M wavelength points, one has to apply a model containing K decay times τ_k, $1 \leq k \leq K$, and $M \times K$ amplitude coefficients a_k^w, $1 \leq w \leq M$. The measured data sets

$$\mathbf{D} = \begin{pmatrix} I_0^0 & \cdots & I_L^0 \\ \vdots & I_l^w & \vdots \\ I_0^M & \cdots & I_L^M \end{pmatrix} \qquad I_l^w = I(t_l, \lambda^w)$$

(measured by means of the TCSPC technique) consist of M time traces each recorded at a wavelength λ^w. One time trace contains L time bins of width Δt, and start time t_l.

Introducing the matrix of spectra

$$\mathbf{S}(\lambda) = \begin{pmatrix} a_1^1 & \cdots & a_K^1 \\ \vdots & a_k^w & \vdots \\ a_1^M & \cdots & a_K^M \end{pmatrix}$$

containing in each column the spectrum of species k and the matrix of decays

$$\mathbf{\Gamma}(\tau, \delta t) = \begin{pmatrix} \exp(-t/\tau_1) \otimes \mathrm{IRF}(t, \delta t_1) \\ \cdots \\ \exp(-t/\tau_K) \otimes \mathrm{IRF}(t, \delta t_K) \end{pmatrix}$$

containing in each row a mono-exponential decay convoluted with the instrument response IRF, one can calculate an estimation $\tilde{\mathbf{D}}$ of the measured data set $\mathbf{D}$ by

$$\tilde{\mathbf{D}} = \mathbf{S}(\lambda) \cdot \mathbf{\Gamma}(\tau, \delta t).$$

To account for minor shifts in time between the decay and the IRF caused

by changes of the light path, the IRF is numerically shifted by an additional fit parameter δt. The figure of merit for the global fitting problem is then given by

$$\chi^2_{\text{global}} = \frac{1}{M} \sum_w \frac{1}{L-p} \left\| (\mathbf{D}_w - \tilde{\mathbf{D}}_w) \oslash \vec{\sigma}_w \right\|^2$$

with $\mathbf{D}_w$ and $\tilde{\mathbf{D}}_w$ denoting row vectors of the measured and estimated data matrices, respectively, and the division element by element $\oslash$. The row vector $\vec{\sigma}_w$ contains the standard deviation per measured data point for the decay recorded at wavelength λ^w.

Secondly, global data analysis was used to extract kinetic rate constants from datasets measured by means of different techniques. As explained in chapter 2, to monitor the states involved in energy and electron transfer of the investigated triads, both, absorption and fluorescence spectroscopic methods had to be applied. The measured kinetic traces can be described by model functions depending on the rate constants of interest and a few more parameters accounting for data normalization and setup specific constants. For a detailed description of the underlying models see chapter 6.4. The rate constants of energy and electron transfer entered the model functions $\vec{m}_\zeta$ as global parameters. The index ζ denotes the measurements with different methods and under different conditions. The overall figure of merit function $\chi^2_{\text{global, red}}$ was computed as the sum of the individual (χ^2_ζ) ones:

$$\chi^2_{\text{global, red}} = \frac{1}{I} \sum_\zeta^I \chi^2_{\zeta,\text{ red}}$$

Since, the standard deviation of data points for data sets obtained by the technique of fluorescence up-conversion or transient absorption spectroscopy was not known from the measurement, the individual values $\chi^2_{\zeta,\text{ red}}$ values had to be normalized iteratively. Without renormalization data sets with higher $\chi^2_{\zeta,\text{ red}}$ values would determine the fitting parameters more than those with lower ones. The normalization factors were chosen in a way to bring the individual values $\chi^2_{\zeta,\text{ red}}$ on the same order of magnitude. The current value of $\chi^2_{\zeta,\text{ red}}$ resulting from the fit of TCSPC data was used to calculate normalization factors for the other $\chi^2_{\zeta,\text{ red}}$ values for the next iteration step.

This method leads to an equal weighting of different measurements even in the case of different statistical certainty of each measurement. However, it seems to be the best approximation so far.

In science, any measured value without a known error is useless! Even in everyday life, one assigns typical confidence intervals to values based on experience and implied rules.

Using the above defined global models, estimation of the confidence intervals was achieved by the support plane method. It is based on comparing the optimal $\chi^2(p_{\mathrm{CI}}^{\mathrm{opt}})$ value with $\chi^2(p_{\mathrm{CI}})$ calculated for a parameter set where one parameter p_{CI} is dragged away from its optimum $p_{\mathrm{CI}}^{\mathrm{opt}}$. The ratio F_χ of both figures of merit follows an F-statistic (Lakowicz, 1999)

$$F_\chi = \frac{\chi^2(p_{\mathrm{CI}})}{\chi^2(p_{\mathrm{CI}}^{\mathrm{opt}})} = 1 + \frac{N_p}{\nu}\,\mathrm{F}(N_p, \nu, P) \tag{4.1}$$

with N_p parameters exhibiting ν degrees of freedom with a probability P that the F_χ value is a result of random noise of the data.

Hence, a statistical test procedure may be performed, to check for a given confidence level boundary of the parameter p_{CI} under question. For estimation of the common one σ confidence interval borders P is set to 0.32, meaning that the tested parameter is inconsistent with the data by chance only with a probability of less than 32 %. The goal of the algorithm is to find the two values p_{CI}^{+} and p_{CI}^{-} where for the fixed probability $P = 0.32$ equation 4.1 is fulfilled. The final result is an estimation of a model parameter p^{opt} with its confidence interval ranging from p_{CI}^{-} to p_{CI}^{+}.

4.3 Algorithmic Details

Parameter estimation is one of the hot topics of numerical mathematics. Metaphorically speaking, the goal is to find the global minimum valley of a hyper-surface. In case of nonlinear models this is mostly an ill-posed problem for which no “best method” exists. Hadamard introduced in 1902 the classification of “well-posed” solutions (Hadamard, 1902; Mandelbrojt and Schwartz, 1965; von Würtemberg, 2011). Later on all non “well-posed” prob-

lems where classified as “ill-posed”.

All methods suffer from at least two main problems: stability and the inability to find the global optimum with certainty. Many algorithms were developed to address this problem. Classified according to the way they work there are algorithms which a) rigorously search a parameter subspace, b) use stochastic or heuristic methods like Monte-Carlo simulation or Downhill-Simplex, c) use information about the slope at the current point on the hyper-surface. Class a) algorithms may be understood as the most pedantic in terms of finding the global minimum, but are slowest ones. The class c) algorithms try to use as much as possible information which is available. However, the calculation of derivatives is per se an unstable operation, which influences also the stability of the optimization. Algorithms of class b) are said to be more stable, but having the drawback of being computational more exhaustive. Since they require furthermore no calculation of derivatives application to all kinds of parameter estimation is easier. For these reasons the Nelder-Mead Downhill-Simplex algorithm (Nelder and Mead, 1965) was chosen for nonlinear optimization.

Following the theoretical work of Golub (Golub and Pereyra, 1973), the fitting program splits the estimation problem into a nonlinear and a linear one. Model functions $f(p,t)$ are linear combinations of nonlinear functions mostly, as for the multi-exponential model like:

$$f(p,t) = \sum_i a_i \, \exp(-t/\tau_i)$$

The parameters within the nonlinear functions (the τ_i in this example) are called nonlinear parameters α_i, shortly denoted with the vector $\vec{\alpha} = (\alpha_i)$. The vector $\vec{a} = (a_i)$ contains the linear parameters a_i.

The main advantage of splitting the problem comes from the fact, that linear estimation problems have a unique and numerically more stable solution compared to nonlinear ones. Therefore, the linear parameters can be determined as precise and unique as possible while reducing the number of nonlinear fitting parameters. The realized algorithm is similar to that described by Krogh (Krogh, 1974).

The main fitting program is organized in two blocks: the outer loop of the Downhill-Simplex algorithm and the inner part of the generalized linear least squares (GLLS) solver (see figure 4.2).

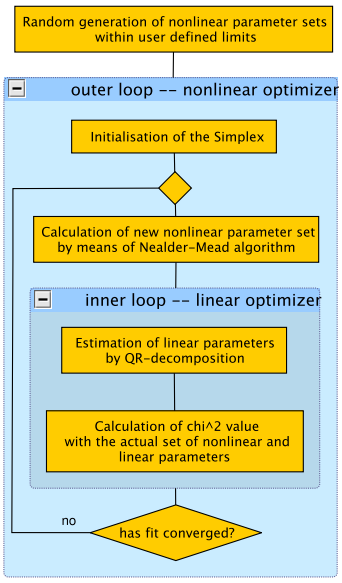

Figure 4.2: Flowchart of the fitting algorithm. For explanation see text.

Initially sets of nonlinear starting parameters are generated randomly from user defined ranges. During each iteration the Downhill-Simplex algorithm needs to benchmark the available sets of nonlinear parameters according to their figure of merit values $\chi^2_j(\vec{\alpha})$. To do so, for each set of nonlinear parameters $\vec{\alpha}$ also the linear parameters are determined by the GLLS solver. The GLLS solver forms the model design matrix $\mathbf{A}(\vec{\alpha})$ of the linear estimation problem based on the nonlinear parameters and functions. Having measured the data $\vec{d}$, the generalized linear least square problem to find $\vec{a}$ to fullfil

$$\mathbf{A}(\vec{\alpha})\,\vec{a} \approx \vec{d}$$

is solved by means of a QR decomposition $\mathbf{Q}\,\mathbf{R} = \mathbf{A}$ of the design matrix. The matrix $\mathbf{A}$ is separated into an unitary matrix $\mathbf{Q}$ and an upper triangular matrix $\mathbf{R}$. Since a system of linear equations equivalent to equation 4.3 is overdetermined and could not be solved directly, it is transformed by applying

the transposed matrix of $\mathbf{Q}$ from the left side

$$\mathbf{Q}^{\mathrm{T}}\mathbf{Q}\,\mathbf{R}\,\vec{a} \approx \mathbf{Q}^{\mathrm{T}}\vec{d}$$

into a directly solvable system of linear equations

$$\mathbf{R}\,\vec{a} = \mathbf{Q}^{\mathrm{T}}\,\vec{d} \quad .$$

The result is a complete set of parameters $(\vec{\alpha}, \vec{a})$ along with its figure of merit value $\chi^2(\vec{\alpha}, \vec{a})$. The $\chi^2(\vec{\alpha}, \vec{a})$ value is reported to the Downhill-Simplex algorithm. Following the scheme of the Nelder-Mead algorithm, out of the current sets of nonlinear parameters a new one is constructed and replaces the worst[1] old set. This way, the nonlinear parameters are improved towards the best fitting set in each iteration step. Likewise the optimal linear parameters are available all the time. The algorithm stops if a defined convergence criterion is reached. It is based on the size of the simplex and the number of iterations without any further reduction of the $\chi^2(\alpha, \vec{a})$ value. The realization of global data analysis was straight forward within this design, since the linked parameters were always nonlinear ones. Thus, it is only a matter of constructing more design matrices from the set of nonlinear parameters and solving more linear equations if more than one data set needs to be fitted globally. The $\chi^2(\vec{\alpha}, \vec{a})$ value is then the sum of all individual values obtained from the solutions of the generalized linear least squares calculations.

[1] The set with the largest χ^2 value.

5 Materials and Methods

5.1 Samples, Solvents, and Cuvettes

The investigated porphyrin-phthalocyanine-heterotriads were synthesized in the group of Prof. Ng (Hongkong University, Hongkong, China). Their synthesis is reported in Ermilov et al. (2006) and in Tannert et al. (2007). The solvent toluene (TOL) Uvasol® was purchased from Merck and dimethylformamid (DMF) spectroscopic grade from Aldrich. All other reagents and solvents were of reagent grade from different suppliers and used as received. Suprasil quartz glass cuvettes for absorption as well as for fluorescence spectroscopy were purchased from Hellma.

5.2 Steady State Absorption and Fluorescence Spectroscopy

The ground state absorption spectra were recorded using a commercial spectrophotometer Shimadzu UV-2501PC at room temperature. Steady-state fluorescence spectra were measured in $1\,\mathrm{cm} \times 1\,\mathrm{cm}$ quartz cuvettes using a combination of a cw-Xenon lamp (XBO 150) and a monochromator (Lot-Oriel, bandwidth 10 nm) for excitation and a polychromator with a cooled CCD matrix as detection system (Lot-Oriel, Instaspec IV) (Korth et al., 1995). To obtain fluorescence quantum yields, solutions of H_2TPP in DMF ($\Phi_{\mathrm{fl}} = 0.11$) (Seybold and Gouterman, 1969) and ZnTPP ($\Phi_{\mathrm{fl}} = 0.033$) (Strachan et al., 1997) in TOL were used as standards.

5.3 Decay Associated Fluorescence Spectra

Time correlated single photon counting (TCSPC) in combination with scanning of the detection wavelength was used to acquire decay associated fluorescence spectra (Knutson et al., 1982). A pulsed, frequency doubled, linear

polarized Nd:VO_4 laser (Cougar, Time Bandwidth Products) with a wavelength of 532 nm, a pulse width of 12 ps, and a repetition rate of 60 MHz was used to synchronously pump a dye laser (Model 599, Coherent) tunable in the range 610–670 nm. The samples were excited with radiation from one of the two lasers mentioned above. Optical density (OD) of the samples was less than 0.2 at the absorption band of lowest energy. Fluorescence was detected with a thermo-electrically cooled micro channel plate (R3809-01, Hamamatsu) under a polarization angle of 54.7 ° relative to excitation. Detection wavelength was chosen by a computer-controlled monochromator (77200, Lot-Oriel). Electrical signals were processed by a PCI TCSPC controller card (SPC630, Becker & Hickl). Data were analyzed by a homemade program applying a variable projection algorithm (Golub and Pereyra, 1973; Krogh, 1974) to the global fitting problem. The Nelder-Mead simplex algorithm (Nelder and Mead, 1965) was used for optimization of the nonlinear parameters, and the support plane approach (Lakowicz, 1999) to compute error estimates of the decay times. Model functions were sums of up to four exponentials convoluted by the instrument response function including a time shift. Decay times and time shift were linked through all measurements of one scan sampled every 2.5 nm in the detection window from 640 nm up to 740 nm.

5.4 Fluorescence Up-Conversion

Fast decay of fluorescence was measured by fluorescence up-conversion. The laser system for generation of ultra fast pulses for gating (800 nm) and excitation (300–1200 nm as desired) consisted of three lasers and an amplifier pumping an optical parametric amplifier (Verdi V6, Coherent; Mira 900D, Coherent; Merlin, Spectra Physics; Spitfire, Spectra Physics; TOPAS, Light Conversion Ltd.). The sample (about 15 ml) was pumped (mzr-7223, HNP-Mikrosysteme GmbH) through a homemade flow cell having a light pathway of 440 µm covered by two 170 µm fused silica windows. Excitation light was focused into the sample. Its polarization was set by a Berek compensator (Model 5540, New Focus). The fluorescence was imaged by a Cassegrain

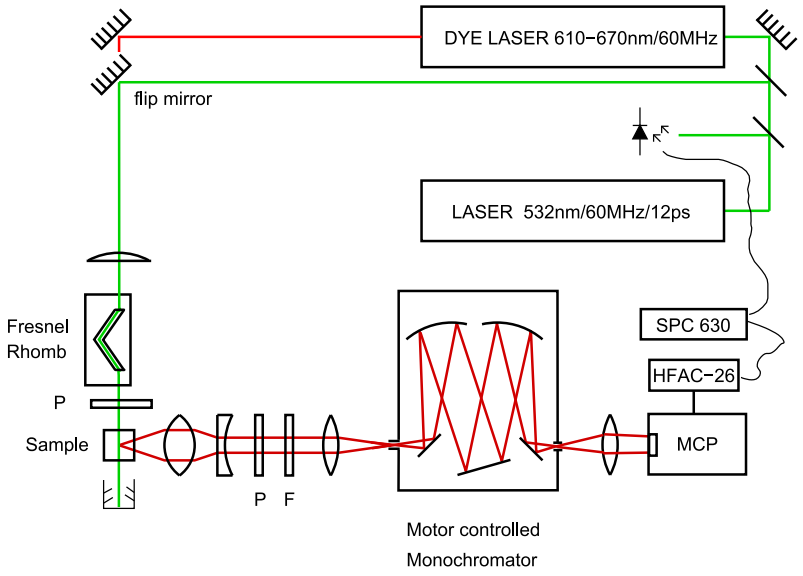

Figure 5.1: Scheme of Time Correlated Single Photon Counting setup. A 532 nm DPSS laser pumps a dye laser. The radiation of either one is used to excite the sample. The combination of a Fresnel rhombus followed by a polarizer P allows to vary the excitation power and sets the polarization. Fluorescence of the sample is collimated and analyzed by a second polarizer P. The cut off filter F enhances stray light rejection from the excitation. A motor controlled monochromator selects a narrow band from the fluorescence emission, which is detected by a multichannel plate MCP. Synchronization signals picked up by a photodiode and the amplified (amplifier HFAC-26) photon counting signals are processed by the TCSPC card SPC 630.

microscope objective (X15 NA 0.5, Ealing) onto a 300 µm thick BBO crystal used in type II interaction configuration. The up-converted light was collimated and refocused by quartz lenses onto the slit of a stepper motor actuated monochromator. Remaining gate beam portions and daylight were cut off by a bandpass filter (DUG11, Schott). An additional raman edge filter (RazorEdge 355nm, Semrock) blocked up-converted excitation stray light for excitation wavelengths below 638 nm. A thermo-electrically cooled photomultiplier (R2027, Hamamatsu) was read out in current mode by a lock-in amplifier (SR530, Stanford Research). The 100 mm long delay stage (M511.11, Physik Instrumente) allowing a maximum of 660 ps delay and the

lock in amplifier were remote controlled via computer. Ten recordings were averaged to give the final data.

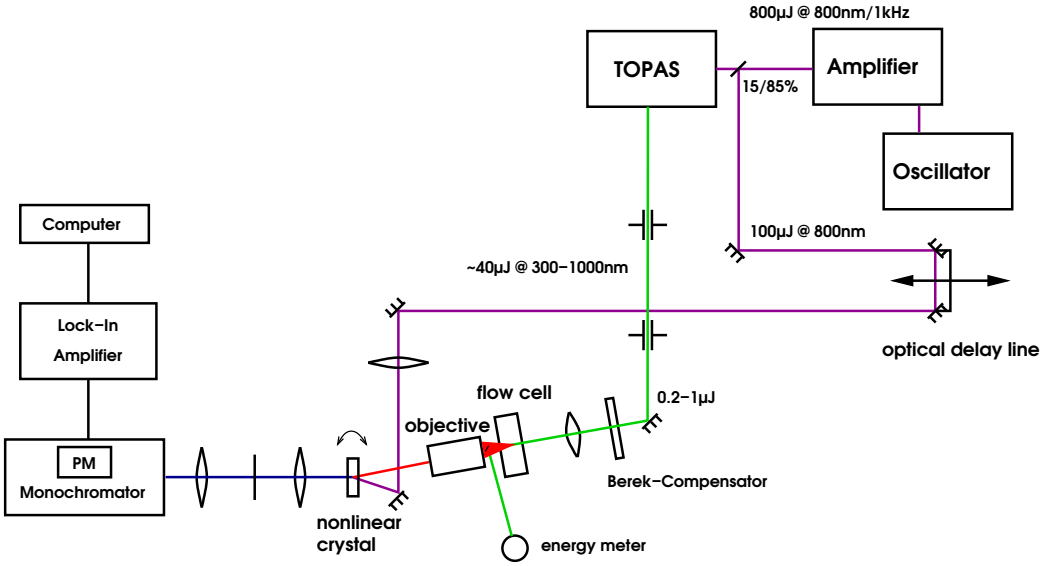

Figure 5.2: Scheme of the fluorescence up-conversion setup.

5.5 Transient Absorption Spectroscopy

TAS in the picosecond time regime

To measure transient absorption spectra, a white light continuum was generated as a test beam in a cell with a D_2O/H_2O mixture using intense 25 ps pulses from a Nd^{3+}:YAG laser (PL 2143A, Ekspla) at 1064 nm. Before passing through the sample, the continuum radiation was split to get a reference spectrum. The transmitted as well as the reference beams were focused into two optical fibers and were recorded simultaneously at different traces on a CCD-matrix (Lot-Oriel, Instaspec IV). Tuneable radiation from an OPO/OPG (Ekspla PG 401/SH, tuning range 200–2300 nm) pumped by the third harmonic of the same laser was used as an excitation beam. The mechanical delay line allowed the measurement of light-induced changes of the absorption spectrum at different delays up to 15 ns after excitation. The OD of all samples was 1.0 at the maximum of the absorption band of lowest

energy. Analysis of experimental data was performed using the compensation method (Rückmann et al., 1997).

5.6 Electron and Energy Transfer Theory

Photo-induced Electron Transfer (PIET)

Two molecules (D and A) may undergo an electron transfer reaction after photoexcitation building up the charge separated (CS) state $D^+ \cdots A^-$. For a comprehensive review read (Kavarnos and Turro, 1986). In this context D is understood as an electron donor and A as the electron acceptor.

$$\begin{aligned} \text{Donor photoexcited:} \quad & D^* \cdots A \quad \rightarrow \quad D^+ \cdots A^- \\ \text{Acceptor photoexcited:} \quad & D \cdots A^* \quad \rightarrow \quad D^+ \cdots A^- \end{aligned}$$

Which and if anyone of these two possible transfer reaction happens is determined by energetical laws. In case of bridged[1] systems with weakly electronically coupled electron donor and acceptor, the semi-classical Marcus theory applies. Important parameters controlling the rate (may also be interpreted as probability) of charge transfer k_{CT} are the free enthalpy ΔG_0 of charge transfer, the reorganization energy λ, the electronic coupling coefficient V, and the temperature T.

$$k_{\mathrm{CT}} = \frac{2\,\pi}{\hbar} \frac{V^2}{\sqrt{4\pi\, k_{\mathrm{B}}\, T\, \lambda}} \exp\left[-\frac{(\Delta G_0 + \lambda)^2}{4\, k_{\mathrm{B}}\, T\, \lambda} \right]$$

For weakly coupled systems, as the P-Pc-P triads under investigation are, the electronic coupling coefficient may only be derived from quantum chemical calculations (Onuchic et al., 1986). It was however beyond the scope of this work to perform these calculations. Therefore, V was treated as an a priori unknown, but well defined number.

The total nuclear reorganization energy λ can be considered as the sum of two parts,

$$\lambda = \lambda_{\mathrm{in}} + \lambda_{\mathrm{out}}$$

[1] Donor and acceptor are hold together by a bridge, denoted as D—A.

the inner λ_{in} and the outer λ_{out} reorganization energy. The inner reorganization energy accounts for the change of binding geometry within donor and acceptor during electron transfer and is therefore independent of solvent properties. For the class of P and Pc compounds its value is small and lies in the range of 0.1–0.3 eV (Gould et al., 1990, 1991). Changes of the free enthalpy due to reorientation of the solvent cage (Brunschwig et al., 1986) are expressed by the outer reorganization energy λ_{out} and can be estimated from the refractive index n and the dielectric constant of the solvent (ϵ_{s}), the separation distance R of the ions and their sizes r_{D^+} and r_{A^-}:

$$\lambda_{\text{out}} = \frac{e^2}{4\pi\,\epsilon_0}\left(\frac{1}{n^2} - \frac{1}{\epsilon_{\text{s}}}\right)\left(\frac{1}{2\,r_{\text{D}^+}} + \frac{1}{2\,r_{\text{A}^-}} - \frac{1}{R}\right)$$

The free enthalpy ΔG_0 of a photo-induced charge transfer reaction is a function of electrochemical, electronic and geometrical properties of the donor–acceptor system. Its theoretical form is called Rehm-Weller equation (Rehm and Weller, 1969; Weller, 1982). Here equation (5.1) is formulated for initially neutral reactants exchanging one electron.

$$\Delta G_0 = e\left(E^{\text{oxd}}_{1/2}(D/D^+) - E^{\text{red}}_{1/2}(A/A^-)\right) - E_{0,0} - \underbrace{\frac{e^2}{4\pi\,\epsilon_0\,\epsilon_{\text{s}}\,R}}_{\text{Coulomb term}} + \underbrace{\frac{e^2}{8\pi\,\epsilon_0}\left(\frac{1}{r_{\text{D}^+}} + \frac{1}{r_{\text{A}^-}}\right)\left(\frac{1}{\epsilon_{\text{ec}}} - \frac{1}{\epsilon_{\text{s}}}\right)}_{\text{Born term}} \tag{5.1}$$

Being a redox reaction, the free enthalpy is mainly determined by the electrochemical reduction potential of the electron acceptor $E^{\text{red}}_{1/2}(A/A^-)$ and the oxidation potential of the donor $E^{\text{oxd}}_{1/2}(D/D^+)$. However, without absorption of a light quantum, the transfer is energetically unfavorable. Uptake of a photon's energy $E_{0,0}$ (i.e. photo-excitation of the donor or acceptor) prepares the system to undergo charge transfer. Therefore, this type of charge transfer is termed "photo-induced". Furthermore, the electrostatic energy of the finally created ions of the charge separated state contributes to the free enthalpy. The coulomb term accounts for the work of the created ions. It

depends on the distance R of both ions and the dielectric constant ϵ_s of the matter in between (Suppan, 1986). As a matter of fact, measurements of the redox potentials are typically conducted in one solvent working well for this type of measurement. However samples undergoing PIET are investigated often in other solvents than the one in which the redox potentials were determined. Using Born's theory about solvation energy of ions (Born, 1920), the redox potentials are corrected for that by the "Born term". It includes the dielectric constant ϵ_{ec} of the solvent of voltammetric measurements, and the dielectric constant ϵ_s of the solvent where the PIET is ongoing. Regrettably, the charge separated state lasts not forever[2], once built up. Charge recombination $D^+—A^- \rightarrow D—A$ destroys the charge separated state with a rate of k_{CR}.

One must be aware of the fact that the constituents of a charge transfer system may exchange their role within the same system depending on initial excitation. Imagine a system $P—Pc$ where P acts as donor D and Pc as acceptor A, if D gets excited initially. Supposed the electron transfer $D^*—A \rightarrow D^+—A^-$ is favorable, its rate will be denoted by k_{ET}. Maintaining the assignments $D \leftarrow P$, $A \leftarrow Pc$, excitation of Pc alias A might result in the following charge transfer reaction: $D—A^* \rightarrow D^-—A^+$, with D not being the electron donor anymore. Following our initial definition one has to reassign the role of P and Pc in terms of donor and acceptor. To avoid confusion the alias names D and A are only used in the general case when D is really the electron donor and A the acceptor, respectively. In order to distinguish between the rate constants of these different charge transfer reactions, the nomenclature in this work is to call the reaction:

$$P^*—Pc \rightarrow P^+—Pc^- \quad \textbf{electron transfer} \text{ with rate } k_{ET}$$

and the reaction

$$P—Pc^* \rightarrow P^+—Pc^- \quad \textbf{hole transfer} \text{ with rate } k_{HT}.$$

[2]The core problem of all the efforts to use sunlight as a source of electric energy.

Charge separation can be a reversible process, and charge back transfer $P^+—Pc^- \rightarrow P—Pc^*$ might happen. The associated rate constant of back hole transfer is denoted k_{BHT}.

Förster Resonance Energy Transfer

Two distinct molecules may exchange electronic energy even without intermediate emission and absorption of photons. One type of this radiation-less energy transfer between fluorophores is called "Förster"- or "Fluorescence resonance energy transfer" (FRET). The first notation honors the extensive work of Theodor Förster in this field of research. He was the first, who interpreted this phenomenon in a profound theoretical framework. (Förster, 1946, 1948, 1949a, 1960)

FRET is a bimolecular process, $D^* + A \rightarrow D + A^*$, where an excited donor molecule D^* transfers its electronic energy to an acceptor A residing in the ground state prior to transfer. The transfer results in an unexcited donor D and an excited acceptor A^*.

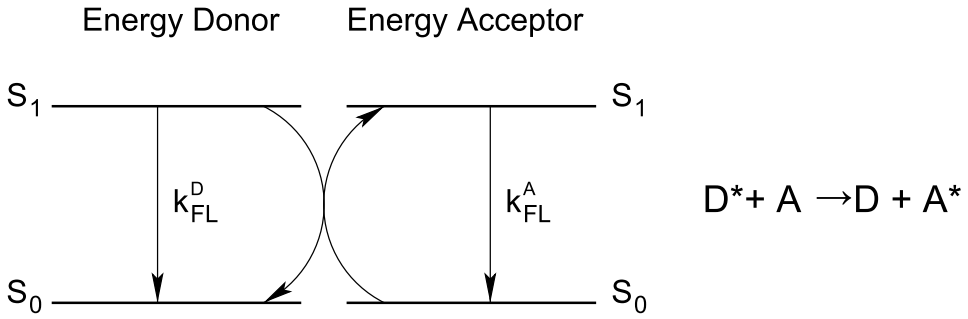

Figure 5.3: Jabłonski diagram depicting directed energy transfer between a donor and an acceptor molecule.

Dipol-dipol interaction leads to transfer of excitation energy if donor and acceptor come close enough to each other and take a favorable orientation. The interaction strength is usually expressed by means of the Förster ra-

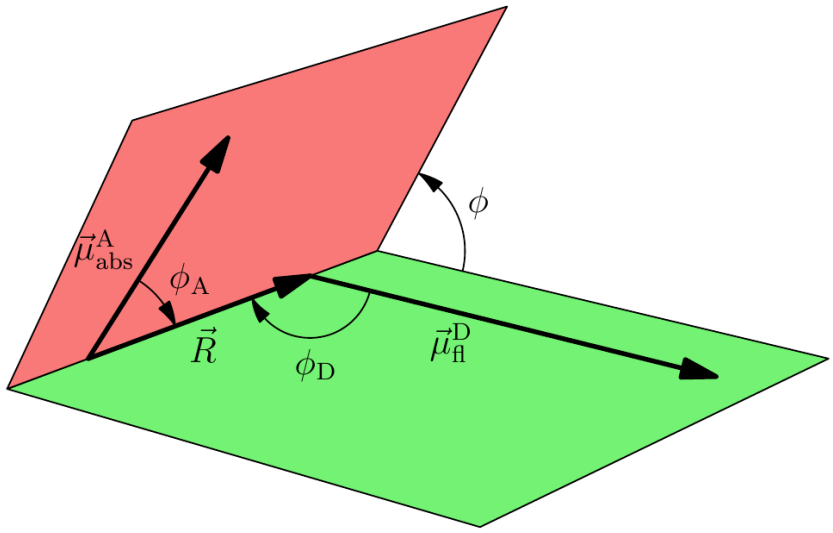

Figure 5.4: Definition of angles (ϕ, ϕ_{A}, ϕ_{D}) for the calculation of the orientation factor (κ^2). Vector $\vec{R}$ describes the distance between the point dipoles of donor (dipole momentum $\vec{\mu}^{\mathrm{D}}_{\mathrm{fl}}$) and acceptor (dipole momentum $\vec{\mu}^{\mathrm{A}}_{\mathrm{abs}}$).

dius R_0 and commonly described by its transfer rate k_{EET}.

$$k_{\mathrm{EET}} = \frac{1}{\tau_{\mathrm{D}}} \left(\frac{R_0}{R}\right)^6$$

The Förster radius is defined as that distance of donor and acceptor, when the energy transfer rate equals the sum of all other depopulating channels of the excited state of the donor. The actual distance of both interacting partners is denoted as R and the experimental donor fluorescence lifetime in the absence of the acceptor as τ_{D}.

Considering two fluorophores, energy transfer becomes favorable if the fluorescence spectrum $I_{\mathrm{fl}}(\tilde{\nu})$ of the energy donating one exhibits a nonzero overlap J with the absorption spectrum $\epsilon(\tilde{\nu})$ of the energy accepting one. Usually, both spectra are expressed in terms of the wavenumber $\tilde{\nu}$.

$$J = \int I^{\mathrm{n}}_{\mathrm{fl}}(\tilde{\nu})\, \epsilon(\tilde{\nu}) \frac{\mathrm{d}\tilde{\nu}}{\tilde{\nu}^4}$$

Normalizing the integrated fluorescence spectrum ($\int I^{\mathrm{n}}_{\mathrm{fl}}(\tilde{\nu})\mathrm{d}\tilde{\nu} = 1$), the fluorescence quantum yield (Φ_{fl}) of the donor in absence of an acceptor enters

the calculation of R_0^6 as a linear scaling factor. Energy transfer, being of electromagnetic nature, also depends on the fourth power of the refractive index of the matter filling the space between donor and acceptor (Knox and van Amerongen, 2002). Avogadro's number (N_A) converts between the amount of substance originating from the absorption coefficient ε and the number of molecules.

$$R_0^6 = \kappa^2 \, \frac{9000(\ln 10)\Phi_\mathrm{fl}}{128\pi^5 n^4 \, N_\mathrm{A}} \, J$$

Finally the strength of interaction depends on the orientation of the interacting dipole moments of donor and acceptor. Assuming the donor and acceptor are fixed in space to each other, κ^2 can be expressed by three angles (ϕ, ϕ_A, ϕ_D), see figure 5.4.

$$\kappa^2 = \Big(\sin(\phi_\mathrm{D}) \, \sin(\phi_\mathrm{A}) \, \cos(\phi) - 2 \, \cos(\phi_\mathrm{D}) \, \cos(\phi_\mathrm{A}) \Big)^2$$

Two intersecting planes are spanned by the emission dipole moment vector $\vec{\mu}_\mathrm{fl}^\mathrm{D}$ of the donor, the absorption dipole moment vector $\vec{\mu}_\mathrm{abs}^\mathrm{A}$ of the acceptor, and the joining vector $\vec{R}$. Vector $\vec{R}$ is coincident with the intersection line of both planes. The angle between these planes is measured as ϕ. In plane, the dipole moments and the joining vector enclose an angle each, ϕ_D and ϕ_A, respectively.

The numerous additional constants in the formula of R_0^6 arise from unit conversions in a way that the numerical values need to be inserted with the following units: $[\varepsilon]$=$\mathrm{M}^{-1}\,\mathrm{cm}^{-1}$ and $[\tilde{\nu}]$=cm^{-1}, resulting in $[R_0^6]$=cm^6.

6 Novel P-Pc-P Heterotrimers

Introduction of Ps and Pcs

While searching for optimal artificial organic light converters, many classes of molecules have been investigated to achieve light harvesting and charge separation. Among all suitable chromophores able to absorb sunlight and exhibiting desirable characteristics to undergo charge separation further on, Ps and Pcs, depicted in figure 6.1, play an important role. Both classes of tetrapyrroles have been extensively investigated and their synthetic chemistry has already been established for a long time. Despite the extensive studies and wide applications of individual Ps and Pcs, the approach of combining Ps and Pcs to build P-Pc hetero-complexes is relatively new, and only a few examples of hetero P-Pc arrays have been described as light-harvesting and/or charge-separation systems until today.

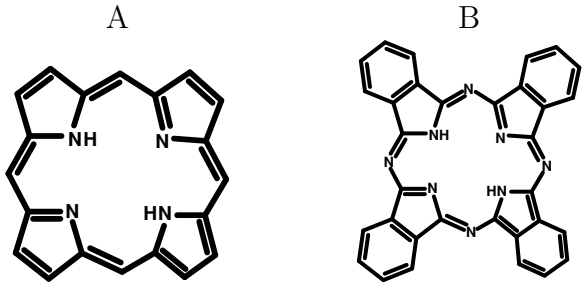

Figure 6.1: Basic chemical structures of A) Porphyrin and B) Phthalocyanine.

From a chemical point of view, free base Ps and Pcs are both cyclic tetrapyrroles belonging to the chemical class of annulenes. Their typical geometry is nearly planar, but special substituents may also bend the molecule (Wiehe et al., 2001b). They exhibit a conjugated cyclic π-electron system. This extended π-system constitutes their optical properties apparent by the strong coloring of Ps and Pcs. They may be classified further as „free base"

(two hydrogen atoms bound in the center) and „metallo" (a metal atom as ligand in the center) -Ps or -Pcs. These two classes differ in their symmetry and the number of conjugated π-electrons. The free bases belong to the D_{2h} symmetry class and exhibit 18 π-electrons, whereas the metal complexes show the higher D_{4h} symmetry and exhibit 16 π-electrons. The different symmetry directly influence their optical properties (Gouterman, 1961; Hollas, 1998). Substituents may strongly influence the photo-physical and electrochemical properties as well. The following more detailed description should, therefore, be understood as a general overview only, since numerous varieties exist. Despite their close relationship, Ps and Pcs differ substantially. Since Pcs may be seen as derivatives of Ps, the latter will be characterized first.

Ps and their derivatives are found manifold in nature. They play a key role in photosynthesis, oxygen transport in the blood, respiration, and act as enzymes in other places (Battersby, 2000). Chemical research on this substance class began about 1840 (With, 1980).

Free base Ps typically show three electronic transitions in the near UV to visible spectral region: a very strong transition, called "B-band" around 400 nm, and two less intense transitions ("Q-bands") ranging from 500 to 700 nm. The latter $\pi \rightarrow \pi^\star$ transitions (Corwin et al., 1968) exhibit a vibrational side band, each. The nomenclature of the absorption band names goes back to Platt (1949, 1950). Due to the higher symmetry, the Q-bands of metallo-Ps degenerate into a single one, such as for zinc tetraphenylporphyrin (ZnTPP).

A first simple theoretical model of Ps absorption spectra was reported by Simpson (Simpson, 1949). An extended description, based on the theory of linear combination of atomic orbitals (LCAO) (Mulliken, 1939a,b) was developed by Platt and coworkers (Longuet-Higgins et al., 1950). Bringing all knowledge together, Gouterman introduced a four orbital model, describing the optical transitions within Ps (Gouterman, 1959, 1961). With this simple model, for the first time the specific oscillator strength of the different bands could be described in a qualitative way. It assigns the experimentally observable bands to transitions between mixed states of four molecular orbitals. The two lowest unoccupied molecular orbitals and the two highest

occupied molecular orbitals are identified with the four mixing states.

Ps do not only absorb strongly, they also exhibit considerable fluorescence quantum yields. Further on, the triplet system is populated by intersystem crossing. A comprehensive overview about Ps is given in the textbooks of Dolphin (1978) and Falk and Smith (1975).

Contrary to the Ps, Pcs are synthetic chemicals. Their discovery dates back to 1907. Braun and Tcherniac (1907) reported the appearance of a blue-colored deposit as an unknown byproduct. In 1927, de Diesbach and von der Weid (1927) described the synthesis of a blue colored compound with high stability and hypothesized that it was a complex salt of copper. However, they did not appreciate its importance and did not fully characterize these complexes. Another accidental synthesis, that of iron Pc in 1928 by a dye producing company, triggered further directed investigations. In 1934 Linstead et al. reported about the synthesis and structure of Pcs in a series of articles (Linstead, 1934a,b,c,d,e,f).

At first used as very stable and very bright green and blue dyes, Pcs were introduced into many other applications over the years. Nowadays they are used in organic solar cells, as semi-conducting layers in printers, as optical limiters, for waste water cleaning, as dyes for optical storage media, organic light emitting diodes, sensors for gases etc. (Claessens et al., 2008).

Similar to Ps, the absorption properties of Pcs are dominated by bands in the near UV and in the red region of the visible spectrum. Whereas the two HOMO orbitals are nearly degenerated in Ps, they have clearly distinct energy levels in Pcs as a consequence of the four aza-groups and the four benzene rings influencing the π electron ring system (Stillmann, 1989; Mack and Stillman, 2003). As a result, the oscillator strength of the Q bands is much higher than that of the B bands in Pcs.

Introduction to P-Pc compounds

In 1984 Gaspard introduced the idea of pairing P and Pc by ionic interaction (Gaspard, 1984). Later, Tran-Thi and colleagues (Gaspard et al., 1986) reported the first covalently bound P-Pc dimer. Another type of mixed P-Pc

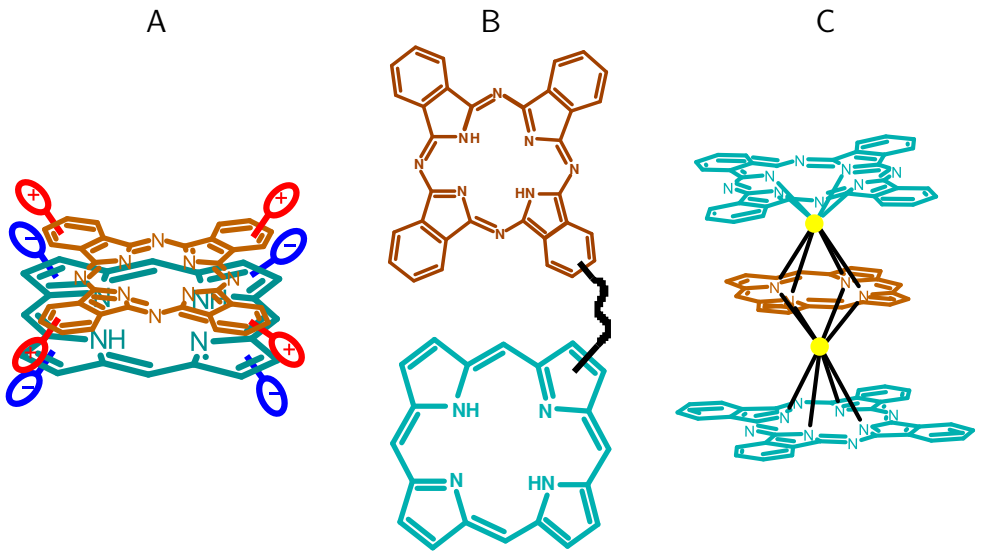

Figure 6.2: Binding motives of P-Pc-heteromers. A) Ionic interaction B) Covalent coupling C) Metal coordination of sandwich type

arrays are sandwich complexes such as the cerium(IV) complex Ce(P)Pc, synthesized by Lachkar et al. (Lachkar et al., 1988). Hence, there are three major groups of P-Pc systems (Tran-Thi, 1997; Ng and Jiang, 1997; Kobayashi, 2002), namely self-assembled ionic systems (figure 6.2A), covalently coupled systems (figure 6.2B), and metal coordinated ones (see figure 6.2C, and figure 6.3). The latter include sandwich-type metal complexes in which the tetrapyrrolic ligands are held face to face by metal atoms, and axially bound systems (Choi et al., 2004; Kobuke, 2006).

Sandwich-type metal complexes and self-assembled ionic systems (both typically face-to-face oriented) are not described in detail in the following section, since there properties differ substantially from the investigated axially bound systems.

A variety of covalently linked and axially bound P-Pc systems have been reported (Gaspard et al., 1986; Kobayashi et al., 1987; Tran-Thi et al., 1989; Tian et al., 1993; Li et al., 1999; Li and Lindsey, 1999; Miller et al., 2000; Yang et al., 2000; Maree and Nyokong, 2001; Sutton and Boyle, 2001; Berber et al., 2003; Cammidge et al., 2005; Zhao et al., 2005a,b; Pereira et al., 2005; Tomé et al., 2006; Ito et al., 2006). However, only a few of them exhibit energy-

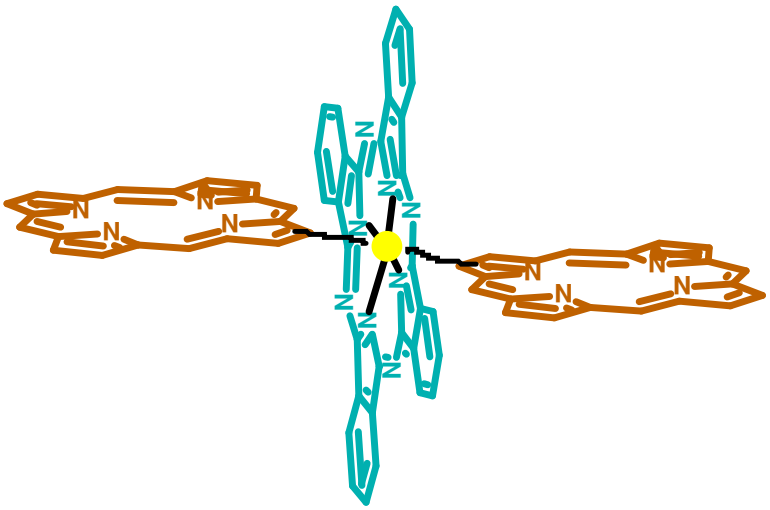

Figure 6.3: Binding motive of a metal-coordinated axially bound P-Pc-P heterotrimer, like the ones investigated in this work. Ps are shown in brown, SiPc is shown in blue, and the coordinating silicon atom is shown in yellow.

and charge-transfer characteristics. (Tran-Thi et al., 1989; Tian et al., 1996; Li et al., 1999; Miller et al., 2000; Yang et al., 2000; Zhao et al., 2005a,b). Lindsey et al. reported a series of mixed P-Pc arrays, which are efficient light harvesters, but electron transfer was not detected in these systems (Li et al., 1999; Miller et al., 2000; Yang et al., 2000).

Tran-Thi et al. carried out a detailed study of competing intramolecular electron and energy transfer processes in a covalently linked P-Pc heterodimer (Tran-Thi et al., 1989), in which the fluorescence of the Pc was quenched and a fast decaying component of Pc emission appeared. This first report on intramolecular transfer processes in a covalently linked P-Pc heterodimer postulated electron transfer competing with energy transfer. Interpretation was based on the quenched fluorescence of Pc and the appearance of a fast decaying component of the Pc. The existence of the assumed more probable electron transfer process was found to be solvent-dependent. It was argued that conformational changes due to solvent polarity favor charge transfer in the polar solvent DMSO. Processes occurring in peripherically, covalently coupled heterodimers, -trimers, and -nonamers (Zhao et al., 2005a,b) were interpreted in the same framework.

Following the successful use of axial coordination by central metal atoms in P and Pc chemistry by Ng et al., this approach became attractive to others. As a result a number of model compounds for artificial photosynthesis utilizing Ps and/or Pcs were synthesized and characterized up to now. Fullerenes coupled to either Ps or Pcs were already used successfully in numerous model systems before (El-Khouly et al., 2004). In the realm of this success fullerenes were coupled by axial ligation to SiPc (El-Khouly et al., 2007; Martin-Gomis et al., 2007, 2008; El-Khouly et al., 2009). The review of Fukuzumi et al. (2009) summarizes structures known in the year 2009. Also other dyes are ligated to SiPc as in the boron dipyrromethene SiPc triad (Ermilov et al., 2009). A self assembling approach is followed in a triad where two cyclodextrins are axial ligands of SiPc. Tetrasulfonated P is able to bind to cyclodextrin and forms then a functional system exhibiting energy and charge transfer (Ermilov et al., 2011).

Later also zinc phthalocyanine (ZnPc) was used in dyads (Maligaspe et al., 2010) exhibiting energy transfer, and in a tetrad built of subPc, triphenylamine, ZnPc, and fullerene (El-Khouly et al., 2010). This tetrad transfers excitation energy efficiently from the subPc to the ZnPc and forms a long-lived charge separated state. Axial ligation was also beneficial to build arrays of Ps and Pcs exhibiting strong and broadband absorption (Zhao et al., 2009, 2010; Cammidge et al., 2011; Tong et al., 2011). These arrays are suggested as light harvesters in DSSCs and OPVs.

Despite axial coordination is considered an easier synthetic route than covalent coupling, there are still a couple of new covalently linked P-Pc supramolecules synthesized (Osati et al., 2010; Pereira et al., 2011; Hausmann et al., 2010).

6.1 Aim of investigating new Heterotrimers

In the year 2000 the big majority of metal-coordinated P-Pc systems, where the detailed photophysics has been investigated before, were of the sandwich type. The strong interaction of the heterocycles in this binding motif, however, does not allow for energy or electron transfer processes within the supra-

molecular framework useful for light conversion. Having the modern design principles for artificial light converters in mind, coordinative chemistry, using stable chromophores with suitably tuned electrochemical properties, seemed to be a way towards new promising light converters, if axial binding of the moieties could be achieved. The first edge-to-face supra-molecular assembly of two Ps and a SiPc by Ng et al. (Li and Ng, 2000) filled that gap and made detailed experimental investigations of this new type of P-Pc-P heteromers possible. During a diploma thesis (Vogel, 2005) these new compounds were investigated initially. However, no final result could be obtained. This work was aimed to clarify the photo-physics in terms of occurring electron and energy transfer in detail.

6.2 Structure of the Investigated Heterotrimers

The heterotrimers under investigation (cf. figure 6.4) are of the axial binding by metal coordination type. They consist of two Ps and one Pc. The central silicon atom of the Pc acts as metal coordination center for the oxygen atom bound to one *meso*-phenyl substituent of each of the two Ps. Since

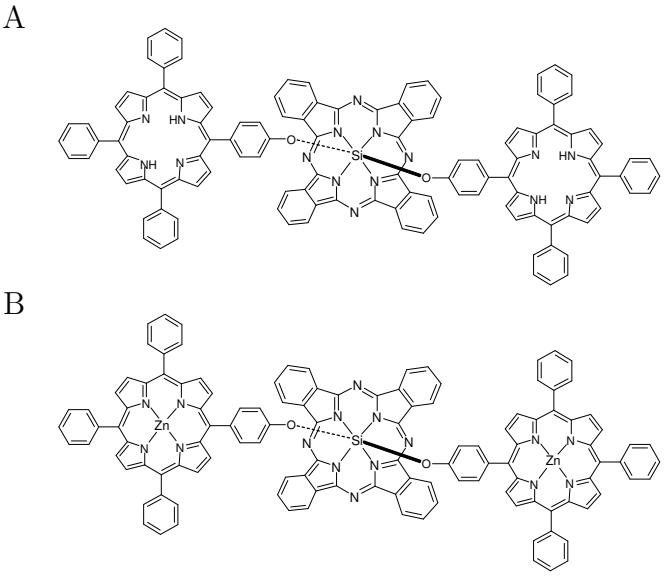

Figure 6.4: Chemical structure of the investigated P-Pc-P heterotrimers. A) Structural formula of H_2TPP-SiPc-H_2TPP B) Structural formula of ZnTPP-SiPc-ZnTPP

the electrochemical properties influence the charge transfer strongly, it is advantageous to compare systems with different properties. For this reason two types of P-Pc-P-heterotrimers were synthesized. In one case the axial ligands are free base tetraphenylporphyrins (H_2TPP), thus yielding H_2TPP-SiPc-H_2TPP (H_2Tr), in the other case ZnTPPs build the metalated form ZnTPP-SiPc-ZnTPP (ZnTr). The axial coordination of the two Ps hinders planar stacking, and thus the build-up of a sandwich type complex. Moreover, solvent polarity should have a minor influence on the molecular geometry in this configuration. This helps to compare and understand the energy and electron transfer independent of steric aspects.

6.3 Electrochemical Properties

In order to estimate the energetics of possible charge transfer processes, the redox potentials of all investigated compounds were measured in the group of Prof. Ng (detailed data not shown). The reference electrode was calibrated with ferrocene. Its redox potential is known in CH_2Cl_2 as +0.45V against a saturated calomel electrode (SCE). The potential was measured as +0.207V against an Ag/Ag^+ electrode within the used setup.

Table 6.1: Electrochemical data[a] of the investigated triads (H_2Tr, ZnTr), and its reference compounds H_2TPP, ZnTPP, and SiPcPy.

Compound	$E_{1/2}(X/X^{2+})$	$E_{1/2}(X/X^{+})$	$E_{1/2}(X/X^{-})$	$E_{1/2}(X/X^{2-})$
H_2TPP	1.30	0.96	-1.29	-1.61
ZnTPP	1.11	0.79	-1.41	-1.64
$SiPcPy_2$	—	1.32	-0.59	-1.00
H_2Tr	1.11	0.90	-0.66	-1.11
ZnTr	1.12	0.77	-0.67	-1.02

[a]Recorded with $[Bu_4N][PF_6]$ as electrolyte in CH_2Cl_2 (0.1 M) at ambient temperature. Potentials were obtained by cyclic differential pulse voltammetry with a scan rate of 100 mV s^{-1}, and are expressed as half wave potentials ($E_{1/2}$) in volts relative to a SCE.

It is reasonable to assume from the data that the first oxidation potential of the triads originates from the Ps and the first reduction potential stems

from the Pc, as these are the closest and most meaningful assignments (c.f. table 6.1).

6.4 Kinetic Models

Excitation, emission, and transfer processes change the electronic state of chromophores. In order to analyze the data obtained by spectroscopic measurements, one needs mathematical models describing the population density of all investigated energy levels. The necessary model is developed in the following. Figure 6.5 shows the four relevant states related to energy

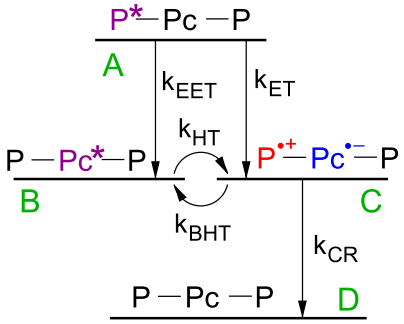

Figure 6.5: The four relevant energy levels and their connecting transitions of the P-Pc-P trimers. The first excited singlet state S_1 is denoted by *. The charge distribution of the charge separated state is indicated by $^+$ and $^-$. Rate constants are abbreviated as follows: energy transfer = k_{EET}, electron transfer = k_{ET}, hole transfer = k_{HT}, back hole transfer = k_{BHT}, charge recombination = k_{CR}

and electron transfer within the P-Pc triads investigated in this work. In ground state D neither a P nor the Pc is excited. This state is reached after an adequate long period past an excitation. Depending on the wavelength of the excitation pulse, state A (P excited) or state B (Pc excited) may be reached by excitation. From state A energy transfer (k_{EET}) leads to state B or electron transfer (k_{ET}) to the charge separated state C. Another pathway of charge transfer, hole transfer (k_{HT}), conveys state B into state C. Also the reverse process, back hole transfer (k_{BHT}), is possible and brings the compound from state C into state B. State C undergoes charge recombination (k_{CR}) leading to the compound residing in the ground state D. The

transitions from state A and B directly into the ground state (namely internal conversion and fluorescence) which of course exist are omitted from the calculation due to their small rate constants compared to the competing processes. For the same reason transitions into the triplet systems of P and Pc are neglected.

From the scheme in figure 6.5 a system of differential equations was derived and solved for the constrained of having only state A populated at time zero. Comparing the short pulse width of the excitation pulse with the rate constants, the approximation of having an instantaneous populated state A holds true.

$$\begin{pmatrix} \dot{A} \\ \dot{B} \\ \dot{C} \\ \dot{D} \end{pmatrix} = \begin{pmatrix} -(k_{\mathrm{EET}} + k_{\mathrm{ET}}) & 0 & 0 & 0 \\ k_{\mathrm{EET}} & -k_{\mathrm{HT}} & k_{\mathrm{BHT}} & 0 \\ k_{\mathrm{ET}} & k_{\mathrm{HT}} & -(k_{\mathrm{BHT}} + k_{\mathrm{CR}}) & 0 \\ 0 & 0 & k_{\mathrm{CR}} & 0 \end{pmatrix} \begin{pmatrix} A \\ B \\ C \\ D \end{pmatrix}$$

Since state D is lonely linked with one transition, the system can be simplified to:

$$\begin{pmatrix} \dot{A} \\ \dot{B} \\ \dot{C} \end{pmatrix} = \begin{pmatrix} -(k_{\mathrm{EET}} + k_{\mathrm{ET}}) & 0 & 0 \\ k_{\mathrm{EET}} & -k_{\mathrm{HT}} & k_{\mathrm{BHT}} \\ k_{\mathrm{ET}} & k_{\mathrm{HT}} & -(k_{\mathrm{BHT}} + k_{\mathrm{CR}}) \end{pmatrix} \begin{pmatrix} A \\ B \\ C \end{pmatrix}$$

The eigenvalues are determined by:

$$\begin{vmatrix} -(k_{\mathrm{EET}} + k_{\mathrm{ET}}) - \lambda & 0 & 0 \\ k_{\mathrm{EET}} & -k_{\mathrm{HT}} - \lambda & k_{\mathrm{BHT}} \\ k_{\mathrm{ET}} & k_{\mathrm{HT}} & -(k_{\mathrm{BHT}} + k_{\mathrm{CR}}) - \lambda \end{vmatrix} = 0$$

Evolving the determinant for its first row gives:

$$\Big(-(k_{\mathrm{EET}} + k_{\mathrm{ET}}) - \lambda \Big) \begin{vmatrix} -k_{\mathrm{HT}} - \lambda & k_{\mathrm{BHT}} \\ k_{\mathrm{HT}} & -(k_{\mathrm{BHT}} + k_{\mathrm{CR}}) - \lambda \end{vmatrix} = 0$$

The first eigenvalue is: $\boxed{\lambda_1 = -(k_{\mathrm{EET}} + k_{\mathrm{ET}})}$

Two additional eigenvalues result from:

$$(k_{\mathrm{HT}} + \lambda)\,(k_{\mathrm{BHT}} + k_{\mathrm{CR}} + \lambda) + k_{\mathrm{HT}}\,k_{\mathrm{BHT}} = 0$$

Introducing

$$k_{\mathrm{S}} = k_{\mathrm{HT}} + k_{\mathrm{BHT}} + k_{\mathrm{CR}}$$

and expanding leads to:

$$\lambda^2 + k_{\mathrm{S}}\,\lambda + k_{\mathrm{HT}}\,k_{\mathrm{CR}} = 0$$

The second and third eigenvalue are: $\boxed{\lambda_{2,3} = -\frac{k_{\mathrm{S}}}{2} \pm \sqrt{\frac{k_{\mathrm{S}}^2}{4} - k_{\mathrm{HT}}\,k_{\mathrm{CR}}}}$

With an exponential ansatz of the form

$$\begin{aligned} A(t) &= A_1\,e^{\lambda_1 t} + A_2\,e^{\lambda_2 t} + A_3\,e^{\lambda_3 t} \\ B(t) &= B_1\,e^{\lambda_1 t} + B_2\,e^{\lambda_2 t} + B_3\,e^{\lambda_3 t} \\ C(t) &= C_1\,e^{\lambda_1 t} + C_2\,e^{\lambda_2 t} + C_3\,e^{\lambda_3 t} \end{aligned}$$

the coefficients of the derivations are identified with that of the system of

equations to:

$$\begin{aligned}
A_1\,\lambda_1 &= -(k_{\mathrm{EET}} + k_{\mathrm{ET}})\,A_1 \\
A_2\,\lambda_2 &= -(k_{\mathrm{EET}} + k_{\mathrm{ET}})\,A_2 \\
A_3\,\lambda_3 &= -(k_{\mathrm{EET}} + k_{\mathrm{ET}})\,A_3
\end{aligned}$$

$$\begin{aligned}
B_1\,\lambda_1 &= k_{\mathrm{EET}}\,A_0 - k_{\mathrm{HT}}\,B_1 + k_{\mathrm{BHT}}\,C_1 \\
B_2\,\lambda_2 &= -k_{\mathrm{HT}}\,B_2 + k_{\mathrm{BHT}}\,C_2 \\
B_3\,\lambda_3 &= -k_{\mathrm{HT}}\,B_3 + k_{\mathrm{BHT}}\,C_3
\end{aligned}$$

$$\begin{aligned}
C_1\,\lambda_1 &= k_{\mathrm{ET}}\,A_0 + k_{\mathrm{HT}}\,B_1 - (k_{\mathrm{BHT}} + k_{\mathrm{CR}})\,C_1 \\
C_2\,\lambda_2 &= k_{\mathrm{HT}}\,B_2 - (k_{\mathrm{BHT}} + k_{\mathrm{CR}})\,C_2 \\
C_3\,\lambda_3 &= k_{\mathrm{HT}}\,B_3 - (k_{\mathrm{BHT}} + k_{\mathrm{CR}})\,C_3
\end{aligned}$$

The equations for state A result in the solution $A_2 = A_3 = 0$ and A_1 determined by the boundary conditions. If A_0 is the population of state A at time zero, $A_1 = A_0$. The values of B_1 and C_1 are determined by a system of linear equations:

$$\begin{aligned}
(\lambda_1 + k_{\mathrm{HT}})\;B_1 \;+\; & -k_{\mathrm{BHT}}\;C_1 &&= k_{\mathrm{EET}}\,A_0 \\
-k_{\mathrm{HT}}\;B_1 \;+\; & (\lambda_1 + k_{\mathrm{BHT}} + k_{\mathrm{CR}})\;C_1 &&= k_{\mathrm{ET}}\,A_0
\end{aligned}$$

$$B_1 = \frac{\begin{vmatrix} k_{\mathrm{EET}}\,A_0 & -k_{\mathrm{BHT}} \\ k_{\mathrm{ET}}\,A_0 & (\lambda_1 + k_{\mathrm{BHT}} + k_{\mathrm{CR}}) \end{vmatrix}}{\begin{vmatrix} (\lambda_1 + k_{\mathrm{HT}}) & -k_{\mathrm{BHT}} \\ -k_{\mathrm{HT}} & (\lambda_1 + k_{\mathrm{BHT}} + k_{\mathrm{CR}}) \end{vmatrix}}$$

$$C_1 = \frac{\begin{vmatrix} (\lambda_1 + k_{\mathrm{HT}}) & k_{\mathrm{EET}}\,A_0 \\ -k_{\mathrm{HT}} & k_{\mathrm{ET}}\,A_0 \end{vmatrix}}{\begin{vmatrix} (\lambda_1 + k_{\mathrm{HT}}) & -k_{\mathrm{CR}} \\ -k_{\mathrm{HT}} & (\lambda_1 + k_{\mathrm{BHT}} + k_{\mathrm{CR}}) \end{vmatrix}}$$

Expanding and introducing two new variables κ and ζ gives:

$$B_1 = \kappa\, A_0 \qquad \kappa = \frac{k_{\mathrm{EET}}(\lambda_1 + k_{\mathrm{BHT}} + k_{\mathrm{CR}}) + k_{\mathrm{BHT}}\, k_{\mathrm{ET}}}{\lambda_1(\lambda_1 + k_{\mathrm{HT}} + k_{\mathrm{BHT}} + k_{\mathrm{CR}}) + k_{\mathrm{HT}}\, k_{\mathrm{CR}}}$$

$$C_1 = \zeta\, A_0 \qquad \zeta = \frac{k_{\mathrm{ET}}\,(\lambda_1 + k_{\mathrm{HT}}) + k_{\mathrm{HT}}\, k_{\mathrm{EET}}}{\lambda_1(\lambda_1 + k_{\mathrm{HT}} + k_{\mathrm{BHT}} + k_{\mathrm{CR}}) + k_{\mathrm{HT}}\, k_{\mathrm{CR}}}$$

The amplitudes B_2, B_3, C_2, and C_3 of the exponential functions are determined by the system of linear equations

$$(\lambda_i + k_{\mathrm{HT}})\; B_i \;\; - \;\; k_{\mathrm{BHT}}\; C_i \;\; = \;\; 0 \qquad i = 2, 3$$

Introduction of $\gamma_i = \dfrac{\lambda_i + k_{\mathrm{HT}}}{k_{\mathrm{BHT}}}$ simplifies the relation between B_i and C_i to $C_i = \gamma_i\, B_i$.

From the boundary conditions $B(t = 0) = C(t = 0) = 0$ it follows that:

$$\begin{array}{rcrcl} B_2 & + & B_3 & = & -B_1 \\ C_2 & + & C_3 & = & -C_1 \end{array} \qquad \text{and also} \qquad \begin{pmatrix} 1 & 1 \\ \gamma_2 & \gamma_3 \end{pmatrix} \begin{pmatrix} B_2 \\ B_3 \end{pmatrix} = \begin{pmatrix} -\kappa\, A_0 \\ -\zeta\, A_0 \end{pmatrix}$$

The explicit solution of B_2, B_3, C_2 and C_3 becomes therefore:

$$B_2 = \frac{-\kappa\,\gamma_3 + \zeta}{\gamma_3 - \gamma_2}\, A_0 \qquad B_3 = \frac{-\zeta + \gamma_2\,\kappa}{\gamma_3 - \gamma_2}\, A_0 \qquad C_2 = \gamma_2\, B_2 \qquad C_3 = \gamma_3\, B_3$$

If state A is not involved in the processes occuring after excitation, an initial instantaneous population of state B is assumed. The system of differential equations for that case is:

$$\begin{pmatrix} \dot{B} \\ \dot{C} \\ \dot{D} \end{pmatrix} = \begin{pmatrix} -k_{\mathrm{HT}} & k_{\mathrm{BHT}} & 0 \\ k_{\mathrm{HT}} & -(k_{\mathrm{BHT}} + k_{\mathrm{CR}}) & 0 \\ 0 & k_{\mathrm{CR}} & 0 \end{pmatrix} \begin{pmatrix} B \\ C \\ D \end{pmatrix}$$

State D can be separated:

$$\begin{pmatrix} \dot{B} \\ \dot{C} \end{pmatrix} = \begin{pmatrix} -k_{\mathrm{HT}} & k_{\mathrm{BHT}} \\ k_{\mathrm{HT}} & -(k_{\mathrm{BHT}} + k_{\mathrm{CR}}) \end{pmatrix} \begin{pmatrix} B \\ C \end{pmatrix}$$

giving the determinant of eigenvalues:

$$\begin{vmatrix} -k_{\mathrm{HT}} - \lambda & k_{\mathrm{BHT}} \\ k_{\mathrm{HT}} & -(k_{\mathrm{BHT}} + k_{\mathrm{CR}}) - \lambda \end{vmatrix} = 0$$

resulting in the characteristic polynomial equation:

$$(k_{\mathrm{HT}} + \lambda)\,(k_{\mathrm{BHT}} + k_{\mathrm{CR}} + \lambda) - k_{\mathrm{HT}}\,k_{\mathrm{BHT}} = 0$$

Introducing

$$k_{\mathrm{S}} = k_{\mathrm{HT}} + k_{\mathrm{BHT}} + k_{\mathrm{CR}}$$

by expanding and sorting the equation simplifies to:

$$\lambda^2 + k_{\mathrm{S}}\,\lambda + k_{\mathrm{HT}}\,k_{\mathrm{CR}} = 0$$

giving two real eigenvalues: $\boxed{\lambda_{1,2} = -\frac{k_{\mathrm{S}}}{2} \pm \sqrt{\frac{k_{\mathrm{S}}^2}{4} - k_{\mathrm{HT}}\,k_{\mathrm{CR}}}}$

With an exponential ansatz of the form:

$$\begin{aligned} B(t) &= B_1\,e^{\lambda_1\,t} + B_2\,e^{\lambda_2\,t} \\ C(t) &= C_1\,e^{\lambda_1\,t} + C_2\,e^{\lambda_2\,t} \end{aligned}$$

the coefficients of the ansatz are identified with that of the system of equations:

$$\begin{aligned} B_1\,\lambda_1 &= -k_{\mathrm{HT}}\,B_1 + k_{\mathrm{BHT}}\,C_1 \\ B_2\,\lambda_2 &= -k_{\mathrm{HT}}\,B_2 + k_{\mathrm{BHT}}\,C_2 \\ C_1\,\lambda_1 &= k_{\mathrm{HT}}\,B_1 - (k_{\mathrm{BHT}} + k_{\mathrm{CR}})\,C_1 \\ C_2\,\lambda_2 &= k_{\mathrm{HT}}\,B_2 - (k_{\mathrm{BHT}} + k_{\mathrm{CR}})\,C_2 \end{aligned}$$

Introduction of

$$\gamma_i = \frac{\lambda_i + k_{\mathrm{HT}}}{k_{\mathrm{BHT}}}$$

gives the relation: $C_i = \gamma_i\,B_i$.

From the boundary conditions $B(t = 0) = B_0$, $C(t = 0) = 0$, and $D(t = 0) = 0$ it follows that:

$$\begin{array}{rcrcr} B_1 & + & B_2 & = & B_0 \\ C_1 & + & C_2 & = & 0 \end{array} \quad \text{and also} \quad \begin{pmatrix} 1 & 1 \\ \gamma_1 & \gamma_2 \end{pmatrix} \begin{pmatrix} B_1 \\ B_2 \end{pmatrix} = \begin{pmatrix} B_0 \\ 0 \end{pmatrix}$$

Therefore the explicit solution of B_1 and B_2 is:

$$B_1 = \frac{\begin{vmatrix} B_0 & 1 \\ 0 & \gamma_2 \end{vmatrix}}{\begin{vmatrix} 1 & 1 \\ \gamma_1 & \gamma_2 \end{vmatrix}} = \frac{\gamma_2}{\gamma_2 - \gamma_1} B_0 \qquad B_2 = \frac{\begin{vmatrix} 1 & B_0 \\ \gamma_1 & 0 \end{vmatrix}}{\begin{vmatrix} 1 & 1 \\ \gamma_1 & \gamma_2 \end{vmatrix}} = \frac{-\gamma_1}{\gamma_2 - \gamma_1} B_0$$

Thus, the mathematical model for the case of P-part or Pc-part excitation is explicitly derived.

6.5 Basic Photophysical Properties

Steady State Absorption

The absorption spectra of H_2Tr and ZnTr show an absorption band at 350 nm, a very strong absorption band around 420 nm, a strong band at 682 nm and several weak bands between 500 and 670 nm (see figure 6.6). The solvent polarity has only a very minor influence (<2 nm shift) on the spectra. A clear difference between H_2Tr and ZnTr is noticable in the band structure between 500 and 650 nm. In case of ZnTPP, two of the four Q absorption bands are degenerated. The missing band at 515 nm is easily detected, whereas the other missing one is in a region, where the absorption of the Pc is overlapping.

From the chemical nature of the linkage between the Ps, and the Pc and the apparent geometry, one would expect nearly no ground state interaction between the chromophores. Detailed analysis reveals that the spectra can be well described as a superposition of minor red shifted spectra of the respective monomers. Knowing the original monomer spectra (depicted in figure 6.7 for comparison), the absorption band assignment becomes clear, the SiPc contributes the UV band around 350 nm, the far red band around 682 nm,

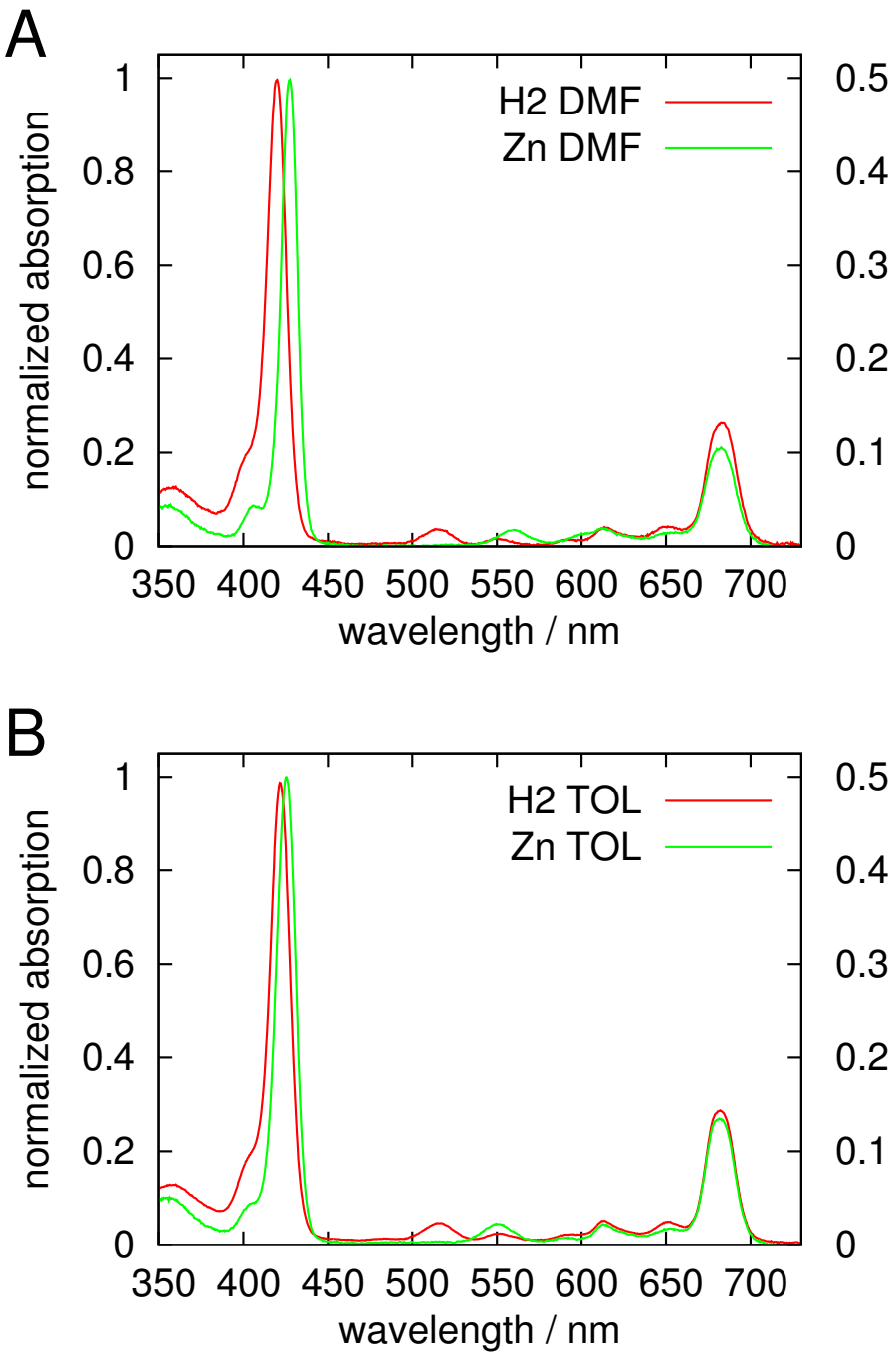

Figure 6.6: Absorption spectra of H_2Tr and ZnTr in A) DMF, and B) TOL.

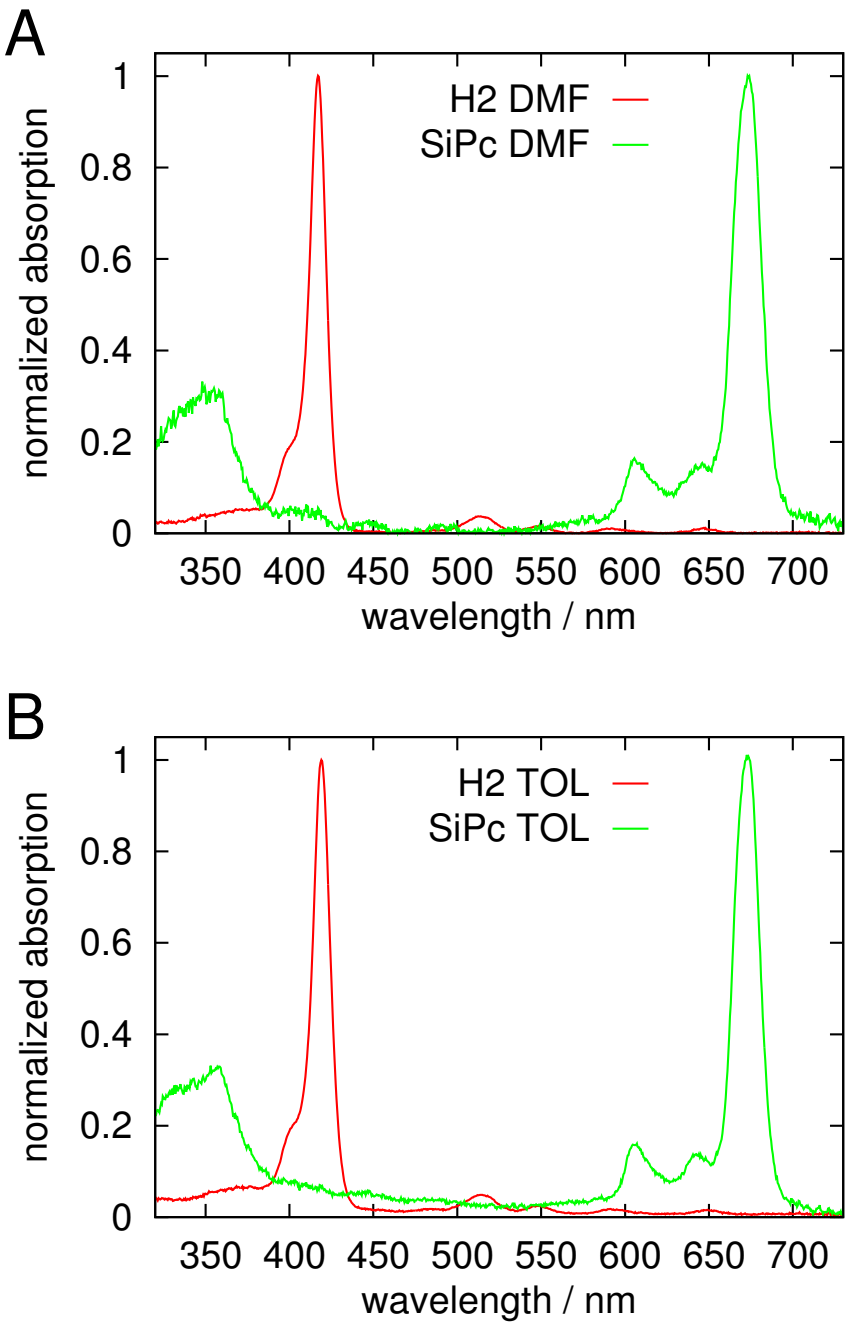

Figure 6.7: Absorption spectra of the reference compounds H_2TPP, and SiPc of H_2Tr in A) DMF, and B) TOL.

and two weak bands around 615 nm and 650 nm. These bands are found at identical positions in H_2Tr and ZnTr as expected, since the Pc-part is in both cases the same SiPc. All other bands originate from the P-part, a strong one about 420 nm and a couple of weak ones from 500 to 650 nm. The different number of weak Q-bands (two for ZnTr and four in case of H_2Tr) is due to the different symmetry of H_2TPP and ZnTPP as described above.

In both solvents all SiPc bands of the trimers are bathochromically shifted by 220 cm^{-1} compared to that of the reference SiPc. This shift is most probably caused by the slightly different axial ligand patterns of the reference SiPc and that within H_2Tr and ZnTr, since the observed bathochromic shifts of the Pc-part absorption bands lie in the range of values reported for different axial ligands attached to $SiPcCl_2$ (Maree and Nyokong, 2001; Lo et al., 2004).

The very small values of the bathochromic shifts of the trimer absorption bands compared to that of the references indicate very weak coupling of the ground states of the P- and the Pc-part. The chromophores can be considered as practically electronically decoupled. Strong ground state interaction, as known from sandwich-type metal coordinated heteromers being a consequence of planar stacking of the π-systems, is prevented by the edge to face linking via axial ligands.

Steady State Fluorescence

Exhibiting complementary, non overlapping absorption properties[1], the Ps and the Pc of the triads are selectively excitable. Limited by the available range of excitation wavelength for all measurements, two wavelength ranges were chosen, which were available on all setups. Selective excitation of the Pc-part of the trimers was accomplished around 615 nm, and selective excitation of the Ps at around 530 nm.

In order to assign the fluorescence bands of the trimers to either the P- or the Pc-part, the spectra of the reference compounds were measured. Presented in figure 6.8, the Ps and the Pc show one typical electronic transition band with an additional vibronic band. The influence of solvent polarity on

[1] At least there are two regions with nearly no overlap of absorption.

spectral shape and position is very small for H_2TPP and SiPc. By contrast, the fluorescence spectrum of ZnTPP is stronger influenced by solvent polarity. The higher polarity of DMF induces a bathochromic shift of both bands. Remarkably, the relative oscillator strength of the vibronic transition band compared to the electronic transition is nearly doubled in the nonpolar TOL.

The experimentally directly available steady state fluorescence spectra (see figure 6.9) of both trimers supported the assumption that there is no interaction between the chromophores in the excited states similar to the situation in the ground states. At a first glance, it seemed that a superposition of the fluorescence spectra of the building blocks was measured. However, time-resolved fluorescence measurements (see next chapter) revealed more species than the non interacting Ps and Pc. Therefore, the interpretation of the steady state fluorescence data is presented in a way that considers also the additional information from time-resolved techniques. By means of measuring decay-associated spectra, small contributions of impurities from educts of the synthesis were uncovered easily. This method assisted in subtraction of these unwanted contributions from the steady state spectra. The fluorescence of the triads emerges as a band, having its maximum at 690 nm (see figure 6.9). This band is found identically in both triads, independently if the P- or the Pc-part is excited. Its wavelength of maximal intensity does not depend on the polarity of the solvent. This fluorescence band is attributed to the fluorescence originating from the Pc-part of the triads. Considering that H_2Tr and ZnTr are composed of an identical Pc-part, this assignment is strongly supported by the similarity of the measured fluorescence band compared to SiPc, namely its maximal wavelength and its dependence on polarity. The observed bathochromic shift by 216 cm^{-1} of the triad fluorescence relative to that of SiPc is nearly the same as already found in the absorption spectrum, additionally indicating that the triad fluorescence is truly that of the Pc-part.

Assuming that the chromophores interact via energy or electron transfer (as wanted by design) their quantum yields should be altered. The quantum yield of the Pc part fluorescence of the triads was measured for P- and Pc-part excitation. The results are presented in table 6.3. Note that these

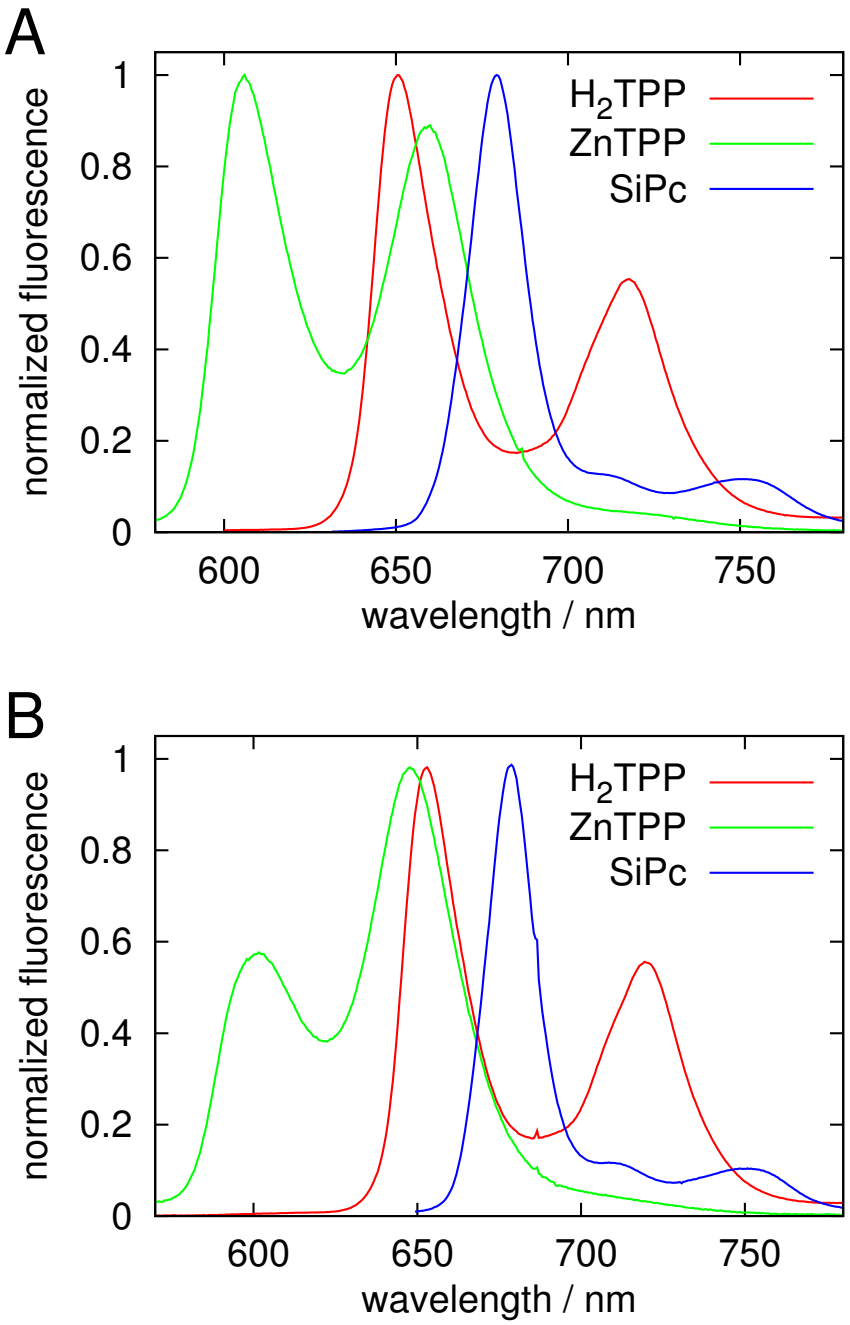

Figure 6.8: Fluorescence spectra of the reference compounds H_2TPP, ZnTPP, and SiPc in A) DMF, and B) TOL.

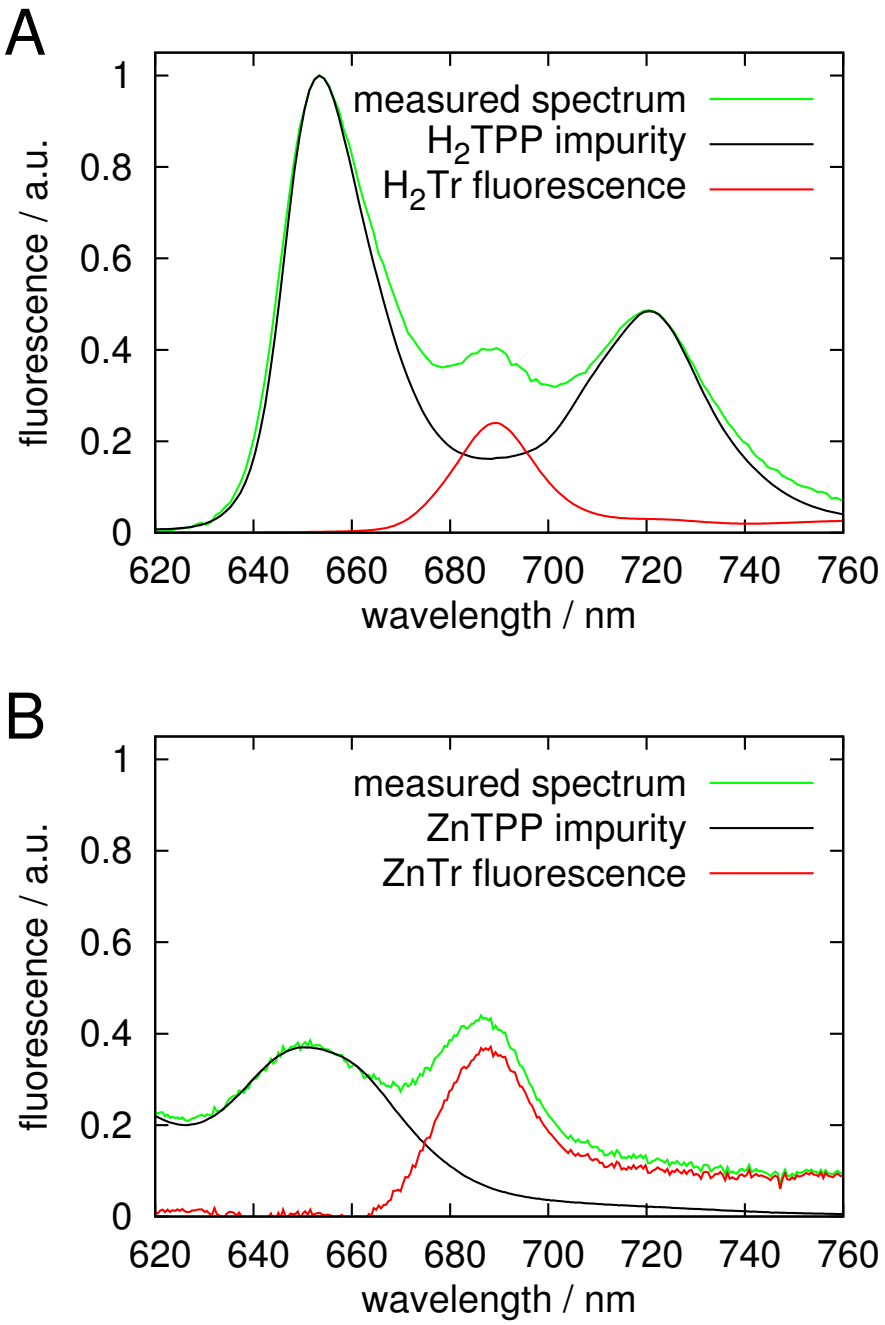

Figure 6.9: Fluorescence spectra of A) H_2Tr in DMF (green), and B) ZnTr in TOL (green). In both cases the P-part was excited at 515 nm. Subtraction of a fluorescence signal attributed to minor traces of precursors (black) resulted in similar spectra for both triads (red). See text for details.

Table 6.2: Absorption and fluorescence maxima of H_2Tr, and ZnTr, and its reference compounds H_2TPP, ZnTPP, and SiPc.

Compound	Solvent	B-band (nm)	Q-band (nm)	λ_{fl} (nm)
H_2TPP	DMF	417	646.5	651, 718
	TOL	419	649	653, 720
ZnTPP	DMF	425	600	606, 659
	TOL	427	601	601.5, 648
SiPc	DMF	356	673.5	680, 751
	TOL	357	673	678.5, 751
H_2Tr	DMF	419.8	683	690 [a]
	TOL	421.8	682	690 [a]
ZnTr	DMF	427.5	682.5	690 [a]
	TOL	429	681.8	690 [a]

[a] Data taken from time-resolved emission scans (DAFS).

values may comprise large errors since the fluorescence intensity originating from the triad is very weak and the covering signal from the impurities much stronger. It is reasonable from theoretical calculations, that an efficient transfer channel quenches the first excited singlet state of the triads Pc-part strongly. It is expected from the quantum yield data (comparing SiPc with the triads) that the transfer rate of the Pc-part quenching channel is on the order of 100 times larger than that of the unquenched depopulation rate. Furthermore, the occurrence of triad fluorescence even after P part excitation with a comparable quantum yield as observed for Pc-part excitation is a first indication for a directed energy transfer process from the Ps to the Pc.

With steady state fluorescence spectroscopy, no fluorescence originating from the P-parts of the triads could be resolved. After subtraction of the fluorescence originating from small traces of synthesis precursors, no patterns similar to that of P fluorescence remained.

Table 6.3: Fluorescence quantum yields of H_2Tr, and ZnTr calculated for the fluorescence band of SiPc after P- and Pc-part excitation.

	H_2Tr		ZnTr	
	excitation of		excitation of	
	P-part	Pc-part	P-part	Pc-part
DMF	$5 \cdot 10^{-4}$	$7.5 \cdot 10^{-4}$	$<5 \cdot 10^{-4}$	$1.0 \cdot 10^{-3}$
TOL	$2.2 \cdot 10^{-3}$	$2.2 \cdot 10^{-3}$	$1.0 \cdot 10^{-3}$	$3.3 \cdot 10^{-3}$

6.6 Fluorescence Kinetics

The time evolution of fluorescence was monitored by two techniques, TCSPC and fsUPC. The former allowed recording of decay associated fluorescence spectra, but provided a limited time resolution. Using the latter, the ultrafast fluorescence decays could be resolved for the triads.

Decay Associated Fluorescence Spectra by TCSPC

Excited state lifetimes give further information about chromophores and their interactions. Complementary to steady state spectroscopy, the signal strength of time-resolved measurements is directly proportional to the initial population of the excited state c_0^* and the fluorescence rate constant k_{fl}. Therefore, even short living excited states can easily be measured if the product $c_0^* \cdot k_{\text{fl}}$ is reasonable large. However, the total number of emitted photons may be to small in these cases to be well detected with standard steady state spectrometers or the spectra of the fast decaying species could be covered by additional species exhibiting high quantum yields.

The fluorescence lifetimes of the reference compounds were measured for comparison and assigning purposes. The values are summarized in table 6.4. They all have mono-exponential decay characteristics as expected from a single homogeneous species of dye molecules.

By measuring maps of time resolved fluorescence intensity over wavelength, one obtains spectra and lifetimes of excited states at the same time. Even mixtures containing many species can be decomposed into an individual spectrum for each species (see chapter 4 for details on data analysis).

Table 6.4: Fluorescence lifetimes of the reference compounds H_2TPP, ZnTPP, and SiPc in the polar solvent DMF and in the unpolar solvent TOL.

	H_2TPP (ns)	ZnTPP (ns)	SiPc (ns)
DMF	10.37 ± 0.02	1.91 ± 0.02	5.06 ± 0.01
TOL	9.19 ± 0.01	1.86 ± 0.02	4.80 ± 0.01

A first investigation revealed that fluorescence of both triads decays multi-exponentially in DMF and TOL. Therefore, a mixture of species was expected. Data sets decomposed into spectra with their associated lifetimes are shown in figure 6.10 and 6.11. In figure 6.10 A the two species found in case of P-part excitation of H_2Tr dissolved in DMF are shown. The strongest signal originates from a species decaying faster than 10 ps and exhibiting a spectrum, bathochromically shifted compared to that of SiPc, whereas a smaller contribution has a lifetime of 9.8 ns and a spectrum shaped like that of H_2TPP. In case of Pc-part excitation (see figure 6.10 C) an identical short living component is identified as by P-part excitation. An additional longer component, however, has a lifetime of 4.6 ns and a spectrum similar to SiPc. The species exhibiting spectra and excited state lifetimes similar to the corresponding reference compounds can very likely be identified as minor traces of the P and Pc precursors from synthesis. They were also found when TOL was used as solvent and are not discussed further. Residing in the nonpolar solvent TOL, H_2Tr shows a different behavior. A second species with a fluorescence pattern identical to the short living species, but with a longer lifetime of around 200 ps (see figures 6.10 B and D) was detected. Also, the lifetime of the first species increases to about 20 ps. One can summarize that the fluorescence of H_2Tr is emitted with a pattern of a bathochromic shifted SiPc shape, indicating that the fluorescence originates from the SiPc of H_2Tr. Further more, identical behavior in case of P-part or Pc-part excitation and no detection of P-part fluorescence reveals a strong energy transfer from the Ps to the central SiPc. In polar environment the Pc of H_2Tr is quenched by an additional depopulation channel with a factor of more than 500, whereas in the nonpolar TOL, two interpretations of the results are possible. The second 200 ps lifetime may stem from a new species or may be due to more

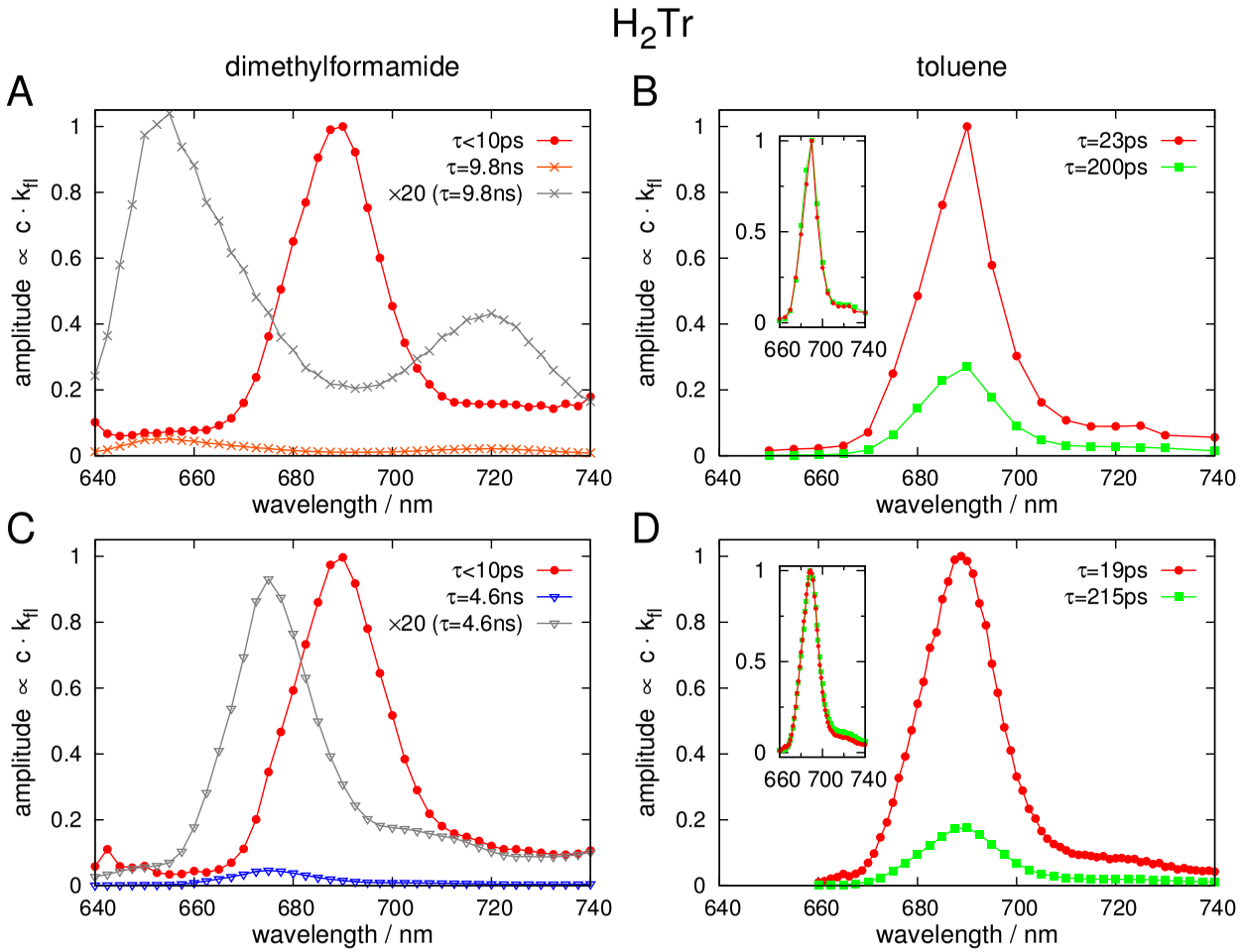

Figure 6.10: Decay associated fluorescence spectra of H_2Tr. A) P-part excitation, DMF B) Pc-part excitation, TOL, inset shows both spectra normalized C) P-part excitation, DMF D) Pc-part excitation, TOL, inset shows both spectra normalized, see text for details.

complex transitions than just quenching of the first excited singlet state of H_2Tr's SiPc. Assuming a new species, solubility and solvent-dependent geometry could be reasons for the heterogeneity in TOL compared to DMF. Since the new appearing species contributes to at least 20 % relative to the fast decaying one, chemical analysis by NMR spectroscopy should have given an indication for a second type of molecule if one expects a different chemical structure. However, no evidence of another chemical structure than H_2Tr was found. Considering the axial binding motif of the triad, two distinct conformations are very unlikely as are stacking of the cyclic rings. The hypothesis of a real second species was rejected, therefore. To enlighten the nature of the second decay time, one has to investigate the origin of the quenching process of the excited state of the Pc-part: energy transfer and excitonic coupling are impossible for energetic reasons (see absorption and fluorescence spectra), however, electron transfer follows other laws. Whereas for energy transfer only the relative energy differences between ground and excited state of donor and acceptor decides about direction and strength of transfer, in case of electron transfer also the absolute energies of the ground states (accessed by electrochemical methods) affect the transfer rate. After careful investigation of the conditions (see next chapter) electron transfer was proven as the quenching process. Due to the thermodynamical nature of electron transfer this can be a reversible process. By introducing back electron transfer as an additional channel into the kinetic model, a second decay time evolves naturally as a solution of the differential equation. Its amplitude coefficient is dependent on the ratio of forward and backward electron transfer. In case of negligible back transfer, the depopulation of the excited state tends to follow a mono-exponential behavior. By employing the model extended by a back electron transfer channel the experimental data could be described well.

For ZnTr in TOL, the analysis gave a 16 ps and a 350 ps decay component in the case of P-part excitation (see figure 6.11A) and a 13 ps and a 280 ps component after Pc-part excitation (see figure 6.11B). The short lifetimes in both cases are very close to the resolution limit of the TCSPC-setup and are therefore unreliable in their absolute value. However, the spectral shape

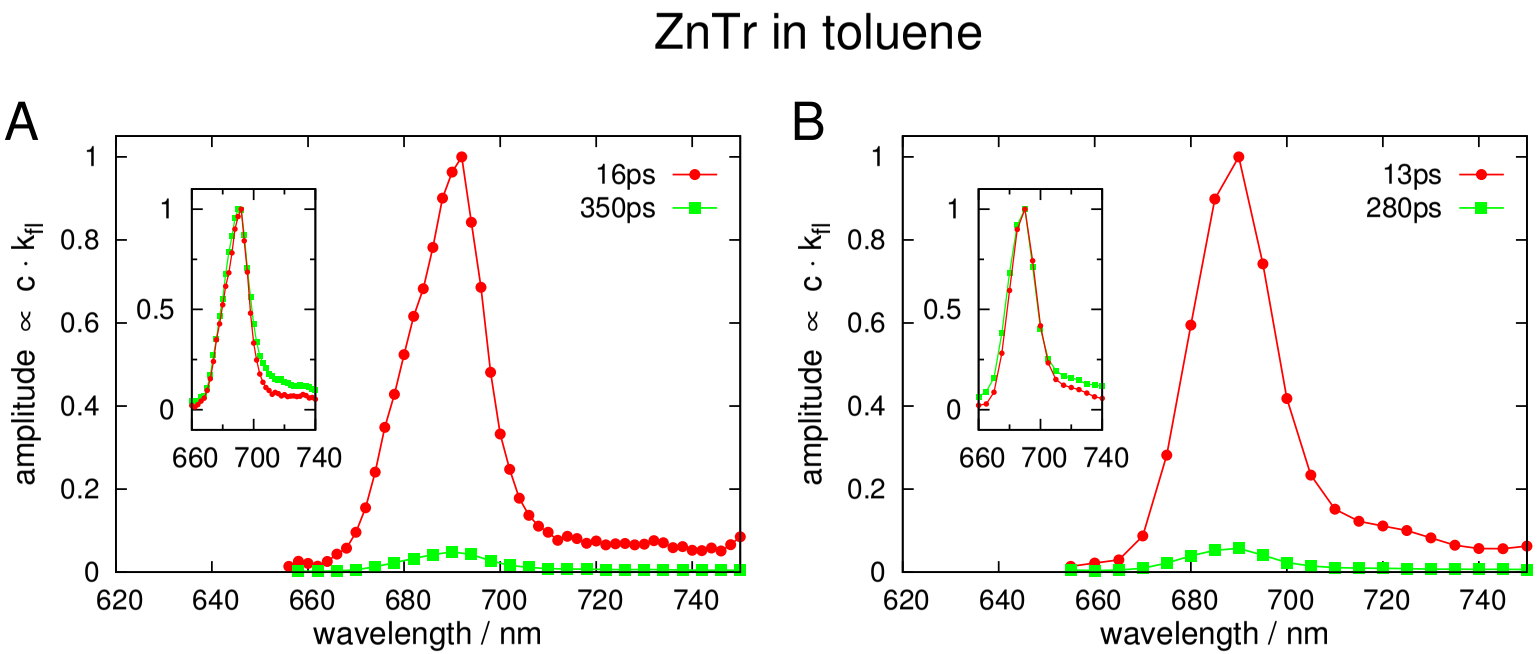

Figure 6.11: Decay associated fluorescence spectra of ZnTr in TOL. A) P-part excitation B) Pc-part excitation, insets show the two bands normalized, see text for details.

of both associated spectra could be resolved. The insets depict the spectra for each solvent in a normalized form. From this representation one can clearly see the spectral congruence of the short and the longer component. Furthermore, the spectra are very close to the spectra of H_2Tr, supporting strongly that the origin of the fluorescence is the SiPc. Like in the case for H_2Tr, no fluorescence from the P-part was detected with the TCSPC-technique in either solvent.

Ultrafast fluorescence decay kinetics by fsUPC

The values of the fluorescence lifetimes of the triads revealed by TCSPC were already at the limit of the method itself. Also the quantum yield measurements indicated very efficient transfer processes. To clarify the transfer rates, the fluorescence lifetimes were additionally measured by fsUPC.

Direct excitation of the Pc-part of H_2Tr dissolved in DMF results in instantaneous emission of fluorescence from the Pc-part (see figure 6.12B) decaying with a time constant of 7.7 ± 0.2 ps. In contrast, excitation of the P-part leads to a raise of the Pc part fluorescence with a time constant of 1.2 ± 0.2 ps, followed by a mono-exponential decay with the same decay time of 7.7 ± 0.2 ps (see figure 6.12A). The raise of Pc-part fluorescence after P-part excitation is the consequence of directed energy transfer from the Ps to the Pc. One should expect that also the fluorescence of the P-part is diminished with the raise time constant of the Pc-part. However, an ultrafast fluorescence decay of the P-part fluorescence was experimentally not resolvable in DMF. In contrast, the decay of fluorescence emission of the P-part of H_2Tr could be measured in the polar solvent TOL after direct excitation of the P-part. It follows a mono-exponential decay with a time constant of 1.3 ± 0.1 ps (see figure 6.16 A). Under the same conditions the fluorescence of the Pc-part raises with a time constant of 1.3 ± 0.1 ps and decays bi-exponentially with time constants of 20 ± 2 ps and 180 ± 10 ps (see figure 6.16 B). In general, similar results were obtained for ZnTr in both solvents. Direct Pc-part excitation of ZnTr dissolved in DMF leads to an instantaneously populated first excited singlet state of the Pc-part which is decaying with a time constant

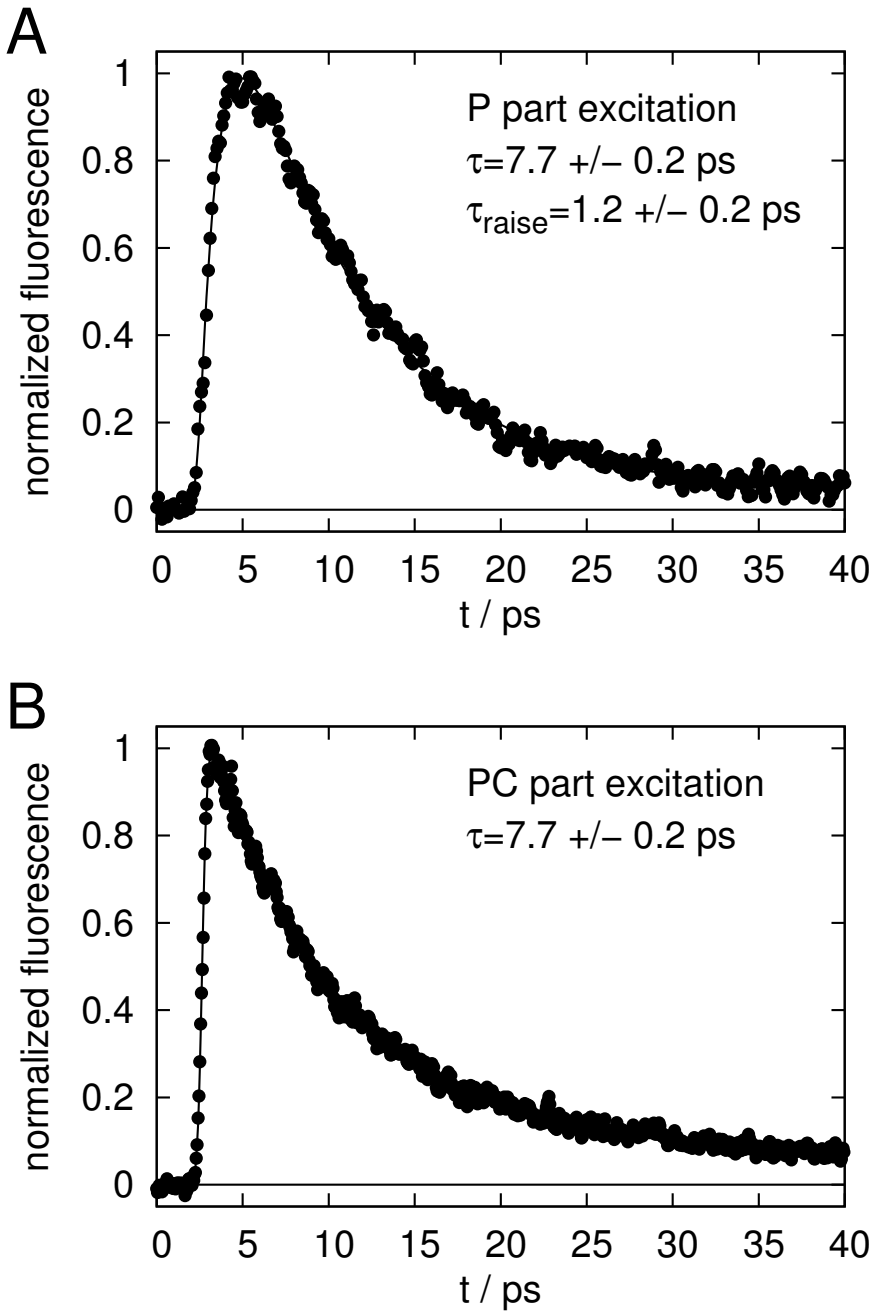

Figure 6.12: Decay of the Pc-part fluorescence of H_2Tr in DMF A) after P-part excitation B) after Pc-part excitation.

of 800±50 ps. Emission from the P-part was not reliably detected for ZnTr in DMF, also the rise time of the Pc-part fluorescence after P-part excitation could not be detected with reasonable error. In polar environment the P-part fluorescence decay of ZnTr could be analyzed and the decay time estimated to 1.2±0.2 ps, yielding an identical value as for H_2Tr in TOL. As expected, the Pc-part's first excited state is populated with the same time constant of 1.2±0.2 ps. Three exponential terms were necessary to describe the fluorescence decay of the Pc-part of ZnTr in TOL adequately. Their time constants were estimated to 900±100 fs, 10±3 ps, and 280±10 ps. The occurrence of three different decay rates was remarkable and violating the model describing the data up to now well. Among various assumptions aggregation of ZnTPP in TOL was discussed and investigated as a possible explanation. Therefore, the relative amplitude coefficients against ZnTr concentration were evaluated. A clear dependency on concentration for the 10 ps component was found, whereas the two other contributions were independent of concentration. Also, by analogy with the other obtained values it was finally concluded that the 10 ps component is very likely an artifact of ZnTPP aggregation and it was excluded from further analyses.

Table 6.5: Fluorescence lifetimes of H_2Tr and ZnTr in DMF and TOL. The investigated parts of the triads were excited directly. — denotes that no fluorescence could be detected.

		P-part (ps)	Pc-part (ps)	
H_2Tr	DMF	—	7.7 ± 0.2	
	TOL	1.3 ± 0.1	20 ± 2	180 ± 10
ZnTr	DMF	—	0.8 ± 0.1	
	TOL	1.2 ± 0.2	0.9 ± 0.1	280 ± 10

6.7 Photo-induced Charge Transfer Pathways

Photo-induced charge transfer should occur in the investigated P-Pc-P heterotrimers by design. The determined redox potentials (see chapter 6.3) show that the formation of only one charge-separated state is allowed, namely $P^{\bullet+}$-$Pc^{\bullet-}$-P, where the P gets oxidized and the Pc reduced. To monitor

its build-up and recombination, transient absorption spectra were recorded. The build-up of the CS state could be recognized (see figure 6.13) by a new occurring absorption band around 580 nm, being a property of the $SiPc^{\bullet-}$ ion (Kodis et al., 2004). Control experiments proved that in all reference substances (H_2TPP, ZnTPP, and SiPc), this band was not observable. The recombination of the CS state could be tracked either by the absorption band of the $SiPc^{\bullet-}$ ion or by the decay of the ground state depletion. Independent of the excited moiety (P- or Pc-part) and the solvent polarity, the formation of the CS state was verified for H_2Tr and ZnTr. Similar decay rates of ground state depletion and the CS state indicate charge recombination as a direct and major pathway to the ground state. This observation is also supported by the fact that the CS state is the lowest excited state for both triads independent of the solvent. Table 6.6 summarizes the obtained lifetimes of the CS state. Whereas the decay of the CS-state has a single pathway

Table 6.6: Lifetimes of the charge-separated state ($P^{\bullet+}$-$Pc^{\bullet-}$-P) of H_2Tr and ZnTr in DMF and TOL.

	DMF (ps)	TOL (ps)
H_2Tr	30 ± 1	180 ± 10
ZnTr	20 ± 1	280 ± 10

($P^{\bullet+}$-$Pc^{\bullet-}$-P→P-Pc-P), its build-up might have two, namely charge separation either after excitation of the P- or the Pc-part (P^*-Pc-P→$P^{\bullet+}$-$Pc^{\bullet-}$-P or P-Pc^*-P→$P^{\bullet+}$-$Pc^{\bullet-}$-P). In order to figure out whether one or both channels may play a role, the energetics of both reactions were examined by means of the Rehm-Weller equation (6.1).

$$\Delta G_{\mathrm{CS}} = e\left(E^{\mathrm{oxd}}_{1/2}(D/D^+) - E^{\mathrm{red}}_{1/2}(A/A^-)\right) - E_{0,0} - \frac{e^2}{4\pi\,\epsilon_0\,\epsilon_{\mathrm{s}}\,R} + \frac{e^2}{8\pi\,\epsilon_0}\left(\frac{1}{r_{\mathrm{D}^+}} + \frac{1}{r_{\mathrm{A}^-}}\right)\left(\frac{1}{\epsilon_{\mathrm{ec}}} - \frac{1}{\epsilon_{\mathrm{s}}}\right) \tag{6.1}$$

The free enthalpy for charge separation (ΔG_{CS}), either from the excited P- or Pc-part, was calculated in electron volts from the half-wave oxidation

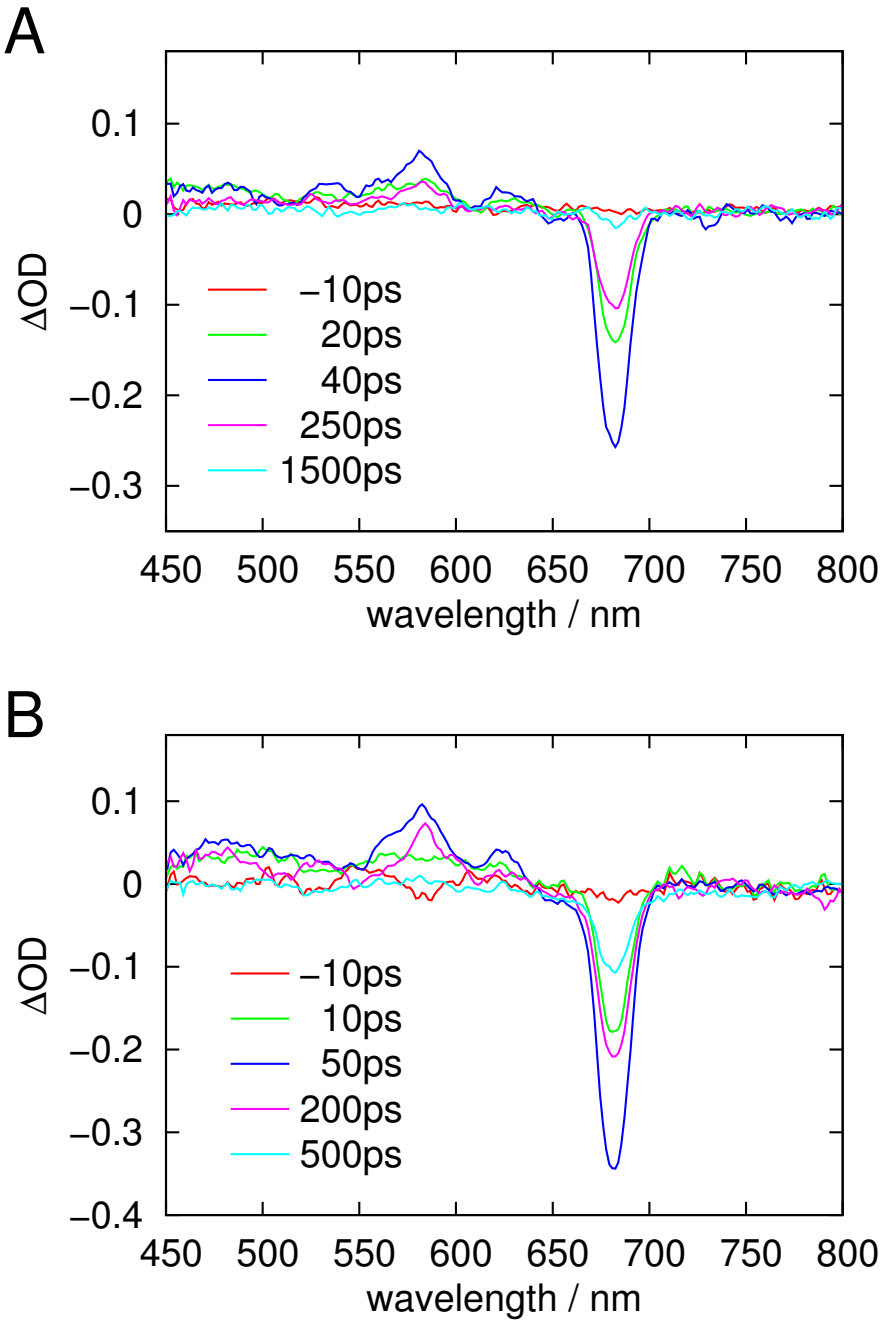

Figure 6.13: Transient absorption spectra of A) H_2Tr dissolved in TOL excited at 518 nm (P-part), and B) ZnTr in DMF excited at 613 nm (Pc-part).

potential of the electron donor $E_{1/2}^{\mathrm{oxd}}(D/D^{+})$ and the half-wave reduction potential of the electron acceptor $E_{1/2}^{\mathrm{red}}(A/A^{-})$ taken in volts. The ground state to first excited singlet state transition energy in electron volts (for P- or Pc-part) is denoted as $E_{0,0}^{\mathrm{P\,(Pc)}}$, respectively. Electrostatic interaction of the uprising ions is considered by the separation distance R of the ions, and the dielectric constant ϵ_{s} of the solvent in which spectroscopic measurements where performed. An additional term accounts for the different dielectric constant ϵ_{ec} of the solvent used for the electrochemical studies compared to that for the spectroscopic ones. It also accounts the effective radii of the cation ($r_{\mathrm{D}^{+}}$) and the anion ($r_{\mathrm{A}^{-}}$) radical. As usual ϵ_0 is the vacuum permittivity and e the charge of the transfered electron. Using measured values of $E_{1/2}^{\mathrm{oxd}} = 0.9\,\mathrm{V}$, $E_{1/2}^{\mathrm{red}} = -0.66\,\mathrm{V}$ for H_2Tr, $E_{1/2}^{\mathrm{oxd}} = 0.77\,\mathrm{V}$, $E_{1/2}^{\mathrm{red}} = -0.67\,\mathrm{V}$ for ZnTr, $E_{0,0}^{\mathrm{H_2TPP}} = 1.92\,\mathrm{eV}$, $E_{0,0}^{\mathrm{ZnTPP}} = 2.07\,\mathrm{eV}$, $E_{0,0}^{\mathrm{Pc}} = 1.84\,\mathrm{eV}$ for DMF, and $E_{0,0}^{\mathrm{H_2TPP}} = 1.91\,\mathrm{eV}$, $E_{0,0}^{\mathrm{ZnTPP}} = 2.06\,\mathrm{eV}$, $E_{0,0}^{\mathrm{Pc}} = 1.82\,\mathrm{eV}$ for TOL, and estimated values of $R = 0.91\,\mathrm{nm}$, $r_{\mathrm{D}^{+}} = 0.43\,\mathrm{nm}$, $r_{\mathrm{A}^{-}} = 0.46\,\mathrm{nm}$ (by use of the HyperChem program package (Hyperchem)), and tabulated values of $\epsilon_{\mathrm{ec}} = 8.9$ for CH_2Cl_2, $\epsilon_{\mathrm{s}}^{\mathrm{DMF}} = 37$, and $\epsilon_{\mathrm{s}}^{\mathrm{TOL}} = 2.4$ the free charge transfer enthalpies were calculated as summarized in table 6.7. The values clearly indicate that

Table 6.7: Calculated charge transfer enthalpies ΔG_{CS} of H_2Tr and ZnTr for the polar solvent DMF and the nonpolar TOL.

	DMF (eV)		TOL (eV)	
charge transfer pathway	H_2Tr	ZnTr	H_2Tr	ZnTr
P-Pc*-P→$P^{\bullet+}$-$Pc^{\bullet-}$-P	-0.57	-0.69	0.07	-0.05
P*-Pc-P→$P^{\bullet+}$-$Pc^{\bullet-}$-P	-0.66	-0.93	0.00	-0.29

hole transfer (P-Pc*-P →$P^{\bullet+}$-$Pc^{\bullet-}$-P) from the excited Pc-part and electron transfer (P*-Pc-P →$P^{\bullet+}$-$Pc^{\bullet-}$-P) from the excited P-part is feasible for both triads in the polar solvent DMF. Refer to chapter 5.6 for a detailed explanation of the naming "hole-" and "electron transfer". The measured fast mono-exponential depopulation (see table 6.5) of the first excited singlet state of the Pc-part of H_2Tr and ZnTr in DMF and the proven charge-separated state (see figure 6.13) agree with the predicted existence of the hole transfer. Contrary, ongoing electron transfer from the excited P-part is not as easy di-

rectly observable since occurring Pc-part fluorescence gives a strong evidence for coexisting energy transfer. This leads to the kinetic scheme depicted in figure 6.14, where electron and energy transfer compete for depopulating the first excited singlet state of the P-moiety. From the solution of the system

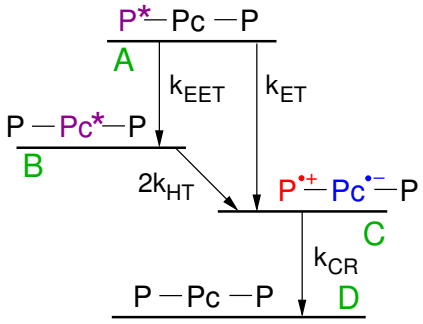

Figure 6.14: Scheme of energy levels and transitions in case of a polar solvent.

of differential equations for that model (refer to chapter 6.4), it follows obviously that only the sum of electron and energy transfer rate (k_{EET}+k_{ET}) is directly observable for all states involved (A, B, and C). It is, therefore, a more complicated task to split the sum rate (k_{EET}+k_{ET}) into a pure energy (k_{EET}) and a pure electron (k_{ET}) transfer rate. One has to characterize also energy transfer to be able to address this task. Chapter 6.8 is dedicated to analyze and describe the results.

A nonpolar environment such as TOL stabilizes the CS state, its lifetime is about ten-fold longer (cf. table 6.6) compared to the polar environment of DMF. Furthermore, the small charge transfer enthalpies favor back hole transfer leading to "delayed fluorescence" of the Pc-part (cf. figure 6.10 B,C and figure 6.11) i.e. appearing of a second decay component (Heitele et al., 1989). The predicted probabilities of back hole transfer (from the calculated charge transfer enthalpies) are also in accordance with the experimental findings of a smaller back transfer rate for ZnTr and a larger one for H_2Tr. Refer hereto the amplitudes of the slow and fast Pc-part fluorescence decay components in figure 6.10 B,C and 6.11. Figure 6.15 depicts the corresponding scheme of transitions for the nonpolar case of TOL.

Also the ΔG_{CS} around zero of H_2Tr in TOL for electron transfer suggests

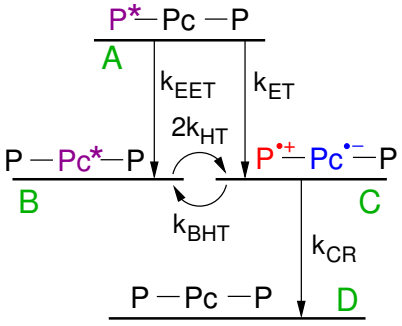

Figure 6.15: Scheme of energy levels and transitions in case of a unpolar solvent.

back electron transfer (i.e. "delayed fluorescence" from the P-part), however no indications of a back electron transfer could be observed for all cases. The final matrix of transfer rates will be given in the next chapter after evaluating also the energy transfer.

6.8 Competing Energy and Electron Transfer

Clear experimental evidence of energy transfer from the P-part to the Pc-part (P*-Pc-P→ P-Pc*-P) was found for H_2Tr and ZnTr in polar and nonpolar environment. In combination, the steady state and time-resolved fluorescence measurements revealed energy transfer as one main depopulation process of the first excited singlet state of the triad Ps by two indications. Firstly, the ratio of Pc-part excitation, Pc-part detection to P-part excitation, Pc-part detection quantum yield is high (see table 6.3). Secondly, observing that the rise of Pc-part fluorescence is identically fast as the decay of the P-part fluorescence, as measured for H_2Tr in TOL, excludes direct excitation of the Pc-part. Since also electron transfer might depopulate the excited state of the Ps, the energy transfer efficiency cannot simply be calculated from the fluorescence decay or fluorescence rise rate of donor or acceptor, respectively. To acquire the whole data directly, one would need to measure absolute amplitude coefficients of populated states, not only at different fluorescence detection wavelengths, but also for transient absorption spectroscopy under exactly the same conditions. This might sound like a not too complicated

exercise, however, turns out to be a difficult metrological procedure, which was not performed in this thesis. Assuming an identical electronic coupling matrix element V for electron and hole transfer, the ratio of both rates can be expressed in terms of known or measured values, as given in formula 6.2.

$$\frac{k_{\mathrm{ET}}}{k_{\mathrm{HT}}} = \exp\left[\frac{\left(\Delta G_0^{\mathrm{HT}} - \Delta G_0^{\mathrm{ET}}\right)\left(\Delta G_0^{\mathrm{HT}} + \Delta G_0^{\mathrm{ET}} + 2\lambda\right)}{4k_{\mathrm{B}}\,T\,\lambda}\right] \tag{6.2}$$

The hole transfer rates and the sum rates of energy plus electron transfer could be measured for H_2Tr and ZnTr in the polar solvent TOL and for H_2Tr in DMF. For these three cases all transfer rates could be calculated with the above mentioned assumption. In order to figure out also the rates for ZnTr in DMF and to verify and support the calculated energy transfer rates with a second approach, energy transfer was treated by means of FRET theory (see chapter 5.6). From the absorption spectra of the Pc-part and fluorescence spectra of the P-part monomers the Förster radii $R_0^{\kappa=1}$ with

$$R_0^{\kappa=1} = \left(\frac{9000(\ln 10)\Phi_{\mathrm{fl}}}{128\pi^5 n^4\, N_{\mathrm{A}}} \int I_{\mathrm{fl}}^{\mathrm{n}}(\tilde{\nu})\,\epsilon(\tilde{\nu})\frac{\mathrm{d}\tilde{\nu}}{\tilde{\nu}^4}\right)^{-\frac{1}{6}} \tag{6.3}$$

were calculated for energy transfer from P- to Pc-part. Commonly, the formula also includes the orientation factor κ, which is sensible dependent on the orientation of the absorption and emission dipole moment of the acceptor and donor, respectively. Please notice, the orientation factor was excluded from the calculation of the Förster radius (i.e. $\kappa = 1$), and therefore included into the calculation of the transfer rate (see formula 6.4) since the orientation factor value is not reliably accessible from geometry optimizations of molecular mechanic calculations.

$$k_{\mathrm{EET}} = \frac{1}{\tau_{\mathrm{D}}}\kappa^2\left(\frac{R_0^{\kappa=1}}{R}\right)^6 \tag{6.4}$$

In formula 6.3 and 6.4, n is the refractive index of the solvent, Φ_{fl} the fluorescence quantum yield and τ_{D} the fluorescence lifetime of the donor (P) in absence of the acceptor, N_{A} Avogadro's number, ϵ the molar absorbance of

Table 6.8: Calculated Förster radii $R_0^{\kappa=1}$ for H_2Tr and ZnTr in DMF and TOL and κ^2 calculated from the estimated energy transfer rate and the Förster radius.

	H_2Tr		ZnTr
	$R_0^{\kappa=1}$ (Å)	κ^2	$R_0^{\kappa=1}$ (Å)
DMF	51	0.78	38
TOL	48	0.81	34

the acceptor (Pc-part) at wavenumber $\tilde{\nu}$, $I_{\mathrm{fl}}^{\mathrm{n}}$, and the normalized fluorescence spectrum of the donor (P-part). The calculated values (summarized in table 6.8) approve the existence of an efficient energy transfer channel from the P- to the Pc-part, comparing the Förster radii of about 40 Å to the center to center distance of donor and acceptor of 9 Å and assuming an appropriate orientation. Theory predicts limiting values of the squared orientation factor κ^2 of zero for the lower and four for the upper limit. Evaluating its value for H_2Tr gives a κ^2 of 0.78 and 0.81 for DMF and TOL, respectively. These values are well within the physically meaningful limits, and, moreover, they are not far from the value of $\frac{2}{3}$, being the magic number for the case of fast, unrestricted, and isotropic motion of the dipole moments. Based on the molecular structure of the triads it is clear that a number of particular orientations leading to prominent values of κ^2 cannot be reached. These include $\frac{2}{3}$, since the motion of P and Pc is restricted in distance, zero, one and four, since perfect perpendicular, parallel or inline orientation is also very unfavorable due to the flexible linking of the two moieties. An intermediate value, as observed, is therefore not violating expectations and seems to be reasonable for the restricted, but flexible structure of the systems. Utilizing the κ^2 data from H_2Tr and assuming an identical orientation of the dipole moments for ZnTr, one can also estimate the energy transfer rate for ZnTr dissolved in DMF, for that measurement data could not be obtained. Hence, all rate constants for H_2Tr and ZnTr in both solvents could be estimated from the measured data and by means of theoretical approaches, see table 6.9 for a compilation.

For the case of H_2Tr dissolved in TOL, data could be measured for three states of the molecule. Hence, global data analysis became possible with this set of data. Utilizing the analytical solution of the differential equation, the time evolution of the P-part fluorescence after P-part excitation, the Pc-part fluorescence after P-part excitation, and the ground state depletion of the Pc-part after P-part excitation could be described and fitted by a comprehensive mathematical model. As a result, the rate constants (k_{EET}, k_{ET}, k_{HT}, and

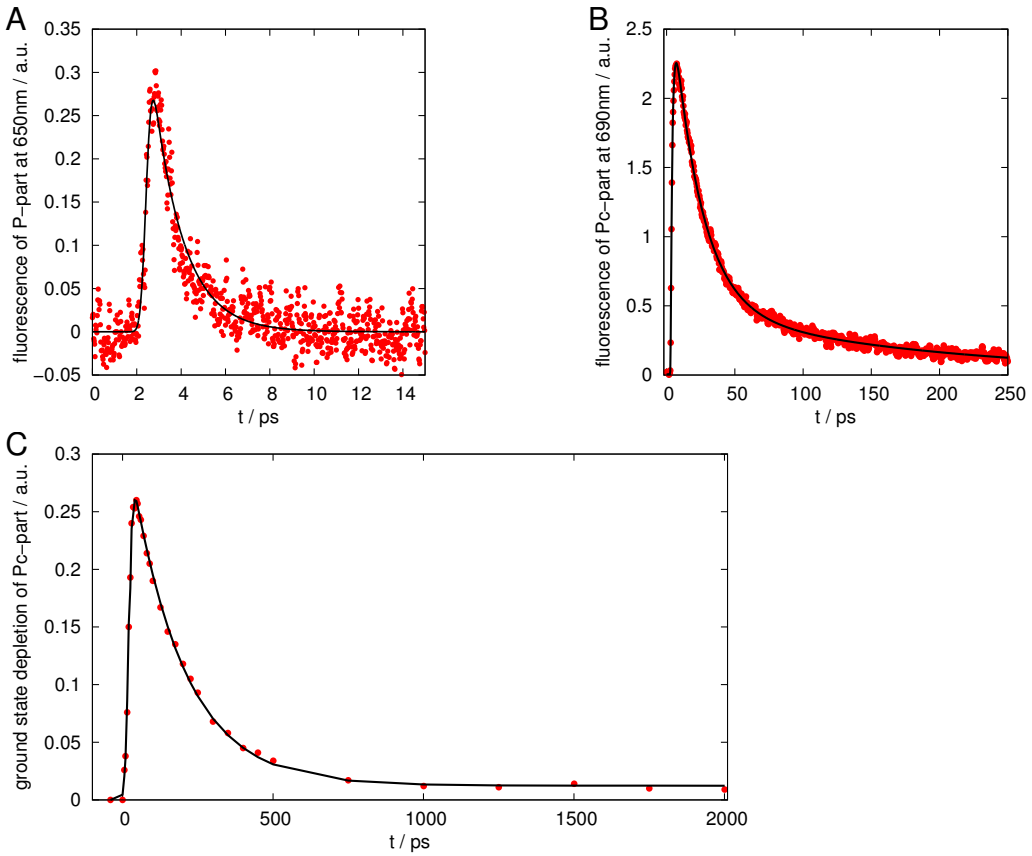

Figure 6.16: Global data analysis of data obtained from H_2Tr dissolved in TOL, all data sets are fitted simultaneously by one mathematical model. A) P-part fluorescence after P-part excitation. B) Pc-part fluorescence after P-part excitation. C) Ground state depletion of the Pc-part after P-part excitation.

k_{CR}) could be extracted and their confidence estimated, see figure 6.16.

The final results are summarized in table 6.9. In order to illustrate the rate constants, the Jałonski diagrams (figure 6.17) for the two different cases of the solvent polarity are shown here once again.

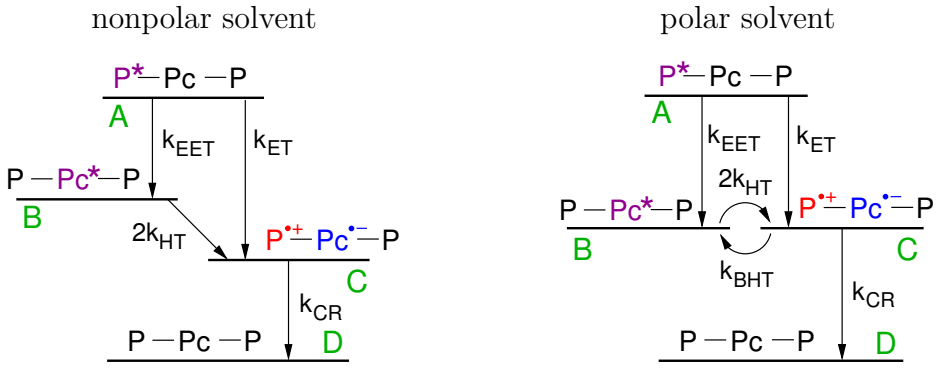

Figure 6.17: Jałonski diagrams for polar (DMF) and nonpolar (TOL) solvent

Table 6.9: Energy (k_{EET}), electron (k_{ET}), hole (k_{HT}), back hole transfer (k_{BHT}), and charge recombination (k_{CR}) rates. See figure 6.17 for detailed information about the levels and transfer channels.

		k_{EET} $(10^{11}s^{-1})$	k_{ET} $(10^{11}s^{-1})$	[a] k_{HT} $(10^{10}s^{-1})$	k_{BHT} $(10^{10}s^{-1})$	k_{CR} $(10^{9}s^{-1})$
H_2Tr	DMF	6.9 ± 0.6	1.39 ± 0.05	6.50 ± 0.03	0	33 ± 2
	TOL	6.5 ± 0.7	0.98 ± 0.02	2.10 ± 0.05	0.61 ± 0.06	6.7 ± 0.2
ZnTr	DMF	7.3 ± 0.8	—	70 ± 10	0	50 ± 2
	TOL	3.8 ± 0.4	4.5 ± 0.5	60 ± 10	14 ± 1	3.6 ± 0.1

[a] Recall that two possible pathways exist for hole transfer from excited Pc to P. Here the rate for only one channel is given.

7 Discussion and Outlook

This work was aimed at analyzing ultrafast energy- and electron-transfer in artificial chemical systems modeling the primary steps of photosynthesis. Spectroscopic and electrochemical methods have been used to measure all necessary properties in order to develop a comprehensive description of the compounds being investigated. The different nature of energy- and electron-transfer requires two different spectroscopic techniques for proper and unambiguous measurements. Energy transfer is preferably monitored by fluorescence detection techniques, whereas electron transfer mostly alters absorption of the sample and needs to be tracked down with transient absorption spectroscopy. The existing portfolio of spectroscopic equipment did not allow for detecting the expected ultrafast transfer processes. Therefore, two new setups were constructed to record fluorescence and absorption of a liquid sample with sub-picosecond time-resolution. Furthermore, the necessary software tools to analyze the obtained data of these complex systems were developed.

Being driven by the need for a sustainable source of energy, there is ongoing research on artificial photosynthetic antenna and reaction center complexes since the 1970s. However, there is still no chemical mimicry of the primary steps of photosynthesis available, which delivers electrical energy in a commercially usable amount. For this reason new model compounds are continuously designed and synthesized. Their structure is based on profound theories, on years of expert knowledge, and on new available synthesis strategies. Even though theoretical predictions may help to narrow the range of potential chemical compounds bearing the desired features, they are not reliable enough to abandon experimental investigation of the promising candidates.

The group of Prof. Ng (Hongkong University) created a new class of model systems by linking two porphyrins and a silicon phthalocyanine axially by metal coordination. Both constituents (P and Pc) are well known as chem-

ically stable molecules exhibiting the proper qualities for efficient energy- and electron-transfer. Therefore, it was expected that the desired properties could be realized. Only a very small number of similar structures was known, and only for a subset of these comparable structures the transfer processes were examined and published. Moreover, the so far published data were obtained by steady-state spectroscopy only and lacked independent confirmation by time-resolved methods. Consequently, nearly no information was available about this new class of light harvesting and charge separating model compounds.

Two types of heterotrimers were synthesized, namely H_2Tr and ZnTr differing in the type of the porphyrins being attached to the silicon phthalocyanine. H_2Tr contains free base tetraphenylporphyrins, whereas in ZnTr the porphyrins bear a zinc atom, complexed by the four nitrogens of the porphyrin core.

Steady-state fluorescence techniques could not clearly identify energy- or electron-transfer in the P-Pc-P triads. Even though these results seemed discouraging at first glance, using time-resolved techniques it could be shown that minor traces of the highly fluorescent precursors of the synthesis deteriorated the steady-state fluorescence spectra. By combining the results of steady-state and time-resolved fluorescence and absorption spectroscopy the interplay of the moieties could be unraveled. With the help of global data analysis a complete scheme of the transfer rates was established. The influence of solvent polarity on electron transfer was investigated by choosing a polar (dimethylformamide) and an unpolar (toluene) solvent as environment.

The new class of porphyrin-phthalocyanine-heterotrimers exhibits very efficient energy transfer from the P moieties to the Pc-part of the triad. The transfer efficiency is larger than 80 % for H_2Tr independent of solvent polarity. For ZnTr in unpolar TOL the efficiency is about 45 %. In parallel, also electron transfer occurs from the initially excited P-part, leading to the formation of the charge separated state $P^{\bullet+}$-$Pc^{\bullet-}$-P. About 15 % of the excited porphyrin molecules contribute to electron transfer in H_2Tr independent of solvent polarity. In contrast, for ZnTr in TOL direct electron transfer from the P-part occurs in 55 % of all transitions. Only less than 0.5 % of H_2Tr

or ZnTr molecules dissipate the energy from the P-part into fluorescence, inter-system crossing, and internal conversion.

Direct or indirect population of the first excited singlet state of the Pc moiety is followed by hole transfer. This hole transfer creates the same charge separated state as electron transfer from the porphyrins does. Hole transfer is also very efficient, nearly 100 % of the excited phthalocyanine molecules transfer their energy into the charge separated state. Once separated, the charges recombine spontaneously after a certain time if they do not get drained. The average recombination time ranges from 20 ps to 280 ps, depending on the type of the porphyrins, and the solvent polarity. The CS state lifetime in polar DMF amounts to 30 ps and 20 ps for H_2Tr, and ZnTr, respectively. A smaller polarity of the solvent stabilizes the CS state for both H_2Tr and ZnTr. This effect is more pronounced for ZnTr, exhibiting a 14 times longer lifetime of the CS state. The lifetime of the CS state is only 6 times longer for H_2Tr in non-polar TOL. The small polarity of TOL not only prolongs the lifetime of the CS state, it also favors a backward hole transfer from the CS state to the first excited singlet state of the Pc-part. Phenomenological, this transfer shows up as a second fluorescence decay component of the Pc-part. Its lifetime is identical to the lifetime of the CS state, as known from other types of delayed fluorescence. Unfortunately, the appearance of the back hole transfer reduces the positive effect of the prolonged CS state lifetime by lowering the net efficiency of the charge separation process.

The ratios of electron and hole transfer rate to the charge recombination rate span the range from 4 to 300. The lowest ratio is found for H_2Tr in DMF, where both ratios (k_{ET}/k_{CR} and k_{HT}/k_{CR}) are about four. The highest and, thus, most favorable ratios in terms of energy retrieval, are found for ZnTr in TOL, where k_{ET}/k_{CR} equals to 125 and k_{HT}/k_{CR} is greater than 300.

A general conclusion from the data can be drawn as follows: Porphyrin-phthalocyanine-heteromers are good candidates for light-harvesting and charge separation complexes. The potential of the two non-sandwich-type metal coordinated heterotrimers acting as both light-harvesting complex and charge separation unit in one molecule could be demonstrated. This approves the

synthetic strategy of ligand coordination by a central metal atom as applicable technique. Energy transfer followed by hole transfer or direct electron transfer produce a charge separated state, efficiently. Even though these results are promising, the investigated P-Pc-P triads are not optimal, yet. Their absorption is very low over the large wavelength band from 450 nm to 650 nm. Also, a longer lifetime of the charge separated state would be desirable to allow the charges to move preferably into electrodes before recombination occurs. A larger ratio between the charge separation and the charge recombination rate would increase the final possible efficiency of energy production furthermore.

After publication of the encouraging results obtained in this thesis, modified compounds were synthesized by the group of Prof. Ng and others as well. In addition to pure P-Pc compounds, subphthalocyanine was utilized as antenna or as electron acceptor (El-Khouly et al., 2008, 2010). The use of fullerene coordinated or covalently linked to zinc porphyrins or zinc phthalocyanines in charge separation assemblies is already established for some time (D'Souza and Ito, 2005). Being promising building blocks, these moieties were utilized again in combination with axial coordination. Martin-Gomis et al. (2007), and El-Khouly et al. (2007) reported about new structures of fullerenes attached by metal coordination to a SiPc core. In the simplest case two fullerene moieties were linked to SiPc. In benzonitrile (PhCN) a CS state lifetime of 5 ns was observed for this system. Even longer lifetimes of the CS state were reported for molecules consisting of a SiPc core coupled to a dendritic structure of four or eight fullerenes. For the nonamer, lifetimes of the CS state longer than 160 ns could be observed in polar PhCN as well as in unpolar TOL. Unfortunately, all these compounds lack absorption in the wavelength range from 400 nm to 600 nm. A supramolecular pentad system (C60-NDI-SiPc-NDI-C60) comprising napthalene diimide (NDI) as a intermediate electron acceptor to the fullerenes showed also a long CS state lifetime of 1 ns (El-Khouly et al., 2009). However, also this system does not feature any strong absorption in the range from 400 nm to 600 nm. Interestingly, it exhibits a ratio of $k_{\mathrm{ET}}/k_{\mathrm{CR}}$ of about 3000. If one could combine such an effective electron transfer exhibiting a long lasting CS state with

broadband absorption, an excellent system would have been created.

Establishing a broader absorption was addressed by substituting the porphyrin moieties with boron dipyrromethene (BDP). Its absorption covers the gap between 400 nm and 600 nm where SiPc does not absorb light. Ermilov et al. (2009) reported about a triad consisting of BDP-SiPc-BDP. For the polar solvent DMF a CS state lifetime of about 30 ps was obtained. Also energy transfer took place from BDP to SiPc. In contrast, the CS state lifetime prolongs up to 4.5 ns in TOL, however the small polarity of the solvent prohibited charge transfer from the excited SiPc. Therefore, direct excitation of SiPc did not contribute to the charge separation efficiency.

A very recent work reported about a pentad where three BDP moities and a fullerene are linked to a zinc porphyrin core by click chemistry (Liu et al., 2011). Both, a singlet and a triplet charge-separated state could be observed. The singlet CS state lifetime has been evaluated to 476 ps in PhCN and to 1 ns in TOL. Unfortunately, it misses absorption above 550 nm, where the major amount of energy from sunlight is available. Furthermore, the estimated triplet state electron transfer rate on the order of $10^6\,s^{-1}$ may limit the duty cycle of energy conversion.

Yet another approach was followed by using host-guest interaction of tetrasulfonated porphyrins with β-cyclo-dextrins linked by coordination to subphthalocyanine (Xu et al., 2010) or SiPc (Ermilov et al., 2011). Remarkably, these compounds are water soluble and can be created easily by mixing two precursors. For the SiPc-based compound utilizing a glycol linker that allows the porphyrin to fold back, a CS state lifetime of 200 ps could be observed.

Unfortunately, all of these recent systems have a drawback at one point or another, too. Also a very limited number of these highly sophisticated light harvesting and charge separating compounds was ever tested in an OPV cell. For a review about investigated systems based on Ps or Pcs see Walter et al. (2010). Moreover, currently there is a trend seen to invest more efforts into research on dye sensitized solar cells, which seem to be more promising at the moment. Not having as high conversion efficiencies as inorganic solar cells yet, the commercial future is expected in segments where properties like

weight, mechanical flexibility, and price are more important than conversion efficiency. This is the case for functionalized fabric or modules incorporated into a bag or rucksack. Companies (i.e. G24 Innovations Limited) already start to market such products based on DSSCs. However, other companies (i.e. Dyesol) started to produce also large scale photovoltaic modules very recently (announced June 2011).

Many organic compounds were tested recently for use in DSSCs. The development looks similar to the beginning of mimicking reaction centers, many things are just tried out. The author believes that more efforts to include the already accumulated knowledge about already existing organic compounds for artificial photosynthesis could be beneficial for developing efficient and sustainable DSSCs and OPV cells. Commercial companies market DSSCs as artificial photosynthesis, however one should keep in mind which compounds are currently used to build a DSSC, most of the material is far from being sustainable.

Concluding, to date, there is still no artificial model of photosynthesis available, which has a high photo-conversion efficiency, a long lifetime, affordable manufacturing costs, and is overall producible in a more sustainable manner than inorganic or hybrid solar cells. Finally, there remains the hope that by targeted design or by chance a really usable artificial system can be realized by mankind faster than it has taken the evolution for the genesis of natural photosystems.

Bibliography

Adams, W. G. and Day, R. E. The action of light on selenium. *Proc. R. Soc. Lond.*, 25(171-178):113–117, 1876.

An, M.-S., Kim, S.-W., and Hong, J.-D. Synthesis and characterization of peripherally ferrocene-modified zinc phthalocyanine for dye-sensitized solar cell. *Bull. Korean Chem. Soc.*, 31(11):3272–3278, 2010.

Barbour, L., Hegadorn, M., and Asbury, J. Watching electrons move in real time: Ultrafast infrared spectroscopy of a polymer blend photovoltaic material. *J. Am. Chem. Soc.*, 129(51):15884–15894, 2007.

Battersby, A. R. Tetrapyrroles: the pigments of life. *Nat. Prod. Rep.*, 17:507–526, 2000.

Bauer, C., Teuscher, J., Brauer, J. C., Punzi, A., Marchioro, A., Ghadiri, E., De Jonghe, J., Wielopolski, M., Banerji, N., and Moser, J.-E. Dynamics and mechanisms of interfacial photoinduced electron transfer processes of third generation photovoltaics and photocatalysis. *Chimia*, 65(9):704–709, 2011.

Becquerel, A. E. Mémoire sur les effets électriques produits sous l'influence des rayons solaires. *Comptes Rendus*, 9:561–567, 1839.

Berber, G., Cammidge, A. N., Chambrier, I., Cook, M. J., and Hough, P. W. Controlled synthesis of ruthenium phthalocyanines and their use in the construction of supramolecular arrays. *Tetrahedron Lett.*, 44:5527–5529, 2003.

Bessho, T., Zakeeruddin, S. M., Yeh, C.-Y., Diau, E. W.-G., and Grätzel, M. Highly efficient mesoscopic dye-sensitized solar cells based on donor-acceptor-substituted porphyrins. *Angew. Chem. Int. Ed.*, 49(37):6646–6649, 2010.

Blankenship, R. *Molecular mechanisms of photosynthesis.* Blackwell Science, 2002.

Born, M. Volumen und Hydratationswärme der Ionen. *Z. Phys.*, 1:45–48, 1920.

Brabec, C. J., Gowrisanker, S., Halls, J. J. M., Laird, D., Jia, S., and Williams, S. P. Polymer-fullerene bulk-heterojunction solar cells. *Adv. Mater.*, 22(34):3839–3856, 2010.

Bradley, D. F. and Calvin, M. The effect of thioctic acid on the quantum efficiency of the hill reaction in intermittent light. *Proc. Nat. Acad. Sci.*, 41(8):563–571, 1955.

Braun, A. and Tcherniac, J. Über die Produkte der Einwirkung von Acetanhydrid auf Phthalamid. *Ber. Dtsch. Chem. Ges.*, 40(2):2709–2714, 1907.

Brown, H. and Escombe, F. Researches on some of the physiological processes of green leaves, with special reference of the interchange of energy between the leaf and its surroundings. *Proc. Roy. Soc. London, Series B*, 76:29–110, 1905.

Brumbach, M. T., Boal, A. K., and Wheeler, D. R. Metalloporphyrin assemblies on pyridine-functionalized titanium dioxide. *Langmuir*, 25(18):10685–10690, 2009.

Brunschwig, B. S., Ehrenson, S., and Sutin, N. Solvent reorganization in optical and thermal electron-transfer processes. *J. Phys. Chem.*, 90:3657–3668, 1986.

Calzaferri, G. Artificial photosynthesis. *Top. Catal.*, 53:130–140, 2010.

Calzaferri, G., Pauchard, M., Maas, H., Huber, S., Khatyr, A., and Schaafsma, T. Photonic antenna system for light harvesting, transport and trapping. *J. Mater. Chem.*, 12:1–13, 2002.

Cammidge, A. N., Berber, G., Chambrier, I., Hough, P. W., and Cook, M. J. Octaalkylphthalocyanato ruthenium (II) complexes with mixed axial

ligands and supramolecular porphyrin:phthalocyanine structures derived from them. *Tetrahedron*, 61:4067–4074, 2005.

Cammidge, A. N., Nekelson, F., Hughes, D. L., Zhao, Z., and Cook, M. J. Stepwise syntheses of complex μ-oxo-linked heterochromophore arrays containing phthalocyanine, porphyrin and subphthalocyanine ligands. *ChemInform*, 42(26), 2011.

Chang, D. W., Ko, S.-J., Kim, J. Y., Park, S.-M., Lee, H. J., Dai, L., and Baek, J.-B. Multifunctional conjugated polymers with main-chain donors and side-chain acceptors for dye sensitized solar cells (DSSCs) and organic photovoltaic cells (OPVs). *Macromol. Rapid Commun.*, 32(22):1809–1814, 2011.

Chapin, D. M., Fuller, C. S., and Pearson, G. L. A new silicon p-n junction photocell for converting solar radiation into electrical power. *J. Appl. Phys.*, 25(5):676–677, 1954.

Choi, M., Choi, C.-F., and Ng, D. Assembling tetrapyrrole derivates through axial coordination. *Tetrahedron*, 60:6889–6894, 2004.

Cid, J.-J., Garcia-Iglesias, M., Yum, J.-H., Forneli, A., Albero, J., Martinez-Ferrero, E., Vazquez, P., Grätzel, M., Nazeeruddin, M. K., Palomares, E., and Torres, T. Structure – function relationships in unsymmetrical zinc phthalocyanines for dye-sensitized solar cells. *Chem. Eur. J.*, 15(20):5130–5137, 2009.

Claessens, C. G., Gonzalez-Rodriguez, D., and Torres, T. Subphthalocyanines: Singular nonplanar aromatic compounds-synthesis, reactivity, and physical properties. *Chem. Rev.*, 102:835–853, 2002.

Claessens, C. G., Hahn, U., and Torres, T. Phthalocyanines: From outstanding electronic properties to emerging applications. *Chem. Rec.*, 8(2):75–97, 2008.

Clarke, T. M. and Durrant, J. R. Charge photogeneration in organic solar cells. *Chem. Rev.*, 110(11):6736–6767, 2010.

Corwin, A. H., Chivvis, A. B., Poor, R. W., Whitten, D. G., and Baker, E. W. The interpretation of porphyrin and metalloporphyrin spectra. *J. Am. Chem. Soc.*, 90(24):6577–6583, 1968.

Dalton, J. and Milgrom, L. R. A novel porphyrin with weak fluorescence due to intramolecular electron transfer quenching. *J.C.S. Chem. Comm.*, pages 609–610, 1979.

de Diesbach, H. and von der Weid, E. Quelques sels complexes des o-dinitriles avec le cuivre et la pyridine. *Helv. Chim. Acta*, 10(1):886–888, 1927.

Deisenhofer, J., Epp, O., Miki, K., Huber, R., and Michel, H. X-ray structure analysis of a membrane protein complex. electron density map at 3 Å resolution and a model of the chromophores of the photosynthetic reaction centre from rhodopsuedomonas viridis. *J. Mol. Biol.*, 180:385–398, 1984.

Deisenhofer, J., Epp, O., Sinning, I., and Michel, H. Crystallographic refinement at 2.3 Å resolution and refined model of the photosynthetic reaction centre from rhodopseudomonas viridis. *J. Mol. Biol.*, 246(3):429 – 457, 1995.

Dexter, D. A theory of sensitized luminescence in solids. *J. Chem. Phys.*, 21:836–850, 1953.

Dirac, P. On the theory of quantum mechanics. *Proc. Roy. Soc.*, A112:661–667, 1926.

Dirac, P. The quantum theory of the emission and absorption of radiation. *Proc. Roy. Soc.*, A114:243–265, 1927.

Dolphin, D., editor. *The Porphyrins*. Academic Press, New York :, 1978.

D'Souza, F. and Ito, O. Photoinduced electron transfer in supramolecular systems of fullerenes functionalized with ligands capable of binding to zinc porphyrins and zinc phthalocyanines. *Coord. Chem. Rev.*, 249(13-14):1410 – 1422, 2005.

Eichwurzel, I., Stiel, H., and Röder, B. Photophysical studies of the pheophorbide a dimer. *J. Photochem. Photobiol. B*, 54(2-3):194–200, 2000.

Einstein, A. Über einen die Erzeugung und Verwandlung des Lichtes betreffenden heuristischen Gesichtspunkt. *Ann. d. Phys.*, 17:132, 1905.

Einstein, A. Zur Quantentheorie der Strahlung. *Mitteilungen der Physikalischen Gesellschaft Zürich*, 18:47–62, 1916.

El-Khouly, M. E., Ito, O., Smith, P. M., and D'Souza, F. Intermolecular and supramolecular photoinduced electron transfer processes of fullerene porphyrin/phthalocyanine systems. *J. Photochem. Photobiol. C: Photochemistry Reviews*, 5:79– 104, 2004.

El-Khouly, M. E., Ju, D. K., Kay, K.-Y., D'Souza, F., and Fukuzumi, S. Supramolecular tetrad of subphthalocyanine-triphenylamine-zinc porphyrin coordinated to fullerene as an "antenna-reaction-center" mimic: Formation of a long-lived charge-separated state in nonpolar solvent. *Chem. Eur. J.*, 16(21):6193–6202, 2010.

El-Khouly, M. E., Kang, E. S., Kay, K.-Y., Choi, C. S., Aaraki, Y., and Ito, O. Silicon-phthalocyanine-cored fullerene dendrimers: Synthesis and prolonged charge-separated states with dendrimer generations. *Chem. Eur. J.*, 13(10):2854–2863, 2007.

El-Khouly, M. E., Kim, J. H., Kay, K.-Y., Choi, C. S., Ito, O., and Fukuzumi, S. Synthesis and photoinduced intramolecular processes of light-harvesting silicon phthalocyanine-naphthalenediimide-fullerene connected systems. *Chem. Eur. J.*, 15(21):5301–5310, 2009.

El-Khouly, M. E., Shim, S. H., Araki, Y., Ito, O., and Kay, K.-Y. Effect of dual fullerenes on lifetimes of charge-separated states of subphthalocyanine-triphenylamine-fullerene molecular systems. *J. Phys. Chem. B*, 112(13):3910–3917, 2008.

Emerson, R. and Arnold, W. The photochemical reaction in photosynthesis. *J. Gen. Physiol.*, 16:191–205, 1932a.

Emerson, R. and Arnold, W. A separation of the reactions in photosynthesis by means of intermittent light. *J. Gen. Physiol.*, pages 391–420, 1932b.

Ermilov, E., Tannert, S., Werncke, T., Choi, M., Ng, D., and Röder, B. Photoinduced electron and energy transfer in a new porphyrin-phthalocyanine triad. *Chem. Phys.*, 328:428–437, 2006.

Ermilov, E. A., Liu, J.-Y., Ng, D. K. P., and Röder, B. Spectroscopic study of electron and energy transfer in novel silicon phthalocyanine-boron dipyrromethene triads. *Phys. Chem. Chem. Phys.*, 11:6430–6440, 2009.

Ermilov, E. A., Menting, R., Lau, J. T. F., Leng, X., Röder, B., and Ng, D. K. P. Switching the photoinduced processes in host-guest complexes of β-cyclodextrin-substituted silicon(iv) phthalocyanines and a tetrasulfonated porphyrin. *Phys. Chem. Chem. Phys.*, 13:17633–17641, 2011.

Eu, S., Katoh, T., Umeyama, T., Matano, Y., and Imahori, H. Synthesis of sterically hindered phthalocyanines and their applications to dye-sensitized solar cells. *Dalton Trans.*, pages 5476–5483, 2008.

Falk, J. and Smith, K. *Porphyrins and metalloporphyrins: a new edition based on the original volume by J. E. Falk.* Elsevier Scientific Pub. Co., 1975.

Fischer, H. Chlorophyll. *Chem. Rev.*, 1920.

Förster, T. Energiewanderung und Fluoreszenz. *Naturwissenschaften*, 33(6):166–175, 1946.

Förster, T. Zwischenmolekulare Energiewanderung und Fluoreszenz. *Ann. Physik*, 437(1-2):55–75, 1948.

Förster, T. Experimentelle und theoretische Untersuchung des zwischenmolekularen Übergangs von Elektronenanregungsenergie. *Z. Naturforsch.*, 4a:321–327, 1949a.

Förster, T. Neuere Untersuchungen über die Phosphoreszenz organischer Stoffe in festen Lösungen. *Naturwissenschaften*, 36(8):240–245, 1949b.

Förster, T. Transfer mechanisms of electronic excitation energy. *Radiat. Res. Suppl.*, 2:326–339, 1960.

Fritts, C. On the Fritts selenium cells and batteries. *Procedings of the American Association for the Advancement of Science*, 33:97–108, 1883.

Fukuzumi, S., Honda, T., Ohkubo, K., and Kojima, T. Charge separation in metallomacrocycle complexes linked with electron acceptors by axial coordination. *Dalton Trans.*, pages 3880–3889, 2009.

Gaspard, S. Face to face porphyrine-phthalocyanine dimers. *Comptes Rendus De L Academie Des Sciences Serie III - Sciences De La Vie-Life Sciences*, 298(14):379–382, 1984.

Gaspard, S., Giannotti, C., Maillard, P., Schaeffer, C., and Tran-Thi, T. The first synthesis of covalently linked mixed dimer complexes containing phthalocyanine and porphyrin. *J. Chem. Soc., Chem. Comm.*, pages 1239–1241, 1986.

GIMP Toolkit. Gimp toolkit. 2002. URL `www.gtk.org`.

Golub, G. H. and Pereyra, V. The differentiation of pseudo-inverses and nonlinear least squares problems whose variables separate. *SIAM J. Numer. Anal.*, 10(2):413–432, 1973.

Gould, I., Ege, D., Moser, J., and Farid, S. Efficiencies of photoinduced electron-transfer reactions: Role of the marcus inverted region in return electron transfer within geminate radical-ion pairs. *J. Am. Chem. Soc.*, 112:4290, 1990.

Gould, I., Young, R., Moody, R., and Farid, S. Contact and solvent separated geminate radical ion pairs in electron transfer photochemistry. *Journal of Physical Chemistry*, 95:2068, 1991.

Gouloumis, A., González-Rodríguez, D., Vázquez, P., Torres, T., Liu, S., Echegoyen, L., Ramey, J., Hug, G. L., and Guldi, D. M. Control over charge separation in phthalocyanine-anthraquinone conjugates as a function of the aggregation status. *J. Am. Chem. Soc.*, 2006.

Gouterman, M. Study of the effects of substitution on the absorption spectra of porphin. *J. Chem. Phys.*, 30(5):1139–1161, 1959.

Gouterman, M. Spectra of porphyrins. *J. Mol. Spectrosc.*, 6:138–163, 1961.

Grätzel, M. Dye-sensitized solar cells. *J. Photochem. Photobiol. C*, 4(2):145–153, 2003.

Grätzel, M. Photovoltaic and photoelectrochemical conversion of solar energy. *Phil. Trans. R. Soc. A*, 365(1853):993–1005, 2007.

Grätzel, M. Recent advances in sensitized mesoscopic solar cells. *Accounts of Chemical Research*, 42(11):1788–1798, 2009.

Guldi, D. M. Fullerene-porphyrin architectures; photosynthetic antenna and reaction center models. *Chem. Soc. Rev.*, 31:22–36, 2002.

Guskov, A., Kern, J., Gabdulkhakov, A., Broser, M., Zouni, A., and Saenger, W. Cyanobacterial photosystem II at 2.9-Å resolution and the role of quinones, lipids, channels and chloride. *Nat. Struct. Mol. Biol.*, 16(3):334–342, 2009.

Gust, D., Moore, T. A., Moore, A. L., Krasnovsky, A. A., Liddell, P. A., Nicodem, D., DeGraziano, J. M., Kerrigan, P., Makings, L. R., and Pessiki, P. J. Mimicking the photosynthetic triplet energy-transfer relay. *J. Am. Chem. Soc.*, 115(13):5684–5691, 1993.

Hackbarth, S., Ermilov, E., and Röder, B. Interaction of pheophorbide a molecules covalently linked to dab dendrimers. *Opt. Commun.*, 248(1-3):295–306, 2005.

Hackbarth, S., Horneffer, V., Wiehe, A., Hillenkamp, F., and Röder, B. Photophysical properties of pheophorbide-a-substituted diaminobutane poly-propylene-imine dendrimer. *Chem. Phys.*, 269(1-3):339 – 346, 2001.

Hadamard, J. Sur les problèmes aux dérivées partielles et leur signification physique. *Princeton University Bulletin*, 13:49–52, 1902.

Hagfeldt, A., Boschloo, G., Sun, L., Kloo, L., and Pettersson, H. Dye-sensitized solar cells. *Chem. Rev.*, 110(11):6595–6663, 2010.

Harbour, J. R. and Tollin, G. In vitro photoreactions of chlorophyll and photosynthetic energy conversion: Chlorophyll-quinone-ethanol at low temperature as an analog of photosystems I and II. *Proc. Nat. Acad. Sci. U.S.A.*, 69:2066–2068, 1972.

Harriman, A. Außergewöhnlich langsame Ladungsrekombination in molekularen Dyaden. *Angew. Chem.*, 116:5093–5095, 2004.

Harriman, A., Mallon, L. J., Elliot, K. J., Haefele, A., Ulrich, G., and Ziessel, R. Length dependence for intramolecular energy transfer in three- and four-color donor-spacer-acceptor arrays. *J. Am. Chem. Soc.*, 131(37):13375–13386, 2009.

Harriman, A. and Sauvage, J. A strategy for constructing photosynthetic models: Porphyrin-containing modules assembled around transition metals. *Chem. Soc. Rev.*, 25:41–48, 1996.

Hauschild, T. and Jentschel, M. Comparison of maximum likelihood estimation and chi-square statistics applied to counting experiments. *Nucl. Instrum. Meth. A*, 457(1-2):384 – 401, 2001.

Hausmann, A., Soares, A. R. M., Martinez-Diaz, M. V., Neves, M. G. P. M. S., Tome, A. C., Cavaleiro, J. A. S., Torres, T., and Guldi, D. M. Transduction of excited state energy between covalently linked porphyrins and phthalocyanines. *Photochem. Photobiol. Sci.*, 9:1027–1032, 2010.

Haycock, R. A., Hunter, C. A., James, D. A., Michelsen, U., and Sutton, L. R. Self-assembly of oligomeric porphyrin rings. *Org. Lett.*, 2(16):2435–2438, 2000.

Heitele, H., Finckh, P., Weeren, S., Pöllinger, F., and Michel-Beyerle, M. Solvent polarity effects on intramolecular electron transfer 1. energetic aspects. *J. Phys. Chem.*, 93:5173–5179, 1989.

Hirade, M., Nakanotani, H., Yahiro, M., and Adachi, C. Formation of organic crystalline nanopillar arrays and their application to organic photovoltaic cells. *ACS Appl. Mater. & Interfaces*, 3(1):80–83, 2011.

Hohmann-Marriott, M. F. and Blankenship, R. E. Evolution of photosynthesis. *Annu. Rev. Plant Biol.*, 62(1):515–548, 2011.

Hollas, J. M. *Modern Spectroscopy*, chapter 4, pages 63–88. John Wiley & Sons, 1998.

Hush, N. S. Adiabatic theory of outer sphere electron-transfer reactions in solution. *Trans. Faraday Soc.*, 57:557–580, 1961.

Hyperchem. *HyperChem 5.02 evaluation release.* HyperCube, Inc., Gainesville, FL, USA, 1997.

Imahori, H., Umeyama, T., and Ito, S. Large π-aromatic molecules as potential sensitizers for highly efficient dye-sensitized solar cells. *Acc. Chem. Res.*, 42(11):1809–1818, 2009.

Imahori, H., Yamada, H., Guldi, D. M., Endo, Y., Shimomura, A., Kundu, S., Yamada, K., Okada, T., Sakata, Y., and Fukuzumi, S. Comparison of reorganization energies for intra- and intermolecular electron transfer. *Angew. Chem. Int. Ed.*, 41(13):2344–2347, 2002.

Ince, M., Claessens, C. G., Brühwiler, D., Calzaferri, G., and Torresa, T. Synthesis of subphthalocyanine-based stopcock for zeolite L. *Macroheterocycles*, 4(4):246–249, 2011.

Ito, F., Ishibashi, Y., Khan, S. R., Miyasaka, H., Kameyama, K., Morisue, M., Satake, A., Ogawa, K., and Kobuke, Y. Photoinduced electron transfer and excitation energy transfer in directly linked zinc porphyrin/zinc phthalocyanine composite. *J. Phys. Chem. A*, 110(47):12734–12742, 2006.

Jeong, N. C., Prasittichai, C., and Hupp, J. T. Photocurrent enhancement by surface plasmon resonance of silver nanoparticles in highly porous dye-sensitized solar cells. *Langmuir*, 27(23):14609–14614, 2011.

Johnson, D., Niemczyk, M., Minsek, D., Wiederrecht, G., Svec, W., Gaines, G., and Wasielewski, M. Photochemical electron transfer in chlorophyll-porphyrin-quinone triads: the role of the porphyrin-bridging molecule. *J. Am. Chem. Soc.*, 115(13):5692 – 5701, 1993.

Jortner, J. Temperature dependent activation energy for electron transfer between biological molecules. *J. Chem. Phys.*, 64(12):4860–4867, 1976.

Kalyanasundaram, K. and Grätzel, M. Artificial photosynthesis: biomimetic approaches to solar energy conversion and storage. *Curr. Opin. Biotechnol.*, 21(3):298 – 310, 2010.

Kalyanasundaram, K., Zakeeruddin, S. M., and Grätzel, M. Photonic and optoelectronic devices based on mesoscopic thin films. *Chimia*, 65(9):738–742, 2011.

Kavarnos, G. and Turro, N. Photosensitization by reversible electron transfer: Theories, experimental evidence, and examples. *Chem. Rev.*, 86:401–449, 1986.

Kearns, D. and Calvin, M. Photovoltaic effect and photoconductivity in laminated organic systems. *J. Chem. Phys.*, 29(4):950–951, 1958.

Kim, H. J., Park, K.-M., Ahn, T. K., Kim, S. K., Kim, k. S., Kim, D., and Kim, H.-J. Novel fullerene-porphyrine-fullerene triad linked by metal axial coordination: synthesis, X-ray structure, and spectroscopic characterizations of *trans*-bis([60]fullerenoacetato)tin(IV) porphyrin. *Chem. Commun.*, pages 2594–2595, 2004.

Kirchhoff, G. and Bunsen, R. Chemische Analyse durch Spectralbeobachtungen. *Pogg. Ann.*, 110(8):161–189, 1860.

Knox, R. and van Amerongen, H. Refractive index dependence of the Förster resonance excitation transfer rate. *J. Phys. Chem. B*, 106:5289–5293, 2002.

Knutson, J., Walbridge, D., and L., B. Decay-associated fluorescence spectra and the heterogeneous emission of alcohol dehydrogenase. *Biochemistry*, 21:4671, 1982.

Kobayashi, N. Dimers, trimers and oligomers of phthalocyanines and related compounds. *Coord. Chem. Rev.*, 227:129, 2002.

Kobayashi, N., Nishiyama, Y., Ohya, T., and Sato, M. Symmetrically tetra-substituted phthalocyanines. *J. Chem. Soc., Chem. Commun.*, pages 390–392, 1987.

Kobuke, Y. Artificial light-harvesting systems by use of metal coordination. *Eur. J. Inorg. Chem.*, 2006(12):2333–2351, 2006.

Kodis, G., , Herrero, C., Palacios, R., Mariño Ochoa, E., Goul, S., de la Garza, L., Van Grondelle, R., Gust, D., Moore, T. A., Moore, A. L., and Kennis, J. T. M. Light harvesting and photoprotective functions of carotenoids in compact artificial photosynthetic antenna designs. *J. Phys. Chem. B*, 108(1):414–425, 2004.

Kolb, H. C., Finn, M. G., and Sharpless, K. B. Click chemistry: Diverse chemical function from a few good reactions. *Angew. Chem. Int. Ed.*, 40(11):2004–2021, 2001.

Kong, J. and Loach, P. Covalently-linked porphyrin quinone complexes as RC models. In P. Dutton, J. Leigh, and S. A., editors, *Frontiers of Biological Energetics — Electrons to Tissues*, volume 1, pages 73–82. Academic Press: New York, 1978.

Korth, O., Hanke, T., Rückmann, I., and Röder, B. High sensitive and spatially resolved absorption / fluorescence measurements on ultrathin Langmuir-Blodgett-films. *Exp. Tech. Phys.*, 41:25, 1995.

Koyama, Y., Miki, T., Wang, X.-F., and Nagae, H. Dye-sensitized solar cells based on the principles and materials of photosynthesis: Mechanisms of suppression and enhancement of photocurrent and conversion efficiency. *Int. J. Mol. Sci.*, 10(11):4575–4622, 2009.

Krogh, F. Efficient implementation of a variable projection algorithm for nonlinear least squares problems. *Commun. ACM*, 17(3):167–169, 1974.

Kroto, H. W., Heath, J. R., O'Brien, S. C., Curl, R. F., and Smalley, R. E. C60: Buckminsterfullerene. *Nature*, 318(6042):162–163, 1985.

Lachkar, M., De Cian, A., Fischer, J., and Weiss, R. Novel sandwich-type complexes: synthesis, structure, spectral, and redox properties of 1 to 1 porphyrin-phthalocyanine cerium(IV) complexes: Ce(Po)(Pc). *New J. Chem.*, 12(8-9):729–31, 1988.

Lakowicz, J. *Principles of fluorescence spectroscopy.* Plenum Press, New York, 1999.

Lee, C. Y., She, C., Jeong, N. C., and Hupp, J. T. Porphyrin sensitized solar cells: TiO2 sensitization with a π-extended porphyrin possessing two anchoring groups. *Chem. Commun.*, 46:6090–6092, 2010.

Li, J., Diers, J. R., Seth, J., Yang, S. I., Bocian, D. F., Holten, D., and Lindsey, J. S. Synthesis and properties of star-shaped multiporphyrin-phthalocyanine light harvesting arrays. *J. Org. Chem.*, 64:9090–9100, 1999.

Li, J. and Lindsey, J. S. Efficient synthesis of light-harvesting arrays composed of eight porphyrins and one phthalocyanine. *J. Org. Chem*, 64:9101–9108, 1999.

Li, X.-y. and Ng, D. Self-assembly of *meso*-pyridylporphyrins and zinc phthalocyanines through axial coordination. *Eur. J. Inorg. Chem.*, 2000(8):1845–1848, 2000.

Lin, C.-F., Zhang, M., Liu, S.-W., Chiu, T.-L., and Lee, J.-H. High photoelectric conversion efficiency of metal phthalocyanine/fullerene heterojunction photovoltaic device. *Int. J. Mol. Sci.*, 12(1):476–505, 2011a.

Lin, J.-Y., Liao, J.-H., and Wei, T.-C. Honeycomb-like CoS counter electrodes for transparent dye-sensitized solar cells. *Electrochem. Solid-State Lett.*, 14(4):D41–D44, 2011b.

Lindsey, J. S. and Mauzerall, D. C. Synthesis of a cofacial porphyrin-quinone via entropically favored macropolycyclization. *J. Am. Chem. Soc.*, 104:4498–4500, 1982.

Linstead, R. P. Phthalocyanines. Part I. A new type of synthetic colouring matters. *J. Chem. Soc.*, 1:1016 – 1017, 1934a.

Linstead, R. P. Phthalocyanines. Part II. The preparation of phthalocyanine and some metallic derivatives from o-cyanobenzamide and phthalimide. *J. Chem. Soc.*, 1:1017–1022, 1934b.

Linstead, R. P. Phthalocyanines. Part III. Preliminary experiments on the preparation of phthalocyanines from phthalonitrile. *J. Chem. Soc.*, 1:1022–1027, 1934c.

Linstead, R. P. Phthalocyanines. Part IV. Copper phthalocyanines. *J. Chem. Soc.*, 1:1027–1031, 1934d.

Linstead, R. P. Phthalocyanines. Part V. The molecular weight of magnesium phthalocyanine. *J. Chem. Soc.*, 1:1031–1033, 1934e.

Linstead, R. P. Phthalocyanines. Part VI. The structure of the phthalocyanines. *J. Chem. Soc.*, 1:1033–1039, 1934f.

Liu, J.-Y., El-Khouly, M. E., Fukuzumi, S., and Ng, D. K. P. Mimicking photosynthetic antenna-reaction-center complexes with a (boron dipyrromethene)3-porphyrin-C60 pentad. *Chem. Eur. J.*, 17(5):1605–1613, 2011.

Lo, P.-C., Huang, J.-D., Cheng, D. Y. Y., Chan, E. Y. M., Fong, W.-P., Ko, W.-H., and Ng, D. K. P. New amphiphilic silicon(iv) phthalocyanines as efficient photosensitizers for photodynamic therapy: Synthesis, photophysical properties, and in vitro photodynamic activities. *Chem. Eur. J.*, 10:4831–4838, 2004.

Longuet-Higgins, H. C., Rector, C. W., and Platt, J. R. Molecular orbital calculations on porphine and tetrahydroporphine. *J. Chem. Phys.*, 18(9):1174–1181, 1950.

Lutz, D. R., Nelson, K. A., Gochanour, C. R., and Fayer, M. D. Electronic excited state energy transfer, trapping by dimers and fluorescence quenching

in concentrated dye solutions: Picosecond transient grating experiments. *Chem. Phys.*, 58:325–334, 1981.

Ma, R., Guo, P., Yang, L., Guo, L., Zhang, X., Nazeeruddin, M. K., and Grätzel, M. Theoretical screening of -NH_2-, -OH-, -CH_3-, -F-, and -SH-substituted porphyrins as sensitizer candidates for dye-sensitized solar cells. *J. Phys. Chem. A*, 114(4):1973–1979, 2010.

Mack, J. and Stillman, M. J. Electronic structures of metal phthalocyanine and porphyrin complexes from analysis of the uv-visible absorption and magnetic circular dichroism spectra and molecular orbital calculations. In K. M. Kadish, K. M. Smith, and R. Guilard, editors, *The Porphyrin Handbook*, volume 16, pages 43–113. Academic Press, San Diego, California, 2003.

Mai, C.-L., Huang, W.-K., Lu, H.-P., Lee, C.-W., Chiu, C.-L., Liang, Y.-R., Diau, E. W.-G., and Yeh, C.-Y. Synthesis and characterization of diporphyrin sensitizers for dye-sensitized solar cells. *Chem. Commun.*, 46:809–811, 2010.

Maligaspe, E., Kumpulainen, T., Lemmetyinen, H., Tkachenko, N. V., Subbaiyan, N. K., Zandler, M. E., and D'Souza, F. Ultrafast singlet-singlet energy transfer in self-assembled via metal-ligand axial coordination of free-base porphyrin-zinc phthalocyanine and free-base porphyrin-zinc naphthalocyanine dyads. *J. Phys. Chem. A*, 114(1):268–277, 2010.

Mandelbrojt, S. and Schwartz, L. Jacques Hadamard (1865-1963). *Bull. Amer. Math. Soc.*, 71(1):107–129, 1965.

Marcus, R. and Sutin, N. Electron transfers in chemistry and biology. *Biochem. Biophys. Acta*, 811(33):265–322, 1985.

Marcus, R. A. On the theory of oxidation-reduction reactions involving electron transfer. I. *J. Chem. Phys.*, 24(5):966–978, 1956.

Marcus, R. A. On the theory of electron-transfer reactions. VI. Unified treatment for homogeneous and electrode reactions. *J. Chem. Phys.*, 43(2):679–701, 1965.

Marcus, R. A. Electron transfer reactions in chemistry. Theory and experiment. *Rev. Mod. Phys.*, 65(3):599–610, 1993.

Maree, M. D. and Nyokong, T. Synthesis, spectroscopy and electrochemistry of octaphenoxyphthalocyaniato silcon complexes. *J. Porphyrins Phthalocyanines*, 5:555–563, 2001.

Marek, P. L., Hahn, H., and Balaban, T. S. On the way to biomimetic dye aggregate solar cells. *Energy Environ. Sci.*, 4:2366–2378, 2011.

Marian, C. M. Spin-orbit coupling and intersystem crossing in molecules. *Wiley Interdiscip. Rev. Comput. Mol. Sci.*, 2(2):187–203, 2012.

Martin-Gomis, L., Ohkubo, K., Fernandez-Lazaro, F., Fukuzumi, S., and Sastre-Santos, A. Synthesis and photophysical studies of a new nonaggregated C60-silicon phthalocyanine-C60 triad. *Org. Lett.*, 9(17):3441–3444, 2007.

Martin-Gomis, L., Ohkubo, K., Fernandez-Lazaro, F., Fukuzumi, S., and Sastre-Santos, A. Adiabatic photoinduced electron transfer and back electron transfer in a series of axially substituted silicon phthalocyanine triads. *J. Phys. Chem. C*, 112(45):17694–17701, 2008.

Martinez-Diaz, M., Ince, M., and Torres, T. Phthalocyanines: colorful macroheterocyclic sensitizers for dye-sensitized solar cells. *Monatsh. Chem.*, 142:699–707, 2011.

Maus, M., Cotlet, M., Hofkens, J., Gensch, T., De Schryver, F. C., Schaffer, J., and Seidel, C. A. M. An experimental comparison of the maximum likelihood estimation and nonlinear least-squares fluorescence lifetime analysis of single molecules. *Anal. Chem.*, 73(9):2078–2086, 2001.

McConnell, I., Li, G., and Brudvig, G. W. Energy conversion in natural and artificial photosynthesis. *Chem. Biol.*, 17(5):434 – 447, 2010.

McNaught, A. D., Wilkinson, A., Nic, M., Jirat, J., Kosata, B., and Jenkins, A. *IUPAC. Compendium of Chemical Terminology, The "Gold Book". XML on-line corrected version: http://goldbook.iupac.org*. Blackwell Scientific Publications, 1997.

Megow, J., Röder, B., Kulesza, A., Bonačić-Koutecký, V., and May, V. A mixed quantum-classical description of excitation energy transfer in supramolecular complexes: Förster theory and beyond. *ChemPhysChem*, 12(3):645–656, 2011.

Meyer, G. J. The 2010 millennium technology grand prize: Dye-sensitized solar cells. *ACS Nano*, 4(8):4337–4343, 2010.

Miller, J. R., Calcaterra, L. T., and Closs, G. L. Intramolecular long-distance electron transfer in radical anions. the effects of free energy and solvent on the reaction rates. *J. Am. Chem. Soc.*, 106(10):3047–3049, 1984.

Miller, R. K., M. A.and Lamm, Prathapan, S., Holten, D., and Lindsey, J. S. A tightly coupled linear array of perylene, bis(porphyrin), and phthalocyanine units that functions as a photoinduced energy-transfer cascade. *J. Org. Chem.*, 65:6634–6649, 2000.

Minimalist GNU for Windows. Minimalist gnu for windows. 2003. URL `www.mingw.org`.

Moser, J. Notiz über Verstärkung photo-elektrischer Ströme durch optische Sensibilierung. *Monatsh. Chem.*, 8:373, 1887.

Mulliken, R. S. Intensities of electronic transitions in molecular spectra I. Introduction. *J. Chem. Phys.*, 7(1):14–20, 1939a.

Mulliken, R. S. Intensities of electronic transitions in molecular spectra VIIIa. Odd-numbered conjugated polyene chain molecules and organic dyes (with notes on optical anisotropy and raman intensities). *J. Chem. Phys.*, 7(8):570–572, 1939b.

Nelder, J. A. and Mead, R. A simplex method for function minimization. *Comput. J.*, 7:308–315, 1965.

Ng, D. and Jiang, J. Sandwich-type heteroleptic phthalocyaninato and porphyrinato metal complexes. *Chem. Soc. Rev.*, 26(6):433–442, 1997.

Nobel Prize. The nobel prize in chemistry. 1999. URL `http://nobelprize.org/nobel_prizes/chemistry/laureates/1999/`. (online, as of March 2012).

Norrish, R. and Porter, G. Chemical reactions produced by very high light intensities. *Nature*, 164:658, 1949.

Noy, D., Moser, C., and Dutton, P. Design and engineering of photosynthetic light-harvesting and electron transfer using length, time, and energy scales. *Biochem. Biophys. Acta*, 1757(2):90–105, 2006.

Ohkubo, K., Kotani, H., Shao, J., Ou, Z., Kadish, K. M., Li, G., Pandey, R. K., Fujitsuka, M., Ito, O., Imahori, H., and Fukuzumi, S. Production of an ultra-long-lived charge-separated state in a zinc chlorin-C60 dyad by one-step photoinduced electron transfer. *Angew. Chem. Int. Ed.*, 43:853–853, 2004.

Olaya-Castro, A. and Scholes, G. D. Energy transfer from Förster-Dexter theory to quantum coherent light-harvesting. *Int. Rev. Phys. Chem.*, 30(1):49–77, 2011.

Onuchic, J. N., Beratan, D. N., and Hopfield, J. J. Some aspects of electron-transfer reaction dynamics. *J. Phys. Chem.*, 90(16):3707–3721, 1986.

O'Regan, B. and Grätzel, M. A low-cost, high-efficiency solar cell based on dye-sensitized colloidal TiO2 films. *Nature*, 353(6346):737–740, 1991.

Osati, S., Safari, N., and Jamaat, P. R. Synthesis and characterization of three covalently linked porphyrin-phthalocyanine pentamers with nucleophilic substitution. *Inorg. Chim. Acta*, 363(10):2180 – 2184, 2010.

Ostwald, W. *Die Mühle des Lebens: physikalisch-chemische Grundlagen der Lebensvorgänge*. Theod. Thomas, 1911.

Pan, X., Li, M., Wan, T., Wang, L., Jia, C., Hou, Z., Zhao, X., Zhang, J., and Chang, W. Structural insights into energy regulation of light-harvesting complex CP29 from spinach. *Nat. Struct. Mol. Biol.*, 18(3):309–315, 2011.

Paul, A., Hackbarth, S., Mölich, A., Luban, C., Oelckers, S., Böhm, F., and Röder, B. Comparative study on the photosensitization of jurkat cells in vitro by pheophorbide-a and a pheophorbide-a diaminobutane polypropylene-imine dendrimer complex. *Laser phys.*, 13:22–29, 2003.

Pelletier and Caventou. Sur la matière verte des feuilles. *Ann. Chim. Phys.*, 9:194–196, 1818.

Pereira, A. M. V. M., Soares, A. R. M., Hausmann, A., Neves, M. G. P. M. S., Tome, A. C., Silva, A. M. S., Cavaleiro, J. A. S., Guldi, D. M., and Torres, T. Distorted fused porphyrin-phthalocyanine conjugates: synthesis and photophysics of supramolecular assembled systems with a pyridylfullerene. *Phys. Chem. Chem. Phys.*, 13:11858–11863, 2011.

Pereira, M. R., Ferreira, J. a. A., and Hungerford, G. Preferential formation of mixed dimers in aluminium containing porphyrin phthalocyanine systems: A photophysical study. *Chem. Phys. Lett.*, 406:360–365, 2005.

Platt, J. Molecular orbital predictions of organic spectra. *J. Chem. Phys.*, 18:1168–1173, 1950.

Platt, J. R. Classification of spectra of cata-condensed hydrocarbons. *J. Chem. Phys.*, 17(5):484–495, 1949.

Porter, G. The bakerian lecture, in vitro models for photosynthesis. *Proc. R. Soc. Lond. A Math. Phys. Sci.*, 362(1710):281–303, 1978.

Rawling, T., Austin, C., Buchholz, F., Colbran, S. B., and McDonagh, A. M. Ruthenium phthalocyanine-bipyridyl dyads as sensitizers for dye-sensitized solar cells: Dye coverage versus molecular efficiency. *Inorg. Chem.*, 48(7):3215–3227, 2009.

Rehm, D. and Weller, A. Kinetik und Mechanismus der Elektronübertragung bei der Fluoreszenzlöschung in Acetonitril. *Ber. Bunsen-Ges. Phys. Chem.*, 73(8-9):834–839, 1969.

Rückmann, I., Zeug, A., Herter, R., and Röder, B. On the influence of higher excited states on the ISC quantum yield of octa-alpha-alkyloxy-substituted Zn-phthalocyanine molecules studied by nonlinear absorption. *Photochem. Photobiol.*, 66:576–584, 1997.

Rühle, S., Shalom, M., and Zaban, A. Quantum-dot-sensitized solar cells. *ChemPhysChem*, 11(11):2290–2304, 2010.

Sauvage, F., Chen, D., Comte, P., Huang, F., Heiniger, L.-P., Cheng, Y.-B., Caruso, R. A., and Grätzel, M. Dye-sensitized solar cells employing a single film of mesoporous TiO2 beads achieve power conversion efficiencies over 10%. *ACS Nano*, 4(8):4420–4425, 2010.

Sauvage, F., Chhor, S., Marchioro, A., Moser, J.-E., and Grätzel, M. Butyronitrile-based electrolyte for dye-sensitized solar cells. *J. Am. Chem. Soc.*, 133(33):13103–13109, 2011.

Seybold, P. and Gouterman, M. Porphyrins: XIII: Fluorescence spectra and quantum yields. *J. Mol. Spectr.*, 31:1, 1969.

Shockley, W. and Queisser, H. J. Detailed balance limit of efficiency of p-n junction solar cells. *J. Appl. Phys.*, 32(3):510–519, 1961.

Simpson, W. T. On the theory of the π-electron system in porphines. *J. Chem. Phys.*, 17(12):1218–1221, 1949.

Snaith, H. J. Estimating the maximum attainable efficiency in dye-sensitized solar cells. *Adv. Funct. Mater.*, 20(1):13–19, 2010.

Stillmann, T., M.J. und Nyokong. Absorption and magnetic circular dichroism spectral properties of phthalocyanines part 1: Complexes of the dianion pc(-2). In A. B. P. Leznoff, C. C. und Lever, editor, *Phthalocyanines: Properties and Applications*, volume 1, pages 133–289. New York: VCH, 1989.

Strachan, J.-P., Gentemann, S., Seth, J., Kalsbeck, W. A., Lindsey, J. S., Holten, D., and Bocian, D. F. Effects of orbital ordering on electronic communication in multiporphyrin arrays. *J. Am. Chem. Soc.*, 119:11191–11201, 1997.

Strickland, D. and Mourou, G. Compression of amplified chirped optical pulses. *Opt. Com.*, 55(6):447 – 449, 1985.

Suppan, P. The importance of the electrostatic interaction in condensed-phase photoinduced electron transfer. *J. Chem. Soc. Faraday Trans I*, 82:509–511, 1986.

Sutton, J. M. and Boyle, R. W. First synthesis of porphyrin-phthalocyanine heterodimers with a direct ethynyl linkage. *Chem. Commun.*, pages 2014–2015, 2001.

Tabushi, I., Koga, N., and Yanagita, M. Efficient intramolecular quenching and electron transfer in tetraphenylporphyrin attached with benzoquinone or hydroquinone as a photosystem model. *Tetrahedron Lett.*, 3:257–260, 1979.

Takechi, K., Shiga, T., Akiyama, T., and Yamada, S. A Z-scheme type photoelectrochemical cell consisting of porphyrin-containing polymer and dye-sensitized TiO2 electrodes. *Photochem. Photobiol. Sci.*, 9:1085–1087, 2010.

Tang, C. W. Two-layer organic photovoltaic cell. *Appl. Phys. Lett.*, 48(2):183–185, 1986.

Tannert, S. *Untersuchung zum photoinduzierten intramolekularen Elektronentransfer in einer Porphyrin-Chinon-Tetrade in Lösung.* Master's thesis, Humboldt-University of Berlin, 1999.

Tannert, S., Ermilov, E. A., Vogel, J. O., Choi, M. T. M., Ng, D. K. P., and Röder, B. The influence of solvent polarity and metalation on energy and electron transfer in porphyrin-phthalocyanine heterotrimers. *J. Phys. Chem. B*, 111(28):8053–8062, 2007.

Tannert, S., Hackbarth, S., Ermilov, E., and Röder, B. Energy migration on pheophorbide a loaded DAB dendrimers. *J. Porphyrins Phthalocyanines*, 8:350, 2004.

Taylor, R. and Walton, D. R. M. The chemistry of fullerenes. *Nature*, 363(6431):685–693, 1993.

Tetreault, N., Arsenault, E., Heiniger, L.-P., Soheilnia, N., Brillet, J., Moehl, T., Zakeeruddin, S., Ozin, G. A., and Grätzel, M. High-efficiency dye-sensitized solar cell with three-dimensional photoanode. *Nano Lett.*, 11(11):4579–4584, 2011.

Thrush, B. A. The genesis of flash photolysis. *Photochem. Photobiol. Sci.*, 2:453–454, 2003.

Tian, H.-J., Zhou, Q.-F., S.-Y., S., and Xu, H.-J. Solvent effects on competitive intramolecular electron transfer and energy transfer in a covalently linked porphyrin-phthalocyanine heterodimer. *Chin. J. Chem.*, 14:412–420, 1996.

Tian, H.-J., Zhou, Q.-F., Shen, S.-Y., and Xu, H.-J. Singlet-singlet intramolecular energy and electron transfer in covalently-linked porphyrin-phthalocyanine heterodimers. *J. Photochem. Photobiol. A: Chem.*, 72(2):163–168, 1993.

Tomé, J. P., Pereira, A. M. V. M., Alonso, C. M. A., Neves, M. G. P. M. S., Tomé, A. C., Silva, A. M. S., Cavaleiro, J. A. S., Martínez-Díaz, M. V., Torres, T., Rahman, G. M. A., Ramey, J., and Guldi, D. M. Synthesis and photophysical studies of new porphyrin-phthalaocyaine dyads with hindered rotation. *Eur. J. Org. Chem.*, pages 257–267, 2006.

Tong, S., Zhang, J., Yan, Y., Hu, S., Yu, J., and Yu, L. Self-assembled supramolecular architecture with alternating porphyrin and phthalocyanine, bonded by hydrogen bonding and π-π stacking. *Solid State Sci.*, 13(11):1967 – 1971, 2011.

Tran-Thi, T.-H. Assemblies of phthalocyanines with porphyrins and porphyrazines: ground and excited state optical properties. *Coord. Chem. Rev.*, 160:53–91, 1997.

Tran-Thi, T.-H., Desforge, C., and Thiec, C. Singlet-singlet and triplet-triplet intramolecular transfer processes in a covalently linked porphyrin-phthalocyanine heterodimer. *J. Phys. Chem.*, 93:1226–1233, 1989.

Turro, N., Ramamurthy, V., and Scaiano, J. *Principles of molecular photochemistry: an introduction*. University Science Books, 2009.

Umena, Y., Kawakami, K., Shen, J.-R., and Kamiya, N. Crystal structure of oxygen-evolving photosystem II at a resolution of 1.9Å. *Nature*, 473(7345):55–60, 2011.

Vogel, J.-O. *Untersuchung des photoinduzierten Elektronentransfers in einem axial verknüpften Porphyrin-Phthalocyanin-Trimer*. Master's thesis, Humboldt-University of Berlin, 2005.

Völker, A. *Erste Femtosekunden-Messungen an Farbstoff-Dendrimer-Komplexen*. Master's thesis, Humboldt-University Berlin, 2003.

von Würtemberg, I. M. *Ill-posed problems and their applications to climate research*. Master's thesis, University of Uppsala, 2011.

Walter, M. G., Rudine, A. B., and Wamser, C. C. Porphyrins and phthalocyanines in solar photovoltaic cells. *J. Porphyrins Phtalocyanines*, 14:787–792, 2010.

Wan, X., Long, G., Huang, L., and Chen, Y. Graphene - a promising material for organic photovoltaic cells. *Adv. Mater.*, 2011.

Wang, M., Anghel, A. M., Marsan, B., Cevey Ha, N.-L., Pootrakulchote, N., Zakeeruddin, S. M., and Grätzel, M. CoS supersedes Pt as efficient electrocatalyst for triiodide reduction in dye-sensitized solar cells. *J. Am. Chem. Soc.*, 131(44):15976–15977, 2009.

Wang, M., Chamberland, N., Breau, L., Moser, J.-E., Humphry-Baker, R., Marsan, B., Zakeeruddin, S. M., and Grätzel, M. An organic redox electrolyte to rival triiodide/iodide in dye-sensitized solar cells. *Nat. Chem.*, 2(5):385–389, 2010a.

Wang, Q., Campbell, W. M., Bonfantani, E. E., Jolley, K. W., Officer, D. L., Walsh, P. J., Gordon, K., Humphry-Baker, R., Nazeeruddin, M. K., and Grätzel, M. Efficient light harvesting by using green Zn-porphyrin-sensitized nanocrystalline TiO2 films. *J. Phys. Chem. B*, 109(32):15397–15409, 2005.

Wang, X.-F., Koyama, Y., Kitao, O., Wada, Y., ich Sasaki, S., Tamiaki, H., and Zhou, H. Significant enhancement in the power-conversion efficiency of chlorophyll co-sensitized solar cells by mimicking the principles of natural photosynthetic light-harvesting complexes. *Biosens. Bioelectron.*, 25(8):1970 – 1976, 2010b.

Wang, X.-F., Tamiaki, H., Wang, L., Tamai, N., Kitao, O., Zhou, H., and Sasaki, S.-i. Chlorophyll-a derivatives with various hydrocarbon ester groups for efficient dye-sensitized solar cells: Static and ultrafast evaluations on electron injection and charge collection processes. *Langmuir*, 26(9):6320–6327, 2010c.

Warburg, E. Die Quantenregeln in der Photochemie. *Naturwissenschaften*, 47:1058–1063, 1924.

Warburg, O. Photochemische Reduktion des Chinons in grünen Zellen und Granula. In *Schwermetalle als Wirkungsgruppen von Fermenten*, pages 171–183. Verlag Dr. Werner Saenger, Berlin, 1946.

Wasielewski, M. Photoinduced electron transfer in supramolecular systems for artificial photosynthesis. *Chem. Rev.*, 92:435–461, 1992.

Weiser, J. and Staab, H. Synthese eines sandwichartig zwischen zwei p-Benzochinon-Einheiten gebundenen Porphyrins. *Angew. Chem.*, 96(8):602–603, 1984.

Weller, A. Photoinduced electron transfer in solution: Exciplex and radical ion pair formation free enthalpies and their solvent dependence. *Z. Phys. Chem.*, 133:93–98, 1982.

Werncke, T. *Entwicklung und Erprobung eines Aufbaus zur Fluoreszenz-Upconversion im fs-Bereich.* Master's thesis, Humboldt-University of Berlin, 2005.

Wiehe, A., Senge, M. O., Schäfer, A., Speck, M., Tannert, S., Kurreck, H., and Röder, B. Electron donor-acceptor compounds: exploiting the triptycene geometry for the synthesis of porphyrin quinone diads, triads, and a tetrad. *Tetrahedron*, 57(51):10089 – 10110, 2001a.

Wiehe, A., Stollberg, H., Runge, S., Paul, A., Senge, M. O., and Röder, B. PDT-related photophysical properties of conformationally distorted palladium(ii) porphyrins. *J. Porphyrins Phtalocyanines*, 5(12):853–860, 2001b.

Willstätter, R. and Stoll, A. *Untersuchungen über Chlorophyll; Methoden und Ergebnisse.* J. Springer, Berlin, 1913.

With, T. K. A short history of porphyrins and the porphyrias. *Int. J. Biochem.*, 11(3-4):189–200, 1980.

Xu, H., Ermilov, E. A., Röder, B., and Ng, D. K. P. Formation and energy transfer property of a subphthalocyanine-porphyrin complex held by host-guest interactions. *Phys. Chem. Chem. Phys.*, 12:7366–7370, 2010.

Yang, S. I., Li, J., Cho, H. S., Kim, D., Bocian, D. F., Holten, D., and Lindsey, J. S. Synthesis and excited-state photodynamics of phenylethyne-linked porphyrin-phthalocyanine dyads. *J. Mater Chem.*, 10:283–296, 2000.

Zanotti, G., Angelini, N., Notarantonio, S., Paoletti, A. M., Pennesi, G., Rossi, G., Lembo, A., Colonna, D., Di Carlo, A., Reale, A., Brown, T. M., and Calogero, G. Bridged phthalocyanine systems for sensitization of nanocrystalline TiO2 films. *Int. J. Photoenergy*, 2010, 2010.

Zanotti, G., Angelini, N., Paoletti, A. M., Pennesi, G., Rossi, G., Bonapasta, A. A., Mattioli, G., Di Carlo, A., Brown, T. M., Lembo, A., and Reale, A. Synthesis of a novel unsymmetrical Zn(ii) phthalocyanine bearing a phenyl ethynyl moiety as sensitizer for dye-sensitized solar cells. *Dalton Trans.*, 40:38–40, 2011.

Zhao, Z., Cammidge, A. N., and Cook, M. J. Towards black chromophores: μ-oxo linked phthalocyanine-porphyrin dyads and phthalocyanine-subphthalocyanine dyad and triad arrays. *Chem. Commun.*, pages 7530–7532, 2009.

Zhao, Z., Cammidge, A. N., Hughes, D. L., and Cook, M. J. Modular face-to-face assembly of multichromophore arrays that absorb across the complete UV-visible spectrum and into the near-IR. *Org. Lett.*, 12(22):5138–5141, 2010.

Zhao, Z., Nyokong, T., and Maree, M. D. Synthesis and photochemical characterization of a zinc phthalocyanine-zinc porphyrin heterotrimer and heterononamer. *Dalton Trans.*, pages 3732–3737, 2005a.

Zhao, Z., Ogunsipe, A. O., Maree, M. D., and Nyokong, T. Synthesis and photophysical properties of a covalently linked porphyrin-phthalocyanine conjugate. *J. Porphyrins Phtalocyanines*, 9:186–197, 2005b.

8 Appendix

The appendix contains the drawings of the electrical circuits designed and built to

- stabilize the temperature of the photodiode lines by driving the internal peltier elements according to the reading from internal temperature dependent resistances, figure 8.1
- drive the readout electronics of the photodiode lines and the laser with a clock and synchronize the readout to the laser pulses, figure 8.2
- convert laser pulses into electrical signals by means of a photodiode, figure 8.3
- blank out the laser pulse generation during photodiode line readout, figure 8.4
- convert the energy of several pump laser pulses into a voltage, figure 8.5
- digitalize the pump laser energy equivalent voltage and transfer it into the computer, figure 8.6

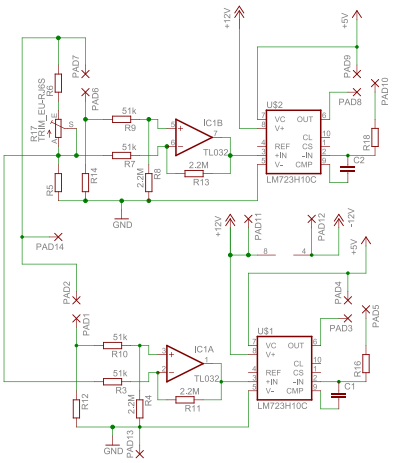

Figure 8.1: Temperature control circuit of the photo-diode lines.

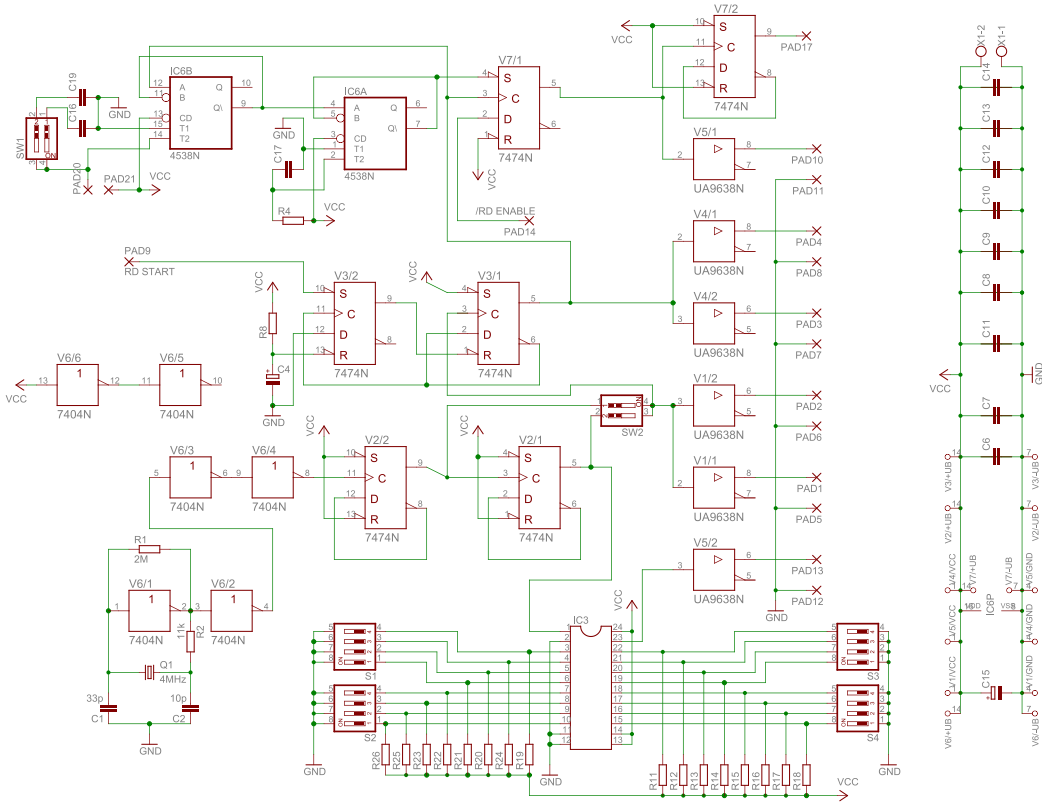

Figure 8.2: Circuit to generate the clock for the photo-diode line drivers and the laser system and to synchronize the read start pulses to the clock.

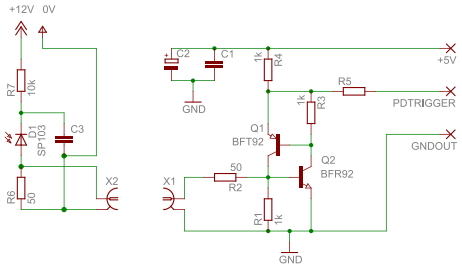

Figure 8.3: Circuit to generate long electric trigger pulses from a photodiode illuminated by the test pulses of femto-second duration to initiate laser pulse synchronized read out of the photo-diode lines.

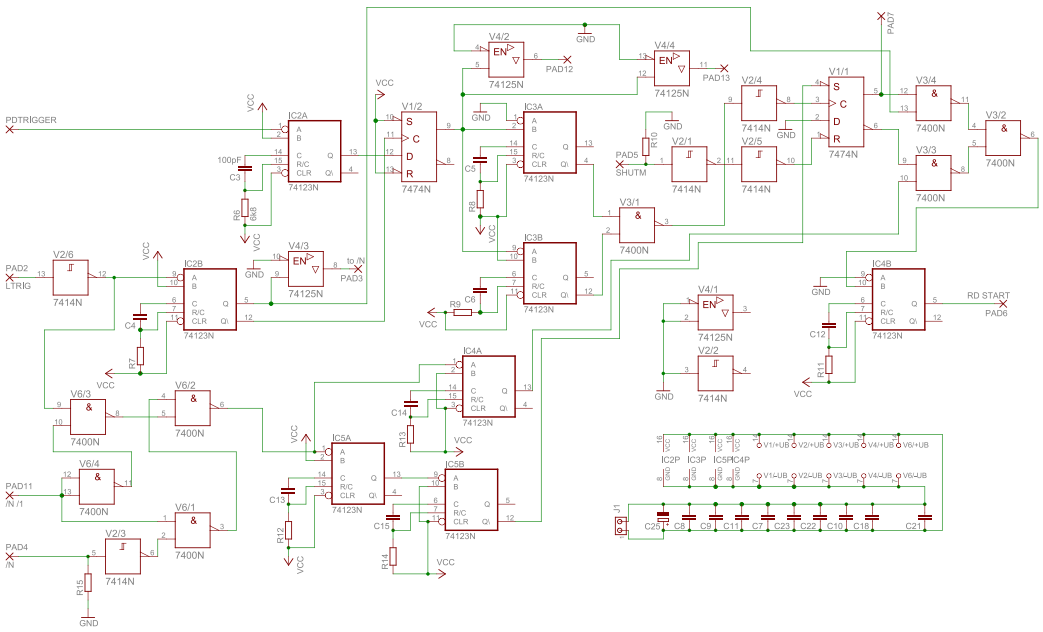

Figure 8.4: Circuit to generate the read start pulses for the photo-diode line drivers and the blank out signal for the pockels cell driver during the read out period.

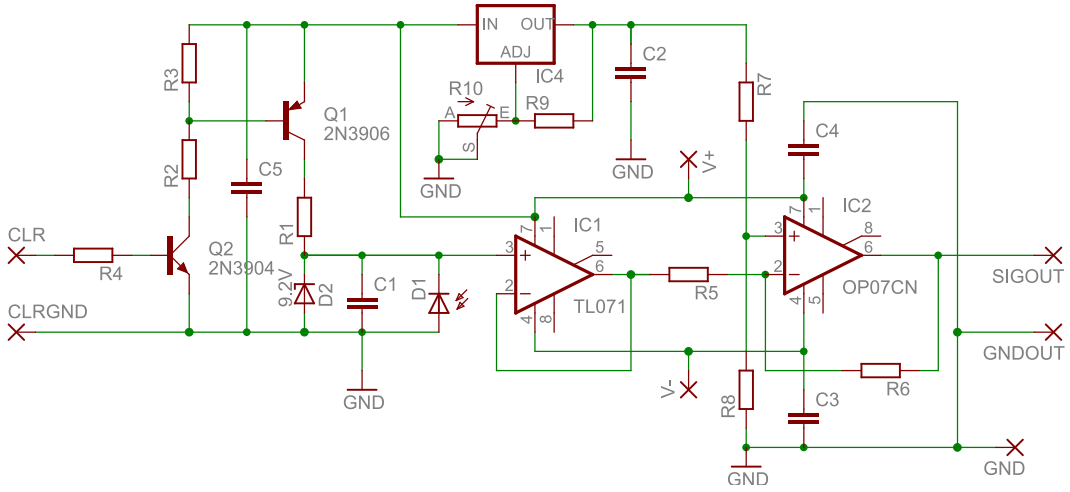

Figure 8.5: Analog electronics part of the synchronous energy detector.

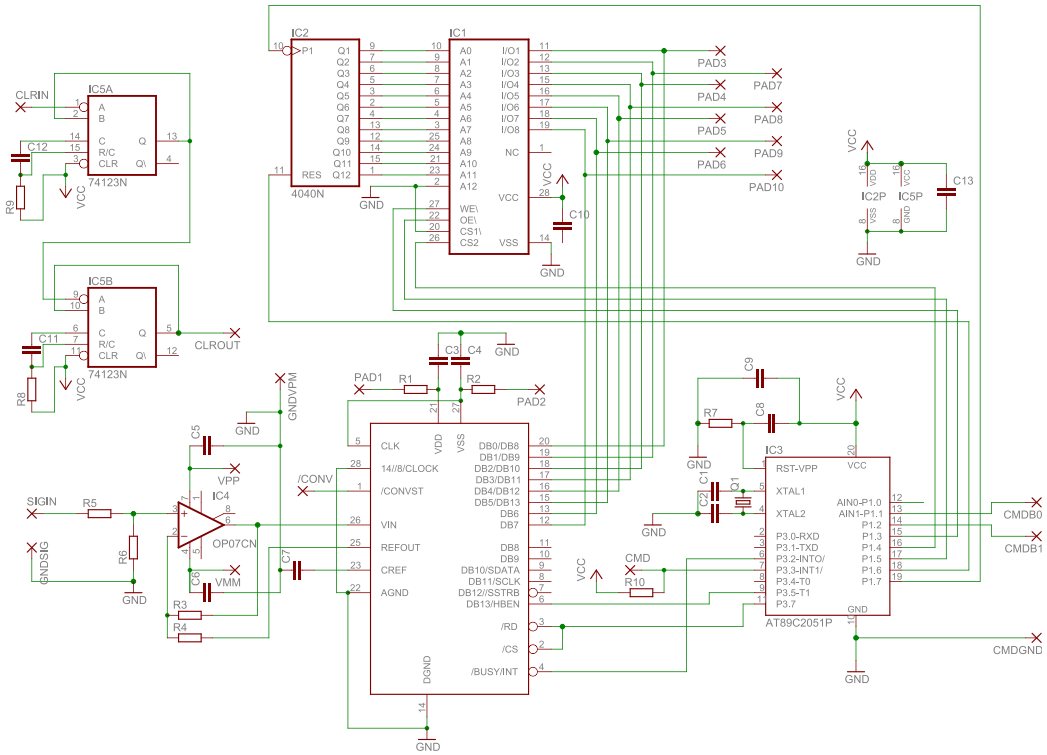

Figure 8.6: Digital electronics part of synchronous energy detector.

Abbreviations

$\boldsymbol{\chi^{(n)}}$	Optical susceptibility of n$^{\text{th}}$ order.
$\boldsymbol{\Delta G_{\mathrm{CS}}}$	Free enthalpy for charge separation.
$\boldsymbol{\varepsilon}$	Molar extinction coefficient.
$\boldsymbol{\epsilon_0}$	Vacuum permittivity.
$\boldsymbol{\epsilon_{\mathrm{ec}}}$	Dielectric constant of the electrochemical solvent.
$\boldsymbol{\epsilon_{\mathrm{s}}}$	Dielectric constant of the solvent.
$\boldsymbol{\gamma}$	Photon.
$\boldsymbol{\kappa^2}$	Orientation factor.
$\boldsymbol{\tilde{\nu}}$	Wavenumber.
$\boldsymbol{\Phi_{\mathrm{fl}}}$	Fluorescence quantum yield.
$\boldsymbol{\sigma_{\mathsf{S_1 \leftarrow S_0}}}$	Absorption cross section.
$\boldsymbol{\sigma_{\mathsf{S_0 \leftarrow S_1}}}$	Stimulated emission cross section.
$\boldsymbol{\sigma_{\mathsf{S_2 \leftarrow S_1}}}$	Induced absorption cross section.
$\boldsymbol{\sigma_{\mathsf{T_2 \leftarrow T_1}}}$	Induced triplet absorption cross section.
BDP	Boron dipyrromethene.
$\boldsymbol{c}$	Concentration.
$\boldsymbol{c_0}$	Speed of light in vacuum.
$\boldsymbol{c_0^*}$	Concentration of excited states directly after excitation.
C60	Fullerene.
CCD	Charge coupled device.
CoS	Cobalt sulfide.
CPA	Chirped pulse amplification.

CS	Charge separation.
CS state	Charge separated state.
CSU	Charge separation unit.
DAB	Diaminobutane.
DAFS	Decay associated fluorescence spectrum.
DMF	Dimethylformamid.
DSSC	Dye sensitized organic solar cell.
$\boldsymbol{E}_{1/2}^{\mathbf{oxd}}$	Electrochemical half wave oxidation potential.
$\boldsymbol{E}_{1/2}^{\mathbf{red}}$	Electrochemical half wave reduction potential.
fsTAS	Transient absorption spectroscopy in the femtosecond time scale.
fsUPC	Fluorescence up-conversion in the femtosecond time scale.
GLLS	Generalized linear least squares.
H_2TPP	Free base tetraphenylporphyrin.
HOMO	Highest occupied molecular orbital.
H_2Tr	H_2TPP-SiPc-H_2TPP triad.
IC	Internal conversion.
ISC	Intersystem crossing.
ITO	Indium-doped tin oxide.
$\boldsymbol{J}$	Overlap integral in Förster radius calculation.
$\boldsymbol{k}_{\mathbf{BHT}}$	Back hole transfer rate constant.
$\boldsymbol{k}_{\mathbf{CR}}$	Charge recombination transfer rate constant.
$\boldsymbol{k}_{\mathbf{EET}}$	Energy transfer rate constant.
$\boldsymbol{k}_{\mathbf{ET}}$	Electron transfer rate constant.
$\boldsymbol{k}_{\mathsf{FL}}$	Fluorescence rate constant.

k_{HT}	Hole transfer rate constant.
k_{IC}	Internal conversion rate constant.
k_{ISC}	Intersystem crossing rate constant.
k_{PHO}	Phosphorescence rate constant.
LCAO	Linear combination of atomic orbitals.
LHC	Light harvesting complex.
LHS	Light harvesting system.
LUMO	Lowest unoccupied molecular orbital.
N_{A}	Avogadro's number.
NDI	Napthalene diimide.
OD	Optical density.
OKE	Optical Kerr Effect.
OPV	Organic photovoltaic.
P	Porphyrin.
Pc	Phthalocyanine.
PhCN	Benzonitrile.
Pheo	Pheophorbide *a*.
PIET	Photo-induced electron transfer.
PS	Photosystem.
r_{A^-}	Radius of the acceptor anion.
RC	Reaction center.
r_{D^+}	Radius of the donor cation.
TOL	Toluene.
$\mathsf{S_0}$	Singlet ground state.
$\mathsf{S_1}$	First excited singlet state.

$\mathbf{S_2}$	Second excited singlet state.
SCE	Saturated calomel electrode.
SFG	Sum frequency generation.
SHG	Second harmonic generation.
SiPc	Silicon phthalocyanine.
SiPcPy	Bis(4-pyridinolato) silicon phthalocyanine.
SNR	Signal to noise ratio.
$\mathbf{T_1}$	First excited triplet state.
$\mathbf{T_2}$	Second excited triplet state.
TAS	Transient absorption spectroscopy.
TCSPC	Time-correlated single photon counting.
UV	Ultraviolet.
VIS	Visible.
ZnPc	Zinc phthalocyanine.
ZnTPP	Zinc tetraphenylporphyrin.
ZnTr	ZnTPP-SiPc-ZnTPP triad.

Acknowledgement

This work would not have been possible without the support of numerous people, to whom I would like to express my thanks.

First of all I would like to thank Prof. Beate Röder for supporting me over the years of this thesis work with helpful comments and advices. Under her supervision I had the freedom to work on many interesting projects.

Moreover, I would like to thank to Prof. Dennis Ng and his group for the very good scientific cooperation, for synthesizing the promising new class of porphyrin-phthalocyanine heteromers, and for giving me the opportunity to investigate their energy- and electron transfer characteristics.

I thank Dr. Eugeny Ermilov and Dr. Arno Wiehe for plenty of fruitful scientific and non-scientific discussions, their supervision on my research, and a stimulating atmosphere.

Dr. Christian Litwinski spent plenty of time on working out new ideas, maintaining the labs, and in discussions with me, many thanks for this time.

Many thanks as well to Thomas Werncke and Andreas Völker. Their assistance paired with an independent working manner was an essential groundwork for the development of two new setups. Jörn Oliver Vogel helped with the preliminary characterization of the heteromers.

I thank Gisela Wöhlecke, and Hartmut Gruber for their excellent technical assistance. Also, I would like to thank the people of the mechanical workshop for their precise and fast work.

Dr. Astrid Tannert, Dr. Michael Wahl, Dr. Christian Litwinski, and Dr. Arno Wiehe proofread the manusscript and gave helpful comments, thanks for that.

Many thanks to Rainer Erdmann and Dr. Felix Koberling for their support to finish this thesis while working at PicoQuant.

Finally, I'm deeply grateful for the time and the support of my wife Astrid, and for the every morning smile of our daughter Rebekka.

Selbständigkeitserklärung

Hiermit versichere ich, dass ich die vorliegende Arbeit selbständig und ohne Benutzung anderer als der angegebenen Quellen und Hilfsmittel angefertigt habe.

Ort, Datum Unterschrift